1-2013

A Method for Evaluating Power Generation Concepts Considering the Optimal Concept of Operations

Tianlei Zhang
University of South Carolina - Columbia

A METHOD FOR EVALUATING POWER GENERATION CONCEPTS CONSIDERING THE OPTIMAL CONCEPT OF OPERATIONS

by

Tianlei Zhang

Bachelor of Science
Xi'an Jiaotong University, 2006

Submitted in Partial Fulfillment of the Requirements

For the Degree of Doctor of Philosophy in

Electrical Engineering

College of Engineering and Computing

University of South Carolina

2013

Accepted by:

Roger A. Dougal, Major Professor

Charles W. Brice, Committee Member

Herbert L. Ginn III, Committee Member

Edward P. Gatzke, Committee Member

Lacy Ford, Vice Provost and Dean of Graduate Studies

DEDICATION

To my loving parents, Yongge Zhang and Jie Bai

ACKNOWLEDGEMENTS

My sincere acknowledgement goes to my advisor, Dr. Roger Dougal. His support and instruction initiated my courage and belief to step into the world of research. His unending guidance and valuable advices have helped me become a professional engineer with the ability to explore wider and deeper knowledge. I am really grateful to him for giving me the opportunity to realize my doctoral degree. More importantly, I would like to thank him for teaching me the thinking of engineers, the altitude towards research, and the skills of technical presentation, which are more important than a diploma and will affect my career development.

I would like to express my gratitude to my dear committee members, Dr. Charles Brice, Dr. Herbert Ginn, and Dr. Edward Gatzke. All of them provided invaluable feedback and suggestions that kept my research work on the right track.

I am very thankful to all the EE faculties and administrative staffs. Especially, I would like to thank Richard Smart for his valuable feedbacks and help with my writing and presentation. I would like to thank Hope Johnson and Valuncha Paterson for their great assistance and support during my study at USC.

I would like to thank all my fellows in Dr. Dougal's research group, Asif Anwar, Paul Young, Blanca Correa, Pietro Cairoli, Huaxi Zheng, Ugo Ghisla, and Dan Li. They provided so many informative discussions and suggestions that made my research easier and smoother. I would also like to thank all the colleagues in my office. They created

such a friendly atmosphere with multi-cultural communications. I have learned so much from all these friends in USC and wish to keep the friendship forever.

My special acknowledgement goes to all my precious friends that I met in Columbia, SC. I specially want to thank Ron and Marianne Parker for their love, care, and encouragement all these years. They made my life filled with parents' love even when I was so far away from my family. I would like to thank Bill Porter for his friendship, help, and support. He brought the most amazing grace into my life that I would keep pursuing. I would also like to give thanks to all my Chinese friends. They made my life in Columbia colorful, meaningful, and memorable. I was so blessed to have them all.

Last but not least, my deepest gratitude goes to my loving parents, Yongge Zhang and Jie Bai. Thank you for your unconditional love and support when I made my decision to fly thousands of miles away from you to pursue the Ph.D. in the US. Thank you for your faith in me and your encouragement to let me realize my dreams without worries. I am very thankful with my grandparents and all my families, especially my aunt, Ling Bai, for their love and care. I love you all forever.

ABSTRACT

When trying to select an appropriate power generation plant for a micro-grid power distribution system like an electric ship, designers must consider both the physical characteristics (e.g., weight, volume, power ratings) and performance characteristics (e.g., fuel consumption, quality of service) of all the design alternatives. Comparing the design alternatives in terms of the physical characteristics is relatively straightforward, but in terms of performance characteristics each design alternative has to be evaluated within its own optimal performance points to make a fair comparison. However, at present no effective method or software tools exist to enable this evaluation at the earliest design stage.

To address this problem, we develop a concept evaluation method to determine the optimized power system concept of operations (CONOPS). Incorporating this method into the power generation plant development allows the design alternatives with undesirable performance to be removed from consideration, and ensures a high level of confidence that no quasi-optimal alternative is eliminated. The CONOPS in this dissertation takes into account the operating setpoints of the generating units on the primary power distribution buses. The optimality of a CONOPS is assessed with respect to its yielded system performance metrics, namely, fuel consumption and the quality of service (QOS). These two are paramount to the operating economy and mission success of micro-grid power systems. As an example, we apply our approach to the set-based

design (SBD) of a shipboard power system to demonstrate its effectiveness. Research is performed using a three step process.

First, we identify the full set of design variables that is applicable to generic power generation and distribution architectures, and use it to formulate the optimization problems of the CONOPS. The optimization problems fit both ac and dc distribution architecture and include the parameters that we identify as essential to describe the architecture. Also, we develop two QOS metrics to investigate the different aspects of system reliability: failure probability, and failure magnitude and duration.

Second, we develop and improve a single-objective particle swarm optimization (SOPSO) and multi-objective particle swarm optimization (MOPSO) to solve the optimization problems of the CONOPS. Both are able to provide enhanced capability and reliability of searching for the global optimum as compared with the previously reported PSOs. For a given system concept and mission (i.e. a description of loading conditions), the results derived by the SOPSO can rapidly reveal the performance tradeoffs of the CONOPS and investigate how the definitions of the performance metrics affect the optimal design of CONOPS. The results derived by the MOPSO, in contrast, help designers identify the quasi-optimal set of design alternatives during SBD with a very high confidence level.

Third, in order to generalize the formulation process of the optimization problems for generic primary generation and distribution architectures and different expressions of the performance metrics, we develop an optimization structure based on the concept of control architecture. We define five broad categories of data to describe the essential parameters and design variables of the optimization problems common to a generic

micro-grid power system application. We also identify the coupling relationship of these categories of data to standardize the co-optimization algorithm of the optimization problems. Therefore, we only need to develop one coding infrastructure that can be applicable to a wide range of design scenarios. In addition, we develop a hierarchical data structure to address the software implementation of this concept evaluation method during SBD. This data structure contains two data exchange/flow block diagrams. One block diagram defines the data sharing method between the early stage models in S3D with an optimization simulation model in MATLAB. The other block diagram defines the data implementation process of resolving the co-optimization problem of the CONOPS in MATLAB. This data structure provides an effective guidance for software engineers to implement the concept evaluation method automatically by means of the two software environments.

TABLE OF CONTENTS

LIST OF TABLES

LIST OF FIGURES

LIST OF ABBREVIATIONS

BBO .....Bio-geography Based Optimization

CDFR ..... Condition-Dependent Failure Rate

CDRD .....Condition-Dependent Repair Duration

CONOPS..... Power System Concept of Operations

EDP .....Economic Dispatch Problem

EP .....Evolutionary Programming

ESM ..... Energy Storage Module

GA..... Genetic Algorithm

GSI .....Gravitational Search Intelligence

HFAC..... High Frequency Alternating Current

HNN.....Hopfield Neural Networks

MLDT .....Mean-Logistics-Delay-Time

MOPSO..... Multi-Objective Particle Swarm Optimization

MTBF.....Mean-Time-Between-Failure

MTTR .....Mean-Time-To-Repair

MVAC.....Medium Voltage Alternating Current

MVDC..... Medium Voltage Direct Current

NGIPS .....the Next Generation Integrated Power System

QOS..... Quality of Service

PBD.....Point-Based Design

PCM ..... Power Conversion Module

PDB ..... Primary Distribution Bus

PDM ..... Power Distribution Module

PGM ..... Power Generation Module

PLM ..... Power Load Module

PMM ..... Propulsion Motor Module

PSO ..... Particle Swarm Optimization

SA ..... Simulated Annealing

SBD ..... Set-Based Design

SFC ..... Specific Fuel Consumption

SOPSO ..... Single-Objective Particle Swarm Optimization

VTB ..... Virtual Test Bed

ZEDS ..... Zonal Electrical Distribution System

CHAPTER 1

INTRODUCTION

1.1. CONTRIBUTIONS OF THIS DISSERTATION

- Development of the optimization problems of the power system concept of operations (CONOPS) for generic micro-grid power generation and distribution systems. These optimization problems are developed to evaluate the quality of power generation concepts in terms of two critical system-level performance metrics—fuel consumption and the system quality of service (QOS). Incorporating these optimization problems at the earliest design stage can further reduce the number of feasible design alternatives compared to traditional methods, considerably reducing the work of the multidisciplinary research team in the preliminary design phase.
- Improvement and validation of a single-objective Particle Swarm Optimization (SOPSO) and a multi-objective Particle Swarm Optimization (MOPSO). Both of the optimization algorithms present an enhanced capability and reliability of locating the global optimum for constrained mixed-integer problems as compared with the previously reported PSOs.
- Application of the SOPSO and MOPSO to the optimization problems of the CONOPS. We demonstrate the performance tradeoff analyses of the CONOPS for different power generation concepts by using the SOPSO. We also present an effective approach to identify the quasi-optimal set of

power generation concepts via the MOPSO according to the stakeholders' preferences on the performance metrics.

- Development of the optimization structure to generalize the modeling process of the optimization problems. Based on the optimization structure, we develop a coding infrastructure of optimization problem formulation that can be imposed on a generic type of micro-grid power generation and distribution architecture. This work reduces the cost of problem formulation and design validation during the exploration of the design space at the earliest stage.
- Development of the data structure to facilitate the automatic software implementation of the concept evaluation method, which accounts for the optimization of the CONOPS, in the set-based design (SBD) phase.

1.2. MOTIVATION

1.2.1. Accounting for the Optimized CONOPS during Concept Evaluation

The primary objective of the power system design process at the earliest stage is to identify and fully explore the feasible regions of the design space. To this end, one should be allowed to combine any applicable type of power generation and distribution architecture (referred to in this dissertation as "system concept") with any feasible combination of generating units (referred to in this dissertation as "design alternative").

However, for a given system concept, assessing the equipment specifications and characteristics (e.g., quantities, power ratings, locations of generating units) is not enough to truly quantify the quality of a design alternative at the earliest design stage. On one hand, although different generation plants are characterized with different hardware parameters, they may behave similarly with appropriate operating setpoint values. For

example, in order to build an 80 MW shipboard power system, one can choose either four generators with the rated power at 5, 15, 20, and 40 MW or four identical generators with rated power at 20 MW. To serve a light load at ¼ power capacity (20 MW), the former design alternative can run two generators: the 20 MW generator is fully operated and 40 MW generator stays as a backup power source in an idling state without producing any power; the latter design alternative can run two 20 MW generators, each producing 10 MW. Under these operating strategies, these two design alternatives may consume a very similar amount of fuel because they all have two generators in service; they also present the same level of QOS because if either operating generator goes offline, the generator left online is still able to fully support the load power demand for the two design alternatives.

On the other hand, the performance of a generation plant can also vary in a significant range with different operating setpoint values. Let us continue with the previous example. To serve the 20 MW load, a generation plant can either dispatch power among all of its generators or just run the minimum number of generators sufficient to support the load. The net fuel consumption of the former case can be several times that of the latter case depending on the load power and quantity of the in-service generating units.

Therefore, in order to derive a fair comparison among the design alternatives at the earliest design stage, one has to identify the quasi-optimal performance of each alternative at the certainty level that can be best achieved or estimated at the stage. Specifically, at the earliest stage where waveform-level controls of power electronic applications are not accessible, it is important to incorporate the optimization of the

system-level operating setpoints into the evaluation of power generation concepts. It is also demanding to generalize this optimization approach for a wide range of system design possibilities (i.e., a "system design" is the combination of the given system concept and one of its design alternatives).

For a micro-grid power system design, the CONOPS are originally referred to by Doerry in [1] as "which power system components are used as well as their configuration for different mission system requirements." In this dissertation, we extend this definition to include more detailed setpoint information of power system components, that is, how much active and reactive power (only for ac distribution system) each in-service power generating unit produces.

1.2.2. Developing the Co-Optimization Problem for Determining the CONOPS

Usually each performance metric requires a design alternative to be operated under specific setpoints to achieve the desired design objectives. When the quality of a design alternative is simultaneously determined by more than one performance metric, these metrics have to be co-evaluated to determine the optimal values of the CONOPS, otherwise, the selection of the best design alternative for a given mission based on one performance metric's optimal value may actually not be valid when considering another performance metric. Similarly, for each design alternative, the selection of the optimal operating point based on one performance metric's value may not be optimal when considering another performance metric.

For example, a shipboard power system with 80 MW power capacity may contain either a few generators with high power ratings (e.g., four 20 MW) or many generators with lower power ratings (e.g., eight 10 MW). If the ship's mission profile includes frequent cruising segments at low speeds, demanding low power for loads (e.g., 32 MW),

the former design may outperform the latter in terms of fuel consumption because the former requires a smaller number of generators in service to fulfill the power demand (i.e. two 20 MW compared with four 10 MW, although both combinations of online generators can be operated at their optimal fuel-saving status, the base fuel consumption to keep a machine operational accounts for a considerable proportion of operating fuel consumption, leading to a high probability that having more generators in service will consume more fuel.) However, the latter design appears to be better in terms of the QOS because the power is dispatched among more generators, offering greater generation redundancy (i.e., 20 MW vs. 30 MW). Therefore, in order to identify the true quality of a design alternative, we need an effective method to fully investigate the performance tradeoffs between fuel consumption and the QOS with different CONOPS.

1.2.3. Incorporating the Concept Evaluation Method Considering the Optimal CONOPS into Set-Based Design

SBD is an important design principle used to fully explore a design space at the early stages. It enables the design process to converge to the best set of potential design alternatives, which will most likely lead to the best solution, in a time frame as short as possible [2][3]. Following the traditional point-based design (PBD) approach, designers quickly assess a range of design alternatives and then arbitrarily select one for further refinement with respect to a range of desired capabilities. In contrast, following SBD, designers do not rush into making decisions but rather eliminate undesirable answers from the design space. This screening process proceeds as additional detailed analyses are added in along design steps until some point when a single design "converges" [4]. Therefore, a far greater range of design alternatives can be evaluated with respect to the desired capabilities with the lowest investment of study effort.

Since SBD produces better solutions faster and offers more flexibility for continued system improvement and integration [2], it has been widely used for applications in the automotive and aerospace industries. Recently, the U.S. Navy has taken actions to adopt SBD for the shipboard power system design process. The SBD model is expected to improve design discovery in the Pre-Preliminary Design (Pre-PD) phase as indicated in Figure 1.1. It will allow more of the design effort to proceed simultaneously and defers detailed specifications until tradeoffs are more fully understood [2][4]. However, the current SBD approach is constructed with the analysis framework only based on physical properties, such as weight, volume, and power capacity. Because of this, the outcome is unable to reflect optimal tradeoffs of system performance. Hence, the design alternatives with inferior performance tradeoffs may also be selected in the Pre-PD, increasing evaluation costs and slowing down design cycles.

Therefore, it is paramount to integrate the optimization of the CONOPS into the current concept evaluation method of SBD. This accomplishment will effectively narrow down the feasible design space at the earliest design stage according to the stakeholders' preferences on the system performance tradeoffs. This work can be done by developing a software coupling method between an external optimization solver, which is advantageous to model and resolve generic optimization problems, and a SBD tool, which is used to generate early stage system models.

1.3. DIFFICULTIES AND CHALLENGES

1.3.1. Formulation and Solution of the Optimization Problems of the CONOPS

In previous literature, fuel consumption, the QOS, and survivability are suggested and discussed most as the critical performance measures of interest at the system level for

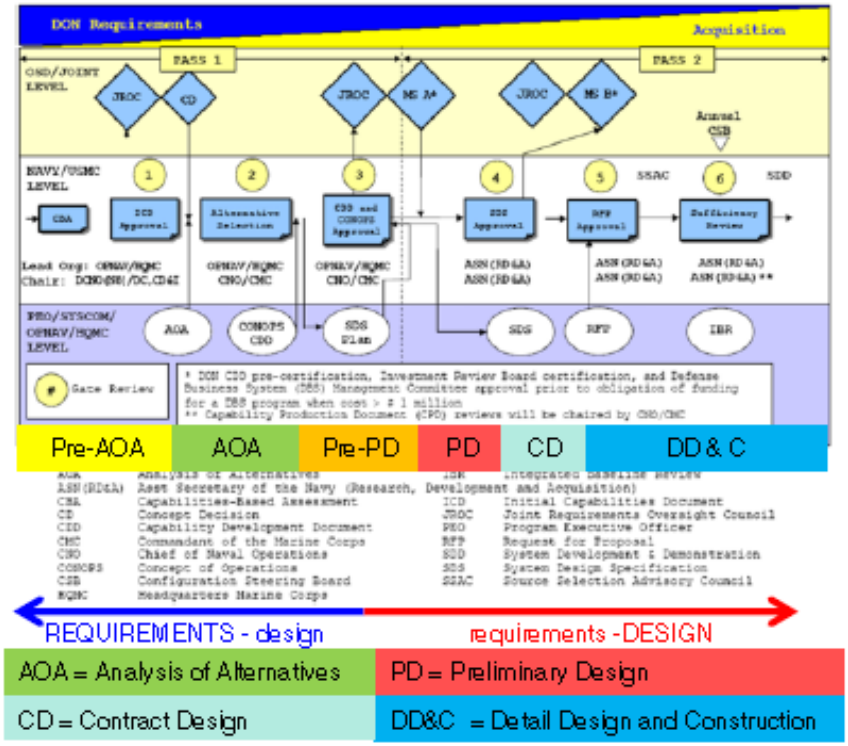

Figure 1.1 Navy Acquisition 2 Pass-6 Gate Acquisition Process and Stages of Design [5][6]

micro-grid power systems [10]-[45]. Fuel consumption is usually minimized for a given mission (or a mission segment) by resolving an economic dispatch problem (EDP). The QOS is the measure of the system's ability to continue serving loads when some generating elements become suddenly unavailable. Survivability measures a system's ability to restore the power supply on a damaged system (i.e., the ability to preserve the power for critical mission loads after damage occurs to the distribution system). In this dissertation, we are only concerned with fuel consumption and the QOS because they are more affected by the refinement of the CONOPS than survivability. In contrast, survivability is mostly predetermined by physical characteristics of both the electric and thermal cooling system layouts (e.g., locations of equipment, the quantity of zones, the

distance between buses) rather than sophisticated operation strategies of power system components when serious damage occurs [35].

However, for micro-grid power systems, the optimization approach for the CONOPS with respective to fuel consumption and the QOS has not been fully addressed at the earliest design stage up to this point. Three main challenges are summarized as follows:

First, the EDPs are previously formulated in terms of the setpoint variables of the CONOPS that mainly reflect the characteristics of terrestrial power plants (i.e., only the real power dispatch is necessary at the end of the generation plant; switching generating units on or off is not necessarily considered; the configurability of a power distribution system is not taken into account.). When applying these variables to the EDPs of micro-grid power systems, the minimum fuel consumption of a system design cannot truly be predicted for acquisition decisions. In addition, the generation redundancy, which is central to micro-grid power systems, is seldom concerned in the previous EDPs.

Second, the optimization problem of the CONOPS with respect to the QOS (referred to in this dissertation as "QOS optimization problem") has not been properly related to any setpoint variables. It has been well acknowledged that ratings of generating units, setpoints of power modules, and the operating status of distribution systems considerably affect the system QOS [44]. However, the existing QOS optimization problems only focus on the QOS enhancement at static operating points of a generation plant rather than the discovery of the optimal operating point of a generation plant for maximizing the QOS. Thus, we need to reformulate the QOS optimization problem from scratch.

Last but not least, although it is essential to have fuel consumption and the QOS co-optimized (see Section 1.2.2), in the past, they have been optimized only in sequence. Specifically, the QOS is always evaluated or improved based on the outcome of an EDP, which determines the power plant setpoint. Thus, it is highly possible to encounter the situation (demonstrated in Chapter 7) that one can never get a satisfactory QOS no matter how he adjust the system hardware around an operating point that implicitly compromises the QOS; or he may have to afford a large investment at that operating point to achieve an acceptable QOS.

How to model these optimization problems and solve the co-optimization problem is also a big challenge for us to address. Considering the complexity of the objective functions and constraints, which are non-convex, nonlinear, and mixed-integer, existing evolutionary algorithms are not effective enough to derive the solution in a reasonable time; thus, this dissertation also has to develop an effective optimization technique to support the optimization process of the CONOPS.

1.3.2. Development of Optimization Structure for a Universal System Design

One has to face two difficulties to impose the optimization problems of the CONOPS on different potential system designs: 1) there is no generic format of the optimization problems that can fit an arbitrary system concept (e.g., the optimization problems formulated for the system with a ring bus cannot be applied for the system with the breaker-and-a-half bus configuration); 2) it is time-consuming in reality to formulate the optimization problems for each system concept one at a time. To address these difficulties, we need to generalize the modeling process and the coding infrastructure of the optimization problems based on the commonality of various system concepts.

As stated by IEEE Std 1676 [46] and recently drafted IEEE Std P1826/D4 [47], control architecture can be effective to generalize the description of normative control functions for different application levels, disregarding a wide range of system architecture types. Specifically, the low level control architecture divides the functional analysis of a generic power electronics system into the control functions ranging from establishing the system mission to managing the specific power devices. The mid-level control architecture (i.e., for power system controls) defines the control functions of a generic zonal electrical distribution system (ZEDS) for properly serving the loads by a customer-supplier agreement, ranging from allocating duties to zones for supporting a mission to identifying the management strategies of zonal power electronic equipment.

The optimization of the CONOPS does not involve the actual control implementations of power system components in time domain, but it determines the overall control objectives of a power system from the primary power generation and distribution level (the power level), that is, how the generating units should be operated in order to guarantee the carrying out of the mission. Since the determination of the CONOPS dictates the operation of the ZEDSs and power electronics system, it is regarded as the control function belonging to the highest level of a power system. Obviously, if the control architecture for this level of a generic micro-grid power system is available, we will be able to develop an optimization structure based on that to standardize the optimization problem of the CONOPS for a universal system design.

Unfortunately, at the moment, the concept of the control architecture is explored only for the low-level power electronic applications and mid-level ZEDSs, but not for the

high-level power systems (the primary power generation and distribution level). Thus, we are missing the basis to develop the corresponding optimization structure.

1.3.3. Automatic Software Implementation of the Concept Evaluation Method

The early stage design software, S3D [48], is developed to provide an environment that enables simultaneous collaborative design across multiple disciplines in the early design process. S3D facilitates the project's transition from a conceptual phase to a detailed design phase. It provides a mechanism for mapping vendor equipment directly to models that are available for detailed designs. It is also able to provide the simulation capability of detailed time-domain design by means of a coupled simulator, called Virtual Test Bed (VTB). Although S3D is advantageous for its quality and efficiency of capturing representative electrical architecture, it lacks the potential to investigate the optimality of a system due to the shortage of an optimization solver.

In contrast, MATLAB contains a large group of powerful tools for numerical computations with vectors and matrices, and offers sophisticated commands for customizing optimization techniques [49]. However, it is insufficient in exploring the design space for system concepts and design alternatives at the earliest design stage. Therefore, the integration of S3D with MATLAB can be an effective solution to incorporate the optimization analysis of the CONOPS into the concept evaluation method. However, at the moment, an effective data sharing method has not yet been developed between the early stage model and the simulation model. Specifically, the transmitted and processed data has not been identified within each software environment and between the two environments. In addition, the procedure to automate software integration and acquisition decisions needs to be defined.

CHAPTER 2

RESEARCH OBJECTIVES

2.1. OVERVIEW OF RESEARCH OBJECTIVES

The objective of this dissertation is to develop a methodology for evaluating the potential power generation concepts for a given micro-grid power system concept, such as a shipboard power system, and selecting a set of quasi-optimal solutions at the earliest design stage. A four-step methodology is developed to meet this goal:

1) Develop the standard optimization problems of the CONOPS with respect to the two critical performance metrics—fuel consumption and QOS—for a generic system design.
2) Formulate the appropriate formats of the optimization problems for each given system concept based on its architecture characteristics.
3) Apply an effective optimization algorithm to co-optimize the optimization problems for the distinct metrics. The quasi-optimal performance tradeoffs are determined based on the concept of Pareto dominance for each potential system design.
4) Compare the quasi-optimal performance tradeoffs of all the potential system designs to select the non-dominated (quasi-optimal) design alternatives and understand their optimal operating strategies.

The entire work is only based on the system-level analyses and eventually applied to SBD for micro-grid power system designs.

2.2. DEVELOPMENT OF THE OPTIMIZATION PROBLEMS OF THE CONOPS

The first objective in this subsection is to identify a set of design variables for a universal system concept and design alternative. This set should be essential to identifying the CONOPS of the micro-grid power generating units. Also, it should be sufficient to allow for tradeoff study between fuel consumption and the QOS for a system design at the earliest stage.

The second objective in this subsection is to formulate the optimization problems of the CONOPS with respect to the distinct metrics. The objective function should be able to quantify the fuel consumption and system QOS in terms of the variable set. The optimization constraints should reflect the operating requirements common to generic micro-grid power systems.

Considering that there are multiple potential topologies of a system concept (e.g., ring bus, split bus, breaker-and-a-half), it is important to identify the appropriate forms of the optimization problems to fit the given one. Therefore, the third objective in this subsection is to identify the essential parameters that characterize a system concept (e.g., the number of independent primary distribution buses, the power distribution configuration of the load zones, the operating status of circuit breakers) and to incorporate them during the optimization problem formulation.

2.3. DEVELOPMENT OF OPTIMIZATION STRUCTURE FOR A UNIVERSAL SYSTEM DESIGN

The objective in this subsection is to develop an optimization structure for defining a universal modeling and coding process of the optimization problems disregarding any specific system concept. Specifically, we need to first define the broad

categories for the data that must be involved in the optimization problems of the CONOPS. This is for generalizing the description of system designs, design requirements, and the formulation procedure. Then we need to identify the relationship among all these categories of data to regulate the co-optimization procedure of the CONOPS. Finally, we need to develop one standard coding infrastructure for imposing the optimization algorithm to the optimization problems, which may correspond to any regular system concept and contain different metric expressions.

We also need to develop a powerful single-objective and multi-objective optimization algorithm to support the optimization and co-optimization approach, respectively. These algorithms should be able to reliably converge to the accurate global optimal solutions in a reasonable number of iterations when dealing with constrained mixed-integer problems. In order to facilitate acquisition decision, we will employ the concept of Pareto optimality to visualize the quality comparison of the design alternatives with the co-optimization approach.

2.4. Development of Data Structure for Software Implementation

Due to software limitations, modeling early stage system designs and optimizing their CONOPS are currently accomplished in two independent software environments—S3D and MATLAB. Therefore, the information of each early stage model studied in S3D has to be manually collected and hard-coded in MATLAB one at a time to generate the appropriate formats of the optimization problems.

The objective in this subsection is to develop a data structure for realizing the automated simulation process by using the two tools. Specifically, we need to identify the data that is required to be collected from a generic system concept in S3D and delivered

to MATLAB for customizing the optimization functions of the CONOPS. In addition, we need to identify the data that are required, processed, and output at each simulation phase of the concept evaluation process implemented in MATLAB. We will finally develop the data flow diagrams for the software data coupling and SBD screening process.

CHAPTER 3

STATE OF THE ART ON THE EARLY-STAGE OPTIMAL DESIGN OF MICRO-GRID POWER GENERATION PLANTS

3.1. OPTIMIZATION PROBLEM FORMULATION

In the previously published efforts, the quality of a micro-grid power generation system design is mainly evaluated in the following aspects at the earliest stage [7][9]: mission-oriented fuel cost, minimization of the number of prime movers, electric power QOS, and benefits of including energy storage devices.

3.1.1. Minimizing Mission-Oriented Fuel Costs

In previous literature, the EDP has been extensively studied for terrestrial power generation plants with various evolutionary optimization algorithms [10]-[24]. Given the mission segments depicting the discrete load power demands, fuel consumption of a power generation plant is minimized by optimizing the operating setpoint of each installed generating unit subject to the operating constraints of interest.

The fuel cost (usually measured in dollars) of each generating unit is formulated by a quadratic or occasionally cubic polynomial in terms of its generated power, P. The quadratic function is expressed as the term in the parentheses of (1). The three coefficients, a_i, b_i, and c_i, are specific to a power generating unit. The fuel cost of a generation plant is expressed as the sum of fuel costs of all N generating units, as shown in (1). When valve point loading effects of generators are concerned, another sinusoidal term has to be added into the polynomial equation, shown as the term in the absolute

operators of (2). The coefficients of e_i and f_i can be determined by fitting the experimental efficiency curve of a generator. However, the sinusoidal term will turn the original convex function into a non-convex one, requiring more advanced evolutionary algorithms to solve the problem [17]-[22].

$$F = \sum_{n=1}^{N} \left(a_n P_n^2 + b_n P_n + c_n \right) \tag{1}$$

$$F = \sum_{n=1}^{N} \left[\left(a_n P_n^2 + b_n P_n + c_n \right) + \left| e_n \sin\left(f_n \left(P_{\mathrm{n,min}} - P_n \right) \right) \right| \right] \tag{2}$$

Constraints imposed on an EDP vary depending on the application of a power generation plant and the accuracy level that designers aim to achieve. Generation capacity and power balance are the compulsory constraints for all situations [15][16]. Apart from these two, extra operating constraints, such as prohibited operating zones [13][15][17]-[20], ramp rate limits [14][21], generator startup fuel consumption [23], transmission line loading limits [1][13], power loss in the transmission lines (normally modeled using the standard or simplified Kron's loss formula) [1][14][17]-[20], the augmentation of spinning reserve capability of a system [22], and the maintenance of the QOS at certain levels [50] can be taken into account for more accurate analysis.

However, it has to be noted that all the previous work fails to address three design concerns, which unfortunately are very significant to micro-grid power systems and SBD applications:

First of all, the reported concepts of EDPs are developed to discover the optimal performance of an already-defined generation plant and system concept, but not to help choose or optimize the specifications of the generation plant for a system concept. Accordingly, the previous EDPs fail to address the early stage design concerns, such as

discovering the minimum number of prime movers and generating units for a system that can yield the minimum fuel consumption for a given mission.

Second, the reported EDPs fail to investigate the effect of the type of electric architecture on the fuel-saving performance of a power generation plant. Since the distributed power factor compensators are installed along the terrestrial AC distribution buses close to the end-use load, the reactive power balance constraint is not required on the side of the generation plant. Therefore, the formulation of the EDP is always regarded to be the same for AC and DC systems. However, considering the weight and cost, a micro-grid power system like an electric ship usually has a limited installation of reactive power compensators. Thus it is necessary to study how the reactive power balance at the end of the generation plant affects the performance of a micro-grid AC power system.

Third, the EDPs formulated for terrestrial generation plants do not consider generation redundancy or any other reliability constraints because of the excessive power support from the grid. However, the power generation capacity of a micro-grid system is always closely sized to the load demands, thus the system usually has little spinning reserve during operations. Therefore, reliability has to be taken into account with fuel consumption when resolving the EDP. Unfortunately, the reported EDPs in literature fail to address this concern.

3.1.2. Improving the Electric Power QOS

The QOS evaluates the ability of a generation plant to preserve the power to loads when certain power generating modules suddenly become unavailable. The QOS is a very important factor to characterize system optimality of a micro-grid power system design [7]. However, the approach to discover the optimal QOS value of a design

alternative at the earliest design stage has not been properly developed. There are three problems with the current existing QOS metrics:

1) Most of them are described in prescriptive languages like "standards" or customer-supplier agreements rather than in algebraic expressions, making the quantitative analysis hard to apply in practice [44].
2) For those very few reported mathematical models of the QOS, they are defined in terms of event-based, not status-based variables and parameters. As a result, a value of the QOS can only represent system reliability measured in a specific failure scenario rather than a good prediction of system reliability in an operating condition. Since the failure scenarios are normally not known at the earliest design stage, these QOS models turn out not to be applicable for SBD purposes [25].
3) Although the determinant factors of the QOS have been well-acknowledged as the generator sizing and CONOPS [44], these factors have not yet been incorporated in the QOS optimization problems.

There are two main methods proposed in literature to determine the QOS of a power generation plant:

The first method involves time-domain analyses, which directly measures certain system state values (e.g., the frequency and bus voltage at certain nodes, the rotor angle of generators, the angle difference between certain buses) to see if any violation occurs for the predefined contingencies [45]. This method can only provide qualitative analysis of the QOS with two states—QOS survival or QOS failure. Therefore, this method is more suitable to be used to generate the conditions for validating the CONOPS obtained

by other means, but not to optimize the CONOPS. In addition, this method requires too many system details that are, unfortunately, not accessible at the earliest design stage.

The second method employs failure and repair rates of generating units to indirectly quantify the QOS. This method provides more flexibility to evaluate the QOS: 1) it allows one to study the individual effect of each generating unit on the QOS of a system; 2) it allows one to estimate the QOS of a system at the preferred level of accuracy by just considering the generating units of interest. This method does not rely on the time-domain analyses; instead, it capitalizes on the accurate estimation of the failure and repair rates of the generating units involved in the system.

Here are the summary of the several important algebraic forms of the QOS metric proposed in literature. Doerry [25] defines the QOS in terms of three factors, namely, mean-time-between-failure (MTBF) values of power components, mission duration, and power interruption events. A QOS failure is defined to occur if a given mission segment cannot be fulfilled in the face of a set of predefined power interruption events during a specified duration. A QOS failure is only regarded to be caused by aggregate component failures; hence a QOS failure rate is directly related to the MTBF values of components. By definition, the QOS failure rate of each component is weighted by the duration of mission segment and that of component online status, as expressed in (3); the weight is calculated in (4). The QOS failure rate of a system is then calculated as the summation of the weighted QOS failure rates of all the components, as shown in (5). The QOS metric is finally defined as the reciprocal of the QOS failure rate of a system, as expressed in (6). This definition of QOS metric is straightforward to comprehend; however, as the author points out, it is difficult to predetermine power interruption events at a high confidence

level because these events can be associated with multiple possibilities and random factors, such as operating-based wear, glitches due to long time operating out of allowable ranges, and human misapplications. In addition, it is costly to test the QOS failure for each failure event (i.e., the time-domain simulation and detailed information of a system design are required).

$$r_{failure(n)} = \frac{f_{qos(n)}}{r_{c(n)}} \tag{3}$$

$$f_{qos(n)} = \sum_{k=1}^{K} f_{om(k)} p_{om(k,\mathrm{n})} q_{om(k,pi_n[j])} \tag{4}$$

$$r_{failure} = \sum_{n=1}^{N} r_{failure(n)} \tag{5}$$

$$QOS = \frac{1}{r_{failure}} \tag{6}$$

For more comprehensive design purposes, Doerry updates the formula of the QOS in [44]. The concept of operational ability, which is defined in terms of three factors of a power component, namely, MTBF, mean-time-to-repair (MTTR), and mean-logistics-delay-time (MLDT), is introduced to evaluate the probability of multiple simultaneous failures, as expressed in (7). This paper points out the necessity to examine multiple simultaneous failures with an A_o less than about 0.995. However, the author does not provide a complete method to estimate the MTTR and MLDT, making this QOS metric difficult for calculation.

$$A_o = \frac{MTBF}{MTBF + MTTR + MLDT} \tag{7}$$

Zapata, et al. [27] measure the QOS in terms of two indices, namely, expected operational outage rate and expected operational unavailability. These indices are

expressed in terms of component failure rates, preventive maintenance rates, false component operating rates, and outage rates due to backup actions. Except for component failure rates, all of the other rates are given as constant parameters, averaged from the historical database. The definition of a QOS failure varies based on the specific system topologies, but the QOS is computed following the same procedures of sequential Monte Carlo simulation. In some literature, the QOS can also be estimated in terms of the capability that a plant can produce the power to the end-use loads at some acceptable levels [28]-[32]. This capability can be evaluated in several measures including loss-of-load probability, loss-of-load duration, and loss-of-energy amount. This measure of the QOS is usually based on the observed or historical data of reliability (i.e., MTBF) and maintainability (i.e., MTTR) of power plant components.

3.1.3. Calculating Failure and Repair Rates of a Generating Unit

Despite the diverse forms of the QOS metric proposed for the second method explained in Section 3.1.2, the factors in common are the failure and repair rates of power plant components. The failure rate of a power plant component is observed to be affected by several factors related to both controllable CONOPS factors (e.g., loading conditions, switching frequency, frequency of setpoint changes) and uncontrollable factors (e.g., aging effect, wear-and-tear, fatigue failure, maintenance schedules, random contingencies). In contrast, the repair rate of a component is more affected by uncontrollable factors (e.g., environmental conditions, nature of failure, diagnostic ability, equipment, repair resources, skills of personnel). At the moment, it is still a problem for manufacturers to estimate or predict these two rates at an acceptable cost [25]. In traditional design practices, designers usually treat failure and repair rates of a power plant component to be constant for universal operating environments and design

scenarios. Their values are given as the averaged value of the inspected historical data of similar products. As a result, one may be surprised to see that the system design appearing to offer a high-level QOS by theoretical analyses behaves far below the expectations during real life operations [28]. In order to make more reliable acquisition decisions, one needs an effective approach at the earliest stage to model dynamic failure and repair rates like those observed from daily operations. Several condition-dependent failure rate (CDFR) models and condition-dependent repair duration (CDRD) models are proposed in recent publications and summarized as follows:

The impact of the setpoint of an electric machine on its failure rate is revealed from the mechanical point of view in [33]. Considering a generation plant with a fixed frequency and sufficient thermal cooling capabilities, the loading condition of each generating unit (i.e., the generated power) is implied to be the most significant factor affecting its dynamic failure rate. Increasing the generated power causes greater torque exerted on the bearings and reduces the fatigue life. This relationship is specified in mathematical expressions in [34]. The author introduces two different CDFR models for a generating unit in terms of its active instantaneous load, P_L. One CDFR model is expressed in (8) as a natural exponential function, which is also employed for the survival analysis in biostatics. The coefficients, λ_o and β, can be determined from a few tested points by data fitting techniques. The other CDFR model is expressed in (9) based on some reference loading points. The parameter λ_C and $P_{L,C}$ are the reference failure rate and the corresponding load, respectively. The parameter y denotes the load dependent exponent. Both models need to capitalize on the historical failure database to determine the parameter values.

$$\lambda(t) = \lambda_o e^{\beta \cdot P_L(t)} \tag{8}$$

$$\lambda(t) = \lambda_C \left[\frac{P_L(t)}{P_{L,C}} \right]^y \tag{9}$$

The uncontrollable factors affecting failure and repair rates are addressed by means of various distribution models and stochastic simulation methods in previous literature. Zapata et al. [27] employ the stochastic point processes (SPP) to model the time-varying failure and repair rates of a generating unit. By evaluating the tendency of randomly generated failure events to change during a period, the appropriate SPP model can be selected from six options. Garazas et al. [28] use a two-parameter Weibull probability distribution (cumulative distribution function) to characterize wear-out and fatigue failures of a gas turbine and adopts a lognormal distribution to derive the repair rate, as expressed in (10) and (11), respectively. These two equations represent statistical reliability and maintainability of a system at time *t*. In (10), the parameters β and η denote the shape parameter and characteristic life of the Weibull distribution, respectively. In (11), the parameters γ and σ denote the mean value and standard deviation of the lognormal distribution, respectively; the function $\Phi(\cdot)$ denotes standard normal distribution cumulative function. These parameters need to be determined based on the historical data.

$$\lambda = 1 - e^{-\left(\frac{t}{\eta}\right)^{\beta}} \tag{10}$$

$$\mu = \Phi\left(\frac{\ln t - \gamma}{\sigma} \right) \tag{11}$$

Wu et al. [23] express the dynamic failure and repair rates in the corresponding bounded ranges. These rates are regarded as the design variables that can be optimized. However, the physical meaning of these optimal rates is not presented.

3.2. Optimization Algorithms

An effective optimization algorithm is prerequisite to solving the co-optimization problem of the CONOPS. The co-optimization problem contains both real and binary variables in the objective functions and constraints. The objective functions are non-convex and thus cannot be resolved by conventional gradient-based methods. In contrast, heuristic techniques are more suitable to be employed.

Heuristic optimization methods, most of which belong to the class of the population-based evolutionary algorithm, do not impose the requirements that systems must be differentiable or continuous; do not limit assumptions regarding the forms or characteristics of the objective functions and constraints; present less likelihood for solutions to be trapped on local optima [51]. However, different heuristic algorithms present different advantages in favor of specific situations.

Popular heuristic methods used for single objective optimization problems include the evolutionary programming (EP) [52], genetic algorithm (GA) [53], simulated annealing (SA) [53], bio-geography based optimization (BBO), gravitational search intelligence (GSI) [54], Hopfield neural networks (HNN) [55], particle swarm optimization (PSO) [56], and various hybrid algorithms [56]-[59]. The limits of these algorithms are summarized as follows: GA, EP, and EA have the common problem that they always fail to guarantee the global optimal solutions compared to the other evolutionary algorithms. Apart from that, GA suffers from the complicated encoding and

decoding schemes and presents degraded efficiency in applications where design parameters are highly correlated; EP converges to near-optimum rather slowly due to its mutation and selection schemes, and can get trapped in sub-optimal states for large scale complex problems; SA is very time-consuming and has difficulties to find the appropriate annealing schedule to account for distinct problems. BBO is typically time-consuming in tuning the parameters, especially for complex systems; its parameters are also problem-specific. The performance of GSI starts degrading significantly in contrast to the other methods when the number of iterations is extended to be large, typically >1000. HNN is more suitable to solve piecewise nonlinear functions but may suffer from excessive numerical iterations, resulting in huge calculations for training the neural network.

In contrast, PSO outperforms all these algorithms in several aspects when tested with the benchmark problems [60]. PSO retains the advantages of the population-based algorithms, being less susceptible to getting trapped in local minima. It balances the global and local exploration such that it converges to the global optimum in shorter time. It is easy to implement with basic mathematics and a limited number of parameters. Its performance does not depend on a user-defined initial point where the simulation iteration starts. Additionally, it can be improved through integrating with other optimization techniques to solve a wide range of problems (e.g., mixed integer problems, multi-objective problems, objective function with stochastic nature, problems with time-sensitive global optima). Hence, we will pick PSO as the algorithm prototype to be improved for solving our co-optimization problem.

The previously reported versions of single-objective PSO (SOPSO) suffer from an ineffective constraint handling capability and premature convergence when dealing with

constrained mixed-integer problems. The previously reported versions of multi-objective PSO (MOPSO) also bear the same problem; even worse, when the constraints contain the mixed integers like our co-optimization problem, current MOPSOs are even unable to converge to a valid solution. Therefore, it is essential to develop an improved SOPSO and MOPSO with better capabilities to deal with mixed-integer variables and avoid premature convergence. In this dissertation, we apply SOPSO to generate the global optimal CONOPS with respect to fuel consumption and the QOS independently. The outcomes are used as the reference to demonstrate the efficacy of the improved MOPSO. The conclusions drawn via these two methods are compared to testify the design improvement of SBD accounting for the optimization of the CONOPS.

CHAPTER 4

BACKGROUND ON MICRO-GRID POWER GENERATION AND DISTRIBUTION SYSTEMS

4.1. ELECTRIC ARCHITECTURE OF MICRO-GRID POWER GENERATION AND DISTRIBUTION SYSTEMS

This dissertation adopts the next generation integrated power system (NGIPS) [7] as the architecture prototype of micro-grid power generation and distribution systems, including those that do not contain electric propulsions. The NGIPS is configured as a zonal electrical distribution system (ZEDS) that represents a simpler, cheaper, and better productivity of commodities (e.g., electricity, chill water) than other system architecture types, such as traditional radial distribution systems or locally producing the commodities [61]. In addition, ZEDSs provide considerable improvement for three measures, namely, survivability, the QOS, and the cost [62].

The NGIPS has three popular types of power generating architecture, namely, medium voltage ac (MVAC), high frequency ac (HFAC), and medium voltage dc (MVDC). Although the details of power interfaces differ from each of them, they all adhere to the same concept of ZEDS and the same types of power modules, as shown in Figure 4.1.

The standard NGIPS power modules are introduced as follows:

- Power Generation Module (PGM): the power source that converts the fuel to electric power. A PGM is normally composed of a mechanical power source

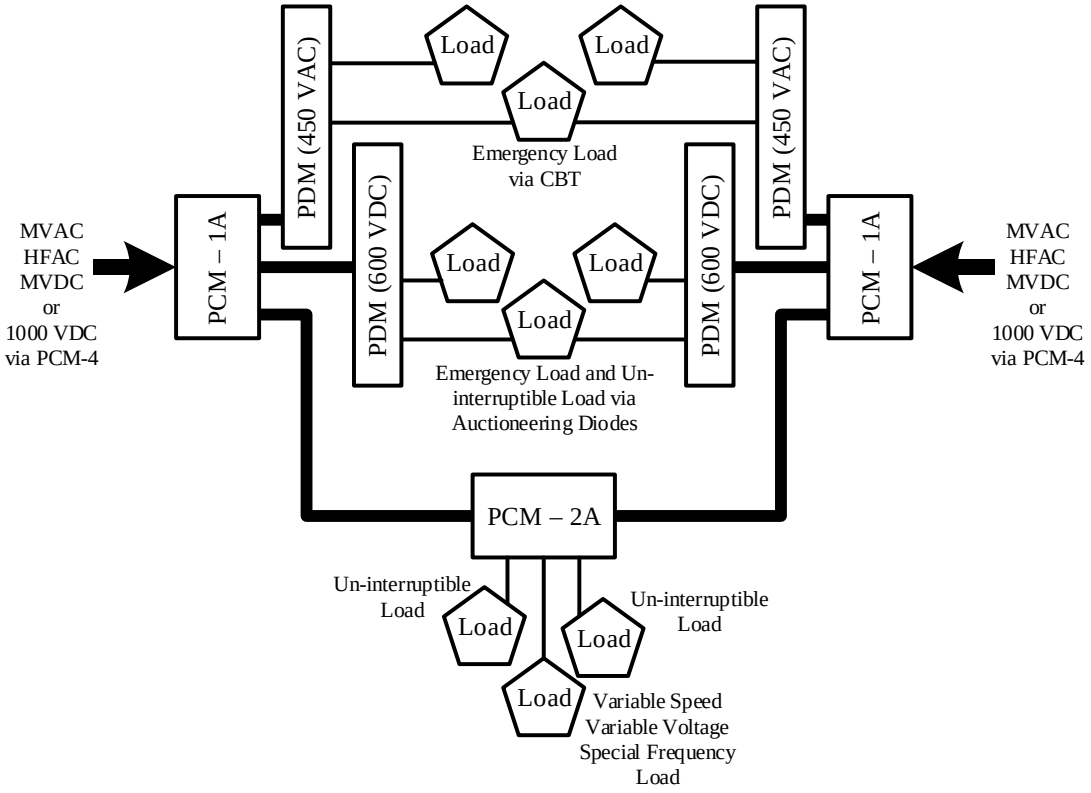

Figure 4.1 Integrated fight thru power zonal electrical distribution architecture (NAVSEA 2007) [7]

(e.g., a prime mover such as a gas turbine or a diesel engine) and an electric generator (e.g., a synchronous machine).

- Propulsion Motor Module (PMM): the load type that converts electric power into the propelling force of a ship, which is the major power consumer at the most of time.
- Power Distribution Module (PDM): the essential elements, including switchgears and cabling, that transport electric power between functional elements.
- Power Conversion Module (PCM): the functional elements, including power transformers and power electronics-based converters, that convert electric power from one type (e.g., voltage, frequency) to another.

- Energy Storage Module (ESM): the storage elements [63], such as batteries, flywheels, and superconducting magnetic energy storage (SMES) etc., that act as a buffer to prevent power disturbances from propagating to loads.
- Power Load Module (PLM): the load that consumes either ac or dc electric power.

In a typical ZEDS, PGMs are connected to the primary distribution bus either on the port or starboard side. After closing all switchgears on the primary buses, the split bus on the port and starboard side can be coupled together to form a big ring bus. PCMs may be necessary between some PGMs and the primary buses depending on the output voltage levels of the PGMs, the bus voltage rating, and the bus voltage type. For the ac distribution architecture, PMMs are the AC loads directly connected to the primary ac buses on either the port or starboard side. In contrast, for the dc distribution architecture, a PMM is usually connected to an appropriate PGM directly (sometimes appropriate transformers may be needed) in place of the power transmission buses.

The zonal load architecture of a ZEDS can be designed in various topologies reflecting compromises between survivability, the QOS, and the cost. For most combatants, the reasonable quantity of the zone is about six to seven, resulting in each zone being roughly fifteen percent of the ship's length [62]. Depending on the bus voltage type, ac or dc, PCMs are employed between the primary distribution buses and in-zone distribution buses. For the latter, one may connect in-zone PGMs and/or in-zone ESMs to improve survivability and the QOS. End-use PLMs are supported with the power from the in-zone distribution buses through necessary PCMs.

In addition to the typical ZEDS with the ring bus topology, several other types of architecture can also be possible [62]: The single bus architecture with zonal generation is generally advantageous if ESMs are not cost effective. This is because single bus architecture involves in-zone PGMs for improving survivability and the QOS. The dual bus architecture with primary bus level storage or zonal level storage is considered for improving service continuity, but it has difficulties in determining the optimal size, location, and control strategies of ESMs. To further enhance survivability from the damage of the loss of primary buses, either integral segmentation or independent segmentation is introduced for the duel bus architecture to pair with zonal ESMs. The hybrid bus architecture is another improved version of the single bus architecture used to better support the critical loads. There are also several versions of the multi-bus system with the advantage of minimizing the number of primary bus distribution nodes, which typically consist of the medium/high voltage switchboard and transformer, both usually large, heavy, and costly. The breaker-and-a-half distribution topology is known to provide more reliability overall than the ring bus topology with a similar ease of scalability, but it demands a greater number of circuit breakers and more sophisticated design of the locations of sources and loads.

Since different types and quantities of power modules are required for different ZEDSs, the optimization problem of the CONOPS developed according to one ZEDS type cannot fit all situations. If a type of NGIPS architecture contains separate primary distribution buses, the optimality of the overall system will be determined by the combination of individual optimal performance of each bus. The minimum fuel consumption and the maximum QOS of the system design are the sum of those of each

bus, respectively. This dissertation makes two assumptions to all system designs: 1) since the efficiency of a PGM is far lower than that of the other types of power system modules, we assume that the latter have fixed power efficiency ratios despite their operating power levels; 2) we assume that all the essential information characterizing a system concept can be easily secured by S3D and used by the optimization solver. The second assumption facilitates MATLAB's automatic selection of the appropriate function of the optimization problem for the ZEDS architecture under study. The "essential" information should include the coupling relationship among modules and between modules and buses, the specifications of PGMs, the operating statuses of PMMs and PLMs, and so on.

4.2. CONTROL ARCHITECTURE

In traditional design practices, designers commonly carry out sequential design procedures to first arbitrarily select a preferred design alternative, and then define controls to fit. Following this method, the hardware cost may be always minimized, but the system performance can hardly achieve or even get close to the global optimum [66]. Our simulation results [64][65] indicate that integrating appropriate control design (referred to as the converter controls for power electronic applications and the equipment setpoint determination for power system designs) with system hardware design (referred to as the circuit components for power electronic applications and the power system components for power system designs) at the earliest design stage can be an effective method to identify the hardware with preferred tradeoff between the cost and system performance quality or with preferred tradeoffs among multiple performance metrics.

However, this method brings up two challenges: For different types of system architecture, how to quickly identify the control variables that should be considered for studying these tradeoffs? How to impose the formulation method of the co-optimization problem to generic system architecture?

The development of the system control architecture can be a good solution to complete the first challenge. IEEE Std 1676 and Std P1826/D4 are two examples of the control architecture. Targeting different levels, namely, the power electronic applications and the ZEDS, they divide the control functions of corresponding system application into standard hierarchical layers according to the temporal responses. Each control function layer identifies the relevant modules and their design variables (i.e., control variables for power electronic devices, setpoint variables for power system components) common to all types of system architecture. Accordingly, the second challenge can be completed by developing an optimization structure in terms of these design variables defined in the control architecture. Considering the commonality of the design variables, a standard formulation structure of the optimization problems described via the design variables should also be possible to impose on a generic type of system architecture.

Therefore, for our concept evaluation method, as long as we have the optimization structure for the primary power generation and distribution system level, we can directly apply it to any given system concept to optimize the CONOPS for each design alterative. Otherwise, one has to repeat the time-consuming problem formulation process for different system concepts one at a time. However, either the control architecture or the optimization structure has not been hitherto discussed for this level. To solve this problem, we need to look into the development of the control architecture for the lower

level applications and apply the same method to develop the control architecture and optimization architecture for the primary power generation and distribution system level.

Despite different system applications, the overall control of an electric system is accomplished by arranging individual control functions and synthesizing their outcomes to yield a desirable control performance. The control functions of a power system application should be classified based on two principles—functionality and temporal response. Each control function is composed of a group of operations within a similar timing range. In the control architecture, each hierarchical layer contains the standard rudimentary control functions integrated based on their temporal responses. In order to accomplish a desired mission assigned to the layer, these rudimentary control functions have to be realized by applying appropriate operating strategies to the standard modules. Normally, the operating strategy of a module (except for data processor modules) can be optimized according to a certain performance metric. However, when the operating strategies of several modules share some design variables (e.g., hardware parameters, control variables), or the operating strategy of a module is intended to achieve multiple control objectives, a multi-objective optimization method needs to be applied to evaluate the performance tradeoffs in either case. In addition, control architecture also defines the standard data that need to be processed between and within hierarchical layers, and their required speed range, facilitating the development of the optimization problem formulation structure.

The control architecture for power electronic applications and that for ZEDSs have been reported in IEEE Std 1676 [46] and Std P1826/D4 [47], respectively. The former mainly focuses on the functional analysis in time domain. Its design variables are

the control signals used to implement the duties of a power electronic system and adjust the behaviors of converters. The latter, in contrast, focuses on the functional analysis in power domain because the purpose of this standard is to modularize a system for rigorous assessment mechanism, interface control management, and proactive conformance testing. Its design variables are setpoint variables used to determine the operating status of the ZEDS components to fulfill a given mission. Next, we will review these two standards in detail.

4.2.1. IEEE Std 1676—IEEE Guide For Control Architecture for High Power Electronics (1 MW and Greater) Used in Electric Power Transmission and Distribution Systems

This document describes the control architecture for broad power electronic applications, whether or not the power electronics is PEBB-based. There are a total of five control layers partitioned from a power electronic system configuration, as shown in Figure 4.2.

- System Control Layer (Sys): all functions involved in the determination of system missions and duties of power electronic systems.
- Application Control Layer (App): all functions involved in the operation of power electronic systems in order to meet the missions determined by the Sys.
- Converter Control Layer (Cnv): all functions that enable the App to perform its mission by implementing many of the functions common to various converters.
- Switching Control Layer (Swt): all functions that enable power electronics to behave as a switch-mode controlled source including modulation control and pulse generation.

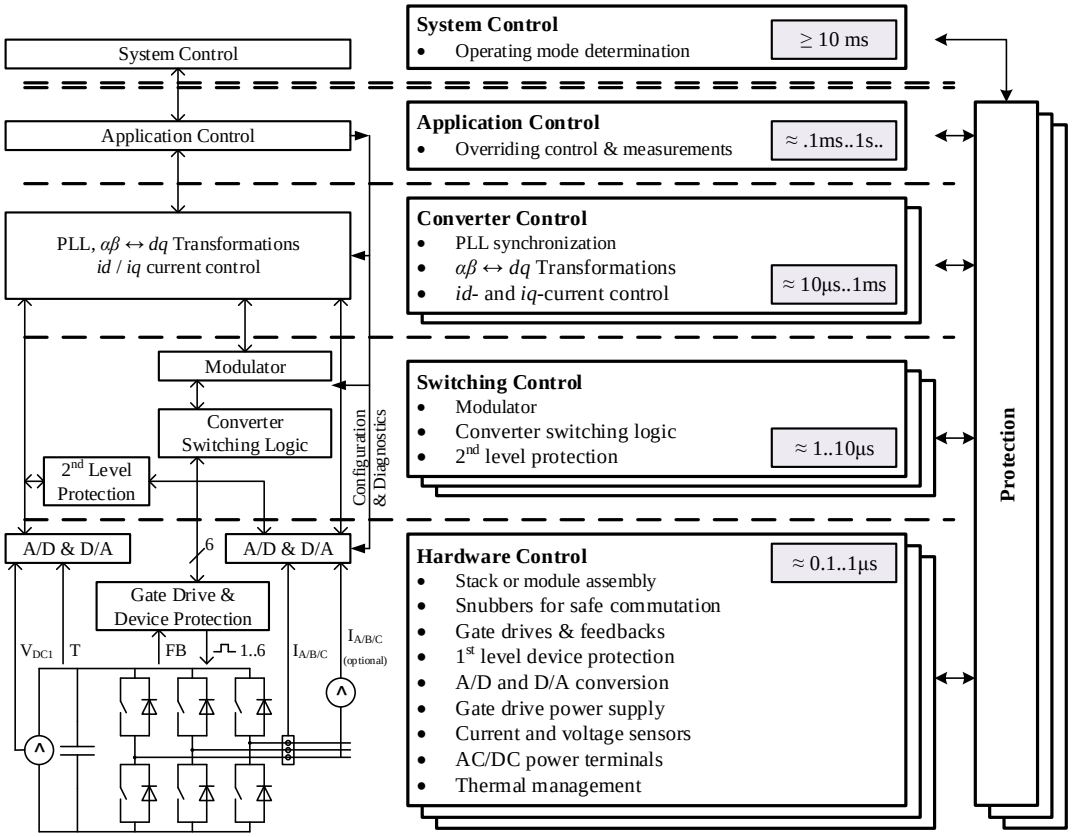

Figure 4.2 Control Architecture for PEBB-based electronics with modifications

- Hardware Control Layer (Hwr): all functions that manage everything specific to the power devices; it may consist of multiple modules depending on the power requirements.

For most power electronic systems, temporal and functional distributions naturally occur at the same boundaries. From the top layer (Sys) to the bottom (Hwr), the timing of control signals is decreasing correspondingly from above 10ms to 0.1µs. The interface requirements are defined based on the temporal partitioning. Signals on the interfaces are classified into three categories, namely, control and protection signals, state signals, and measurement signals, and their transmission logics are also defined.

Following the control architecture, any power electronic system can be consistently expressed with the standard integrated functional diagrams. In [65], we have already demonstrated the benefits of using this control architecture to optimize the converter control layer through an example of buck converter design. Instead of choosing hardware parameters, namely, inductance and capacitance, and then designing the feedback control system in traditional practices, we co-optimize the parameters of hardware and PI controller (i.e., K_i and K_p) defined in this layer. As a result, the converter performance metrics (i.e., inductor current ratio and output voltage overshoot) are improved by 14%.

4.2.2. IEEE P1826/D4—Draft Standard for Power Electronics Open System Interfaces in Zonal Electrical Distribution Systems Rated Above 100 kW [70]

This document is recently drafted to define the control architecture for the ZEDSs with power electronic interfaces between the zones. Specifically, this standard extends the control function described in the Sys level of IEEE Std 1676 into three detailed control functions at the system level. This document applies the Open System concepts to the ZEDSs and identifies the Open System interfaces, facilitating the plug-and-play operability of components. It also formulates specific interface requirements that can be universally applied to maintain total power system performance and efficiency.

The partitioned control layers and power electronic interfaces are shown in Figure 4.3. The basic control functions and partitioning criteria of each layer are explained as follows:

- Multi-Zone Control Layer (Mzn): all functions that are involved in the operation of the overall system mission, and in the allocation of duties to each

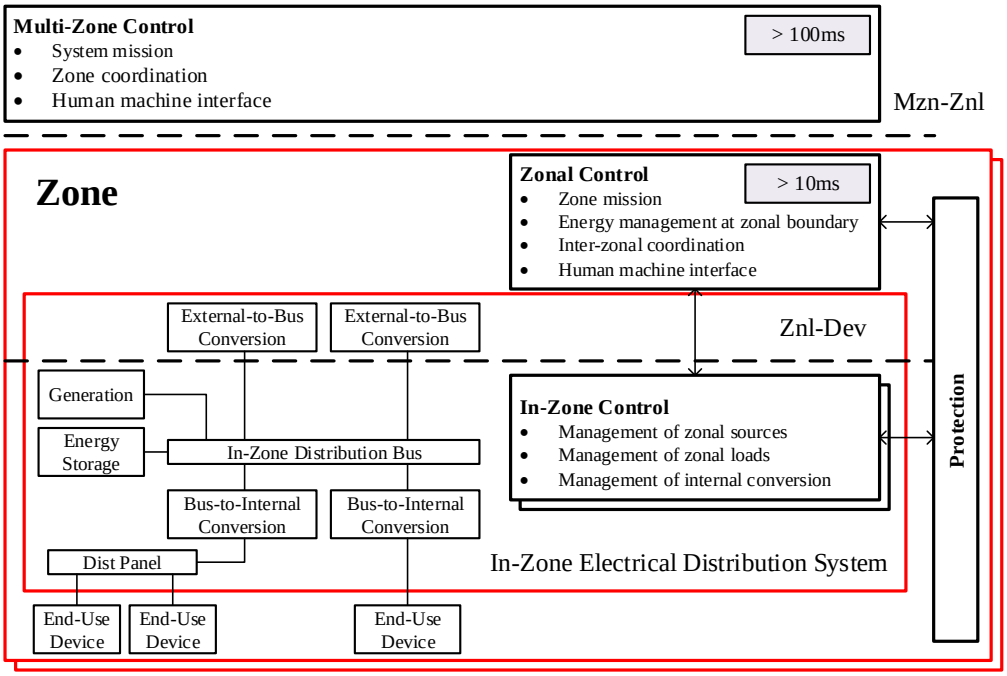

Figure 4.3 Control Architecture for zonal electrical distribution systems with power electronics open system interfaces

zone or to a group of zones supporting that mission. The following control functionalities are required at minimum:

- Determine and set the operating state of a zone.
- Coordinate zones, when applicable.
- Receive health/status from, and provide control commands to, zonal level control.
- Provide a human-machine interface.

▪ Zonal Control Layer (Znl): all functions that are involved in the determination of zone missions and the method of coordination of In-Zone controls. The following control functionalities are required at minimum:

- Provide control of energy flow at zonal interface.
- Provide health/status to, and receive control commands from, the Mzn.

- Provide coordination for fault detection, isolation, and reconfiguration.
- Provide in-zone coordinate, when applicable.
- Provide a human-machine interface to detect and handle equipment problems at zonal interface.

- In-Zone Control Layer (Izn): all functions that are involved in performing zone missions and duties of power electronics systems. The following control functionalities are required at minimum:
  - Provide autonomous control of in-zone elements, configuration, and faults.
  - Provide health/status to, and receive control commands from, the Znl.
  - Provide power flow management in accordance with power allocations provided by the Znl.
  - Provide a human-machine interface to detect and handle problems of in-zone equipment.
  - Respond to changing load conditions.

The communications between these control functions are realized by the appropriate designs of the power electronics applications at the layer interfaces, which accommodate the timing defined in Figure 4.2. As we use this ZEDS control structure for the system level optimization design, we always assume that the derived control strategies can be correctly implemented at the power electronics level.

Depending on the locations where modules are connected to the ZEDS, some of the standard power modules explained in Section 4.2.1 are further classified in IEEE P1826/D4. PGMs are categorized into external PGMs and in-zone PGMs. Operation of the former is first determined by a given mission at the highest power-generating level, as

this dissertation is mainly focusing on. Then the derived control strategy is notified to the Mzn layer for coordinating zones. The latter are controlled through optimizing the performance metrics associated with the Izn layer, providing an optional strategy for protecting the in-zone QOS from faults occurring at the top layers. PCMs are categorized into external-to-bus PCMs and bus-to-internal PCMs. Operating status of the former is determined in the Znl layer to convert the power originated from external PGMs to the type and quality desired by the main in-zone PDMs. The operating status of the latter is determined in the Izn layer to convert the power from the type and quality of in-zone PDMs to those desired by end-use PLMs. (Specific setpoints of PCMs are calculated by applying the control structure in IEEE Std 1676.) The power distribution panel in Figure 4.3 refers to the in-zone PDMs, which provide the appropriate type of power to end-use PLMs when the power type of end-use PLMs does not match the output of the main in-zone PDMs (e.g., dc loads for an ac type of power architecture).

CHAPTER 5

DEVELOPMENT OF OPTIMIZATION ALGORITHM

5.1. ORIGINAL DEFINITION OF PARTICLE SWARM OPTIMIZATION

The original PSO was developed to perform as a flexible population-based stochastic search method [67]. Compared with the other evolutionary algorithms, PSO is especially advantageous to combine and balance the global and local exploration capacities. The particle populations in PSO are able to heuristically converge to the global optimum by learning from their own best previous experiences and by communicating with each other to learn the hitherto best experience of the overall population. The integration of the global exploration and local exploitation by PSO is expressed in (12) in terms of four groups of variables: the current position of each particle, x_d; the current velocity of each particle, v_d; the hitherto best position found by all particles (known as the global best, x_{gbest}); the best history position of the individual particle (known as the personal best, x_{pbest}):

$$v_{id}(t+1) = w \cdot v_{id}(t) + c_1 \cdot U(0,1) \cdot \left[x_{gbest} - x_{id}(t) \right] + c_2 \cdot U(0,1) \cdot \left[x_{pbest} - x_{id}(t) \right] \quad (12)$$

$$x_{id}(t+1) = x_{id}(t) + K \cdot v_{id}(t+1) \quad (13)$$

$$K = \frac{2}{\left| 2 - \varphi - \sqrt{\varphi^2 - 4\varphi} \right|}, \quad \text{where} \quad \varphi = c_1 + c_2 > 4 \quad (14)$$

$$w = \frac{w_{min} - w_{max}}{iter_{max}} \times t + w_{max} \quad (15)$$

where K and w are the constriction factor and the inertia weight, respectively, introduced to improve the searching performance and convergence; c_1 and c_2 are the acceleration factors of the population, reflecting the influence degree of the global best and personal best, respectively; $U(0,1)$ is a uniformly distributed number from the interval (0,1); i denotes each individual particle in the population; t is the current iteration number. Usually, w is a linearly decreasing value from w_{max} to w_{min} during the maximum allowed number of iterations $iter_{max}$ for faster convergence. v_{id} is limited by its maximum value v_{idmax}, which is usually set to be the maximum dynamic range of the corresponding variable.

The original PSO is essentially developed in continuous space without the capability to deal with constraints and binary variables. Unfortunately, the optimization problem of the CONOPS for micro-grid power systems involves binary variables in both objective function and constraints. Therefore, we develop two new versions of PSO to support our work, one for single-objective and one for multi-objective optimization problem. These two versions successfully present performance improvements beyond the current PSOs in two aspects when dealing with the problems containing binary variables: one is the enhanced capability of effectively avoiding premature convergence; the other is the improved capability of more accurately and reliably locating the global optimum.

5.2. Improvement of Single-Objective Particle Swarm Optimization

5.2.1. Handling Method for Discrete Binary Variables

For handling discrete binary variables, we employ the method to let SOPSO interpret the particle velocities as the probabilities of changing the binary variables from one state to the other (1 or 0) via (16) [68].

$$u_{id} = \begin{cases} 1 & U(0,1) < S(v_{id}) \\ 0 & U(0,1) \geq S(v_{id}) \end{cases}, \quad S(v_{id}) = \frac{1}{1+e^{-v_{id}}} \tag{16}$$

where $S(v_{id})$ is a sigmoid limiting transformation to limit the velocity-based probability to the interval (0,1). Then the maximum allowable velocity v_{idmax} is interpreted as the limit of probability that u_{id} will be 1 or 0.

5.2.2. Constraint Handling Scheme

There are four constraint handling methods— *preserving feasibility method*, *repair algorithm*, *rejecting approach* and *penalty function*—commonly applied to tackle the equality and inequality constraints of a single-objective optimization problem. *Preserving feasibility method* always keeps the initial point and intermediate points during iteration in the feasible space by using certain updating scheme, such as saturation masking for bounded variables and embedded equality handling in coding [69]. However, the variable updating scheme is highly problem-dependent, especially suitable for solving the easy constraint expressions. When the constraints are nonlinear, or comprise polynomials and discrete expressions, the coding of the variable updating scheme becomes very challenging. *Repair algorithm* method is also problem-specific, that is, restoring feasibility might be as difficult as solving the optimization problem itself. *Rejecting approach method* evaluates every intermediate solution in all constraints and then rejects those with any constraint violation. Hence, applying this method consumes remarkable calculation time. In addition, as the number of variables increases, the heuristic computation mechanism needs to be largely improved in order to be capable of generating the feasible solutions [70].

In contrast, *penalty function* directly integrates the constraints with the objective function through certain weights. Accordingly, the violation of constraints can be

straightforwardly reflected as an unacceptably large value added to the objective function [71]. Penalty function is also more in favor of the heuristic optimization process of PSO because it is able to quantify a constraint violation in magnitude; in contrast, the other constraint handling schemes only treat a constraint violation as a discrete state, either feasible or infeasible. Specifically, for a common constrained minimization problem in (17), the corresponding unconstrained objective function containing the penalty functions can be expressed in (18). Equation (19) and (20) provide the effective forms of the penalty terms for common use.

$$\begin{aligned} &\min\ f(x) \quad \text{subject to} \\ &g_j(x) \le 0, \qquad j = 1, 2, \cdots, n \\ &h_j(x) = 0, \qquad j = n+1, n+2, \cdots, m \end{aligned} \tag{17}$$

$$F(x) = f(x) + \sum_{j=1}^{m} k_j \times H_j(x) \tag{18}$$

$$k_j = (C \cdot t)^{\alpha}, \qquad H_j(x) = \sum_{j=1}^{m} D_j^{\beta}(x) \tag{19}$$

$$\begin{aligned} D_j(x) &= max\{0, g_j(x)\}, \qquad j = 1, 2, \cdots, n \\ D_j(x) &= max\{0, |h_j(x)|\}, \qquad j = n+1, n+2, \cdots, m \end{aligned} \tag{20}$$

where $x = [x_1, x_2, \cdots, x_p]$ is the vector with p input variables; $f(x)$ is the original objective function subjected to n equality and $(m\text{-}n)$ inequality constraints; k_j and $H_j(x)$ are the penalty weight and the penalty factor of constraint j, respectively; C is a constant denoting the initial penalty effect; α and β are the constants defining the form of the penalty function.

However, the traditional penalty functions have some noticeable disadvantages with parameter selection, that is, a high value of the penalty term will result in easily

getting trapped to the local optimum while a low value might lead to non-convergence of the objective function. To address this problem, four forms of dynamic penalty function has been reported in [70][71], as expressed in (21). Since there is no clear conclusion on which form outperforms the others for a given optimization problem, we incorporate all the four forms with our developed SOPSO to facilitate one's testing on his specific problems.

$$\begin{cases} P(\alpha,\beta): \quad P(1,1), P(1,2), P(2,2) \\ \text{Multi-stage:} \qquad k_j = \sqrt{t} \quad or \quad t\sqrt{t}, \quad H_j = \sum_{j=1}^{m} \theta_j \cdot D_j^{\gamma_j} \end{cases}$$

$$\text{where } \theta_j = \begin{cases} 10 & D_j \in [0, 0.001) \\ 20 & D_j \in [0.001, 0.1] \\ 100 & D_j \in (0.1, 1] \\ 300 & D_j \in (1, \infty) \end{cases}, \quad \gamma_j = \begin{cases} 1 & D_j \in [0,1) \\ 2 & or\, else \end{cases} \tag{21}$$

It is worth mentioning that the multi-stage penalty function normally outperforms the other dynamic penalty functions in most complicated problems, including our optimization problem. One of the main reasons is the adoption of the varied penalty factors for different levels of constraint violation. This "adaptive" learning process is advantageous to avoid the difficulties of choosing the appropriate penalty factor for different problems, and to speed convergence to the optimum. The other main reason is the application of a more strict screening process of the obtained particles along the training process. The penalty weight increases at each iteration step, creating more chances for the particles to explore the whole searching space at the beginning but to hold the feasible solutions later on. Therefore, the multi-stage penalty function is always automatically taken as the first choice of the constraint handling method when our developed SOPSO is applied.

5.2.3. The Mutation Operator and Archive Vector

In order to prevent premature convergence due to a limited number of feasible points in the binary space, we introduce a "mutation" operator and an "archive" vector to the searching process so that the particles are able to be released from the local optima and self-initiated for a new searching process.

We assign the probability of mutation w_1 to a random number of particles for enhancing their global exploration capabilities. If g_{best} fails to improve after s iterations, the velocities of some arbitrarily selected real variables will be set to a random value within their velocity bounds, and the states of certain binary variables will be reversed (i.e., "1" changed to "0" and "0" changed to "1"), as shown in (22).

$$\begin{cases} \text{real:} & v_{pid}(t+1) = U(0,1)\cdot V_{pidmax} \quad U_{pi}(0,1) \le w_1 \\ \text{binary:} & x_{pid}(t+1) \Rightarrow \text{reverse} \quad U_{pi}(0,1) \le w_1 \end{cases} \tag{22}$$

where v_{pid} denotes the particle i's velocity of design variable x_p; U_{pi} (0,1) is a random number in (0,1) for the particle i of x_p.

The number of particles that should be considered for mutation is controlled by a function of influence rate, as expressed in (23) [64]. This influence rate and the chance for each selected particle to be mutated are all proportional to the iteration number of training particles. The pseudocode of the particle mutation process based on the influence rate is developed in Figure 5.1.

$$influence\ rate = 1 - e^{-\frac{w_i}{w_{\max}}} \tag{23}$$

where w_i is the instantaneous inertia weight in the current iteration loop; w_{max} is the initial value of the inertia weight as defined in (15).

```
for   i = 1 : training iteration
   ...
   Calculate the new velocities of particles;
   % mutation starts
   Give a static mutation rate, m;
   for   j = 1 : the population of particles
      Generate a random value s = rand(0, 1);
      if   s <= influence rate
         Randomly select a binary variable of the
particle;
         Generate a random value t = rand(0, 1);
         if   t <= m
            Change the state of the binary variable;
         end
      end
   end
   % mutation ends
   Update the new velocities of particles;
   ...
end
```

Figure 5.1 Pseudocode of the particle mutation process based on the influence rate

Apart from the mutation operator, we also introduce a method to automatically create the opportunities for the trapped particles to escape from the local optima. It is like introducing a "ranger" patrolling around during the optimization process. The duty of the ranger is to look for the particles that fail to update in a certain number of steps, forcibly relocate them, and reactivate a new search. However, since there is no effective method to distinguish a local optimum from the global optimum, it is possible that the particles converge to the global optimum may also be relocated. To address this concern, we create an archive to store the best g_{best} that has been obtained along the searching process. Therefore, once the stopping criteria of the SOPSO are met, the stored value in the archive will be the global optimum. The detailed procedure to apply the archive method is explained as follows:

Specifically, when g_{best} fails to update in a predefined number of iteration steps, the current g_{best} will be evaluated to see if it is a valid solution with null penalty. If so, the

values of both x_{gbest} and g_{best} will be stored in an "archive" vector. And then g_{best} will be mutated (i.e., some of the binary variables in x_{gbest} are reversed at a probability w_{gbest}). Thus, the trend of all the particles flying to the premature converged point is disturbed and a new searching behavior is automatically initiated. If not, the archive will not be operated. g_{best} will still be mutated to release the particles from flying to the premature convergence. If the archive is empty, the first valid pair of g_{best} and x_{gbest} will be directly stored. If the archive has already had a pair of g_{best} and x_{gbest}, the new g_{best} will be compared against the stored g_{best}. If the new g_{best} is smaller, the new pair will replace the existing one; otherwise, the new pair will be disregarded. The data flow logic of mutation and archive operation is shown in Figure 5.2.

The efficacy of this new SOPSO is demonstrated using the design problem introduced in Section 6.4. The derived simulation results are compared with those obtained via a previously reported binary version of SOPSO [59]. Our developed SOPSO is able to consistently find the results closer to the global optimum and present 32% smaller standard deviation in 50 times of simulation trials.

It is important to point out that by using the archive vector, the searching process of the particles will not stop based on convergence because the convergence at each time is also a new start of searching. Hence one needs to define the maximum times of updating the archive. Based on our observation, basically, the probability to find the global optimum is proportional to the number of maximum times, for which the archive is allowed to be updated. Considering the tradeoffs between the simulation speed and result quality, we suggest taking the number from 5 to 10 for common problems with 16 to 20 design variables.

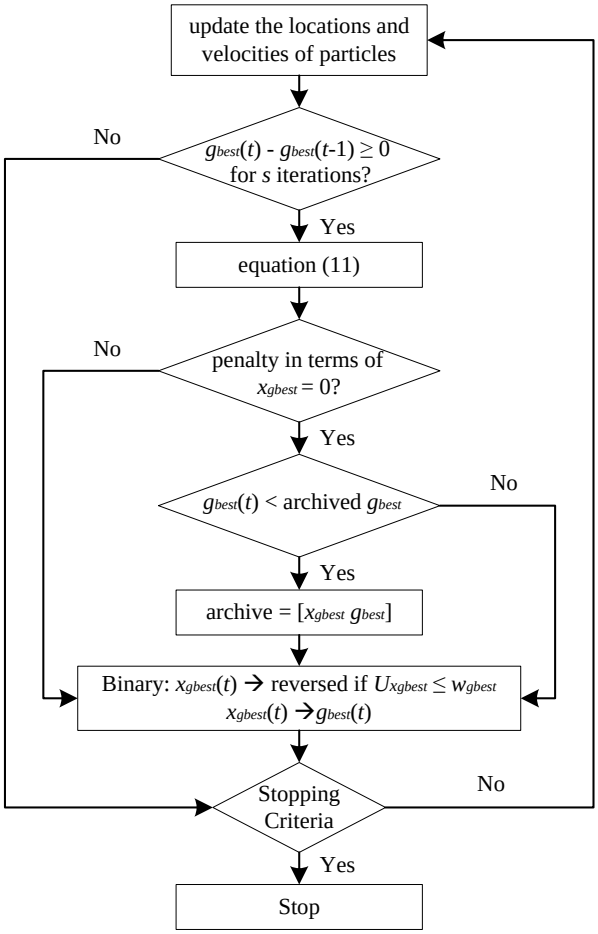

Figure 5.2 The data flow chart of applying the mutation operator and archive vector

5.3. IMPROVEMENT OF MULTI-OBJECTIVE PARTICLE SWARM OPTIMIZATION

The constrained MOPSO is originally presented in [72] to just deal with real variables. It uses a relatively simple scheme without penalties to screen out the solutions with any constraint violation. Unfortunately, this constraint handling method is suffering from a very limited capability of generating the feasible solutions in complicated problems. To address this problem, we improve the MOPSO by employing a multi-stage penalty function as introduced in Section 5.2.2. In addition, the mutation operators in (22) and (23) are also incorporated in the particle searching process.

For benchmark problems [72], our developed MOPSO shows equally good performance as the original constrained MOPSO. However, when we solve the co-optimization problem of the CONOPS containing equality and inequality constraints as well as binary variables (details are explained in Chapter 9), the original constrained MOPSO cannot converge at all. In contrast, our developed MOPSO is able to successfully locate the Pareto optimal points whose border values successfully meet the expectations of the SOPSO (see Chapter 8).

CHAPTER 6

FORMULATION OF THE ECONOMIC DISPATCH PROBLEM FOR MICRO-GRID POWER SYSTEMS

6.1. DEFINITION OF BROAD CATEGORIES OF DATA

Referring to the developing method of the control architecture for the lower-level system applications, we define five broad categories of data to describe system designs and control functions for the primary power generation and distribution level, formulate the optimization problems of the CONOPS, and construct the optimization structure.

- *Setpoint Variables*: the set of variables that determines the CONOPS. This set is composed of both real and discrete binary variables. Based on the investigation of different ZEDS prototypes (e.g., MVAC, MVDC, HFAC), this set is defined to accommodate a considerably wide range of system architecture for the early-stage performance analyses.
  - *Real Variables*: the active power outputs and the power factors of PGMs;
  - *Binary Variables*: the online status (0=offline, 1=online) and power factor status (0=lagging, 1=leading) of PGMs;
- *Measurement*: the measured information that indicates the characteristics of the power components or modules in terms of efficiency and reliability. The information about efficiency, including the power efficiency, fuel efficiency, and instantaneous power consumption, is used to derive the network power flow relationship. The information about reliability, including the reference

points of MTBF values of equipment, is essential to be used for the QOS analysis;

- *System State*: the sensor information (i.e., it indicates the coupling status and operating status, on/off, of power modules) and any other essential parameters (e.g., health states of power modules, electric architecture types (ac or dc), switch locations) that determine the instantaneous topology of the primary power distribution system;
- *Mission Objective*: the user-defined or generated information (e.g., maneuver signals of mechanical load systems, mission segments, power quality) that describes the missions required to be fulfilled by a control function;
- *Constraint*: the system- or equipment-specific requirements that have to be fulfilled during system operations;
  - *Static Constraint*: the constraints whose parameters and expressions are time-independent, such as PGM nameplate ratings and PGM operating limits;
  - *Dynamic Constraint*: the constraints whose parameters or expressions are time-sensitive or mission-dependent, such as configuration-related power balance constraints and decision-based redundancy requirement.

6.2. FORMULATION OF OBJECTIVE FUNCTION

Considering the total N generating units connected to a primary power distribution bus, the real design variables of the EDP for that bus include the active power output, $P_{gout,n}$, and power factor, pf_n, of PGM n. The binary variables include the online

status, u_n, and power factor status, v_n, of PGM n. We use $u=1$ for "ON" status, $u=0$ for "OFF" status, $v=1$ for lagging power factor, and $v=0$ for leading power factor.

Therefore, the objective function of the EDP for the bus is expressed in (24).

$$\min f\left(P_{gout}, pf, u, v\right)=\sum_{n=1}^{N} u_n \times\left\{v_n \cdot f_{t,n}\left[f_{g,n}(P_{g,n})\right]+(1-v_n)\cdot f_{t,n}\left[f_{g,n}(P_{g,n})\right]\right\} \quad (24)$$

where, $P_{g,n}$ is the total active power generated by PGM n, considering the power losses of following principal components: bearing friction, windage losses, conductor losses in the excitation circuit, energy loss in both the magnetic material and the winding copper, and other heat dissipation [75].

Function $f_{t,n}$ is the expression of the thermal efficiency curve of prime mover n (the prime mover of a PGM in this dissertation is consistently referred to as a gas turbine), indicating the relationship between its input fuel and output power at shaft. Function $f_{g,n}$ is the expression of the power efficiency curve of generator n, indicating the relationship between its input power and output power. Function $f_{t,n}$ and $f_{g,n}$ for a PGM should be tested and provided by the manufacturer of the equipment brand. Since we lack this information for the moment, in design demonstration, we adopt a per-unit-based efficiency curve for $f_{t,n}$ and $f_{g,n}$ individually for each PGM.

The thermal efficiency curve is developed based on the concept of specific fuel consumption (SFC) in this dissertation. SFC measures the ratio of the fuel mass flow of an engine to its output power during a time unit. The SFC curve for a generic gas turbine rated at 30000 hp is provided in [73]. The power load is expressed in per unit value, and the unit of SFC is defined as *lbm/hp-hr*, as shown in Figure 6.1. This curve trend can be used to approximate the relationship between SFC and the operating power for an arbitrary gas turbine. Depending on the power rating, this curve can be adjusted by

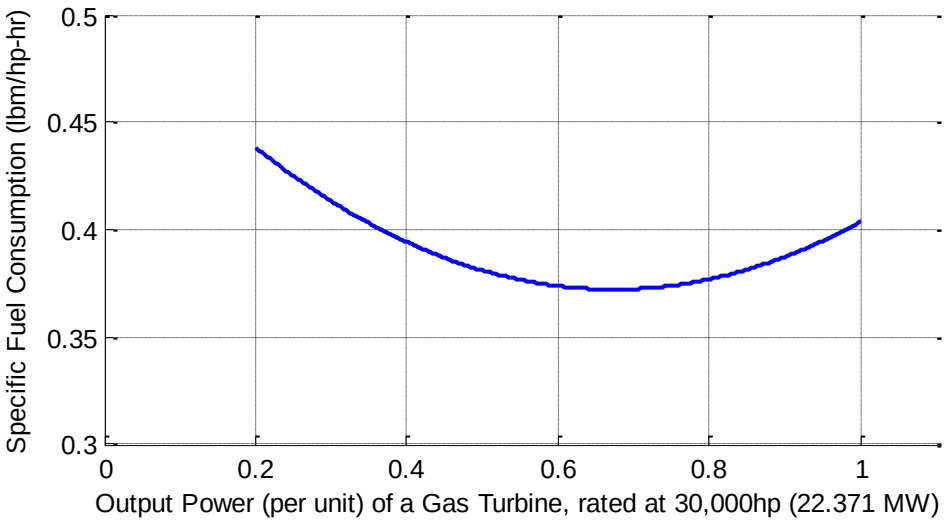

Figure 6.1 Specific fuel consumption curve for a Gas Turbine rated at 30000 hp

moving up or down for a certain degree to match its lowest value (i.e., the highest efficiency) provided by the manufacturer. The equipment database in S3D contains this information for some off-the-shelf gas turbines. General Electric also includes the rated SFCs in the specifications of their marine gas turbines with the power rating at 4.47 MW, 14.91 MW, 25.06 MW, 30.20 MW, 35.32 MW, and 42.43 MW [74]. For conceptual study at the earliest design stage, we can use this information to scale the SFC curve for any arbitrary power-level gas turbines. Specifically, the SFC curve can be expressed with a second order polynomial equation by curve fitting techniques, as shown in (25). The scale to adjust the curve in terms of gas turbine nominal power can be determined with a third order polynomial equation, as shown in (26). The relationship between the input fuel (measured in *lbm/hr*) and the output power of a gas turbine can be expressed in a seven order polynomial equation. This equation can satisfactorily reflect the fuel consumption at engine's idle, which is regarded as 10% of that at the nominal power. The error between the derived curve from this equation and the given curve is within $\pm$0.05%.

$$SFC = a_{sfc} P_{shaft,p.u.}^2 + b_{sfc} P_{shaft,p.u.} + c_{sfc} \tag{25}$$

$$SFC_{rate} = a_r P_{t,rate}^3 + b_r P_{t,rate}^2 + c_r P_{t,rate} + d_r \tag{26}$$

The efficiency curve of a generator is mainly affected by two factors—the operating power and power factor. In [75], the efficiency curve of BDAX 7-290ERJT (80 MW, 13.8 kV, 3 Ph, 60Hz) at power factor of 1.0, 0.9, 0.85, and 0.80 are plotted as separate lines in the same figure. As the power factor reduces, the operating power level yielding the maximum efficiency decreases; meanwhile, the efficiency obtained at the rated power drops, as shown in Figure 6.2. Since a single curve fitting is not able to address these two characteristics affected by the power factor, we capitalize on (27) to incorporate the physical meanings of power loss to the estimation of the generator efficiency [77].

$$\eta = \frac{P_{g,pu,n}}{P_{g,pu,n} + \frac{1-\eta_{rate,n}}{\eta_{rate,n}}\left[\left(1-F_{copper,n}\right) + F_{copper,n} P_{g,pu,n}^2\right]} \tag{27}$$

$$F_{copper,n} = \frac{1}{1+P_{\max eff,n}^2} \tag{28}$$

$$f_{g,n} = \frac{P_{g,n}}{\eta} \tag{29}$$

The efficiency of generator n at the operating power $P_{g,pu,n}$ (per unit value) is formulated in terms of both load-independent power loss and load-dependent power loss. The former includes the losses in magnetic material and mechanical frictions. The latter refers to the power losses in the winding copper. In (27), $F_{copper,n}$ denotes the fraction of the total losses in the winding copper. This value can be uniquely determined in (28), where $P_{maxeff,n}$ is the operating power that yields the maximum efficiency. $P_{maxeff,n}$ can be

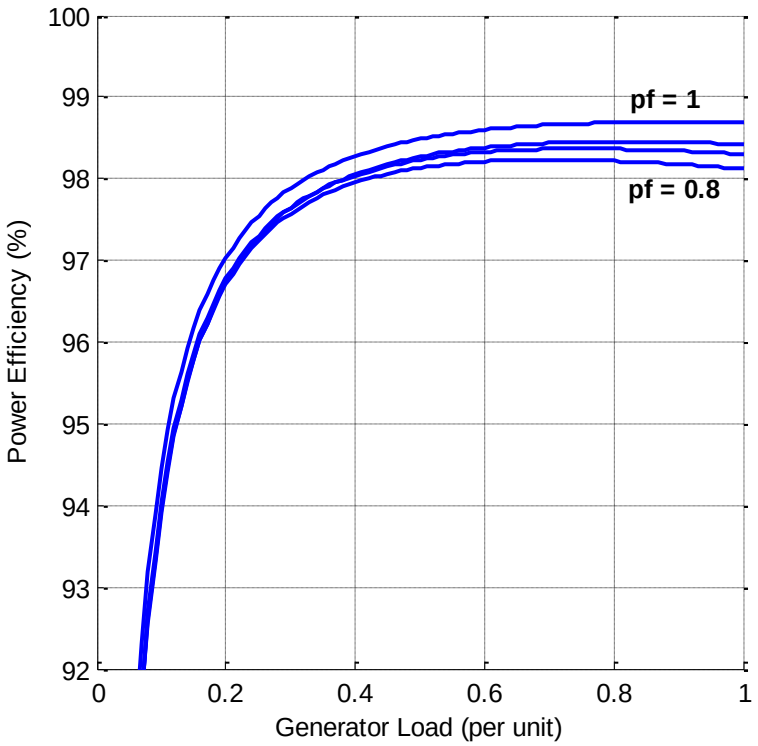

Figure 6.2 Variation of power efficiency with the load and power factor for a generic generator rated at 80 MW (the line from the top down corresponds to *pf* = 1, 0.9, 0.85, and 0.8, respectively) [75]

measured for each power factor value. For the moment, since the efficiency curve for any arbitrary power factor is not accessible, in this dissertation, we choose to estimate both $\eta_{rate,\,n}$ (the efficiency at the rated power) and $P_{maxeff,n}$ based on the curves given in Figure 6.2 through the interpolation method.

In addition, the efficiency curve plot of another generator with a lower power rating, the BDAX 7-193ER (60 MW, 13.8 kV, 3 Ph, 60 Hz) is given in [76]. By comparison, we notice that the higher power rating, the higher overall efficiency could be normally reached. Therefore, based on these two documents, we can also approximate the efficiency curve plot for any sized generator through the interpolation method.

6.3. FORMULATION OF OPTIMIZATION CONSTRAINTS

Four constraints are considered in our EDP.

1) Real and Reactive Power Balance Constraint

$$\sum_{n=1}^{N}\left(u_n \cdot P_{g,n}\right) - P_{loss} - P_{load} = 0, \quad \sum_{n=1}^{N}\left(u_n \cdot Q_{g,n}\right) - Q_{load} = 0 \tag{30}$$

where

$$P_{loss,\mathrm{PDM}} = \alpha \cdot \sqrt{\left(\sum_{n=1}^{N} P_{g,n}\right)^2 + \left(\sum_{n=1}^{N} Q_{g,n}\right)^2} \tag{31}$$

$$Q_{g,n} = \frac{P_{g,n} \cdot \sqrt{1 - pf_n^{\,2}}}{pf_n} \tag{32}$$

$$P_{loss,\mathrm{PCM}} = \beta \cdot \sqrt{\left(\sum_{n=1}^{N} P_{g,n} - P_{loss,PDM}\right)^2 + \left(\sum_{n=1}^{N} Q_{g,n}\right)^2} \tag{33}$$

$$P_{loss} = P_{loss,PDM} + P_{loss,PCM} \tag{34}$$

P_{load} and Q_{load} are the active power and reactive power demands of the aggregate load of the shipboard power system in a mission segment, respectively; $P_{loss,\,PDM}$ is the conductor power loss occurring in the PDMs on the primary power distribution bus and zonal distribution buses; $Q_{g,n}$ is the reactive power output of PGM n; $P_{loss,\,PCM}$ is the aggregate power loss occurring in the PCMs on the power flow paths. For estimating the power loss during transmission and distribution, we assume all the PCMs are located close to the PLMs. Therefore, the power at the input of the PCMs is obtained by deducting $P_{loss,\,PCM}$ from the power generated at the output of the PGMs.

Energy losses in the PDMs and PCMs are considerably small as compared with that in the PGMs. Power losses in the PDMs are mainly regarded as conductor losses, which accounts for about 1% to 2.5% of the transmitted power [78]. In contrast, the

conversion efficiency in a PCM is approximately 96.5% at 40-100% rated load [79]. Since the number of employed PCMs is hard to estimate at the earliest design stage, in order to make a fair comparison, we conservatively assume that every online load needs a PCM for appropriate power conversion. As a result, we set α equal to 0.025 and β equal to 0.035 consistently for every primary power distribution bus of all the potential system designs.

2) Generation Capacity Constraint

$$u_n \cdot \sqrt{P_{g,n}^2 + Q_{g,n}^2} - P_{rate,n} \le 0 \tag{35}$$

where $P_{rate,n}$ is the rated generation capacity of PGM n.

3) Constraint of the Power Factor Adjusting Range

A PGM is able to work in either lagging or leading power factor status. However, we limit the power factor value to certain intervals for stability purposes. We define a real variable pf to denote the power factor value and use a binary variable v_n to indicate the power factor status.

When v is equal to 0, a PGM works with a leading power factor, the value of pf is bounded in $\left[-1, \quad -pf_{lead,\max}\right]$, as expressed in (36). The negative sign indicates the reactive power flow direction.

$$\begin{aligned} &u_n \cdot (1-v_n)(-1-pf_n) \le 0 \\ &u_n \cdot (1-v_n)\left(pf_{lead,\max,n} + pf_n\right) \le 0 \end{aligned} \tag{36}$$

When v is equal to 1, a PGM works with a lagging power factor, pf is positive and bounded in $\left[pf_{lag,\min}, \quad 1\right]$, as expressed in (37).

$$\begin{aligned} u_n \cdot v_n \cdot \left(pf_{lag,\min,n} - pf_n \right) \le 0 \\ u_n \cdot v_n \cdot \left(pf_n - 1 \right) \le 0 \end{aligned} \tag{37}$$

4) Generation Redundancy Constraint

For each primary power distribution bus, system redundancy needs to be evaluated in order to avoid single-point failures. The two aspects of generation redundancy are expressed in (38) and (39). *U* is the least number of PGMs that must be in service to support an independent distribution bus during a mission segment. P_{vload} is the power demand of the vital loads supported by an independent distribution bus during a mission segment.

$$U - \sum_{n=1}^{N} u_n \le 0 \tag{38}$$

$$P_{vload} - \left(\sum_{n=1}^{N} u_n \cdot P_{rate,n} - \max\left\{ n = 1,2...N \mid u_n \cdot P_{rate,n} \right\} \right) \le 0 \tag{39}$$

6.4. THE DESIGN PROBLEM FOR DEMONSTRATION

In order to demonstrate the design improvement of our concept evaluation method compared against the traditional design approaches, we employ two prototypes of ZEDS—MVAC and MVDC—to represent a generic micro-grid power system. They are consistently used in this dissertation for both single- and multi-objective optimization purposes.

The primary power generation and distribution topology of the ZEDS is constructed with a ring bus, as shown in Figure 6.3. Since all the loads receive the power from the same bus, no vital load allocation strategy is necessarily taken into account. However, if a ZEDS topology with multiple independent primary distribution buses is

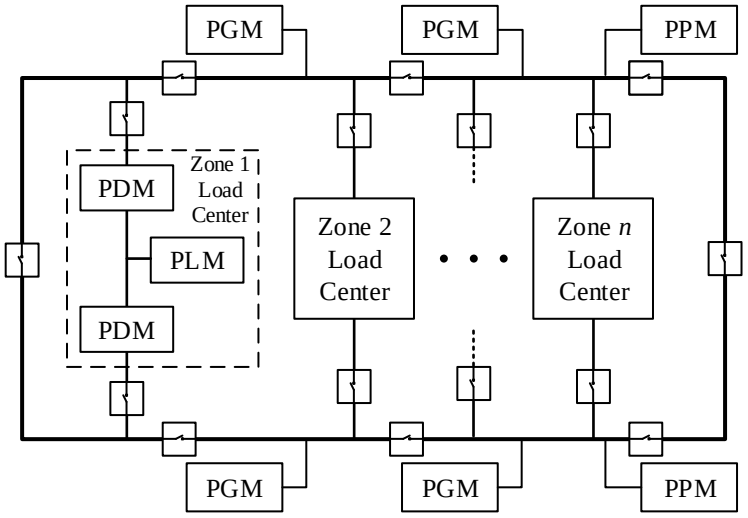

Figure 6.3 The prototype of the shipboard ZEDS used for demonstrating our design method

under study, the optimization of the CONOPS will be carried out for each bus independently; therefore, the non-vital load profile and the allocated power demands of the vital loads have to be known for each bus.

The main design parameters are listed in Table 6.1. The PGM candidates are provided by the equipment database in the S3D simulation environment, which contains seven off-the-shelf gas turbine generators for different power level applications. The goal of our design is to choose the quasi-optimal generator combinations for an 80 MW shipboard power system. Due to the limitations of weight and volume, only the combinations with four or five generators are investigated. Therefore, there are a total of eight feasible design alternatives, which correspond to eight system designs, generated by the MATLAB script, as listed in Table 6.2. For stability and efficiency purposes, we define the minimum lagging power factor of a generator as 0.5 and the maximum leading power factor as 0.95.

Table 6.1 The parameter list of the shipboard power system design

Parameters of Shipboard Power Generation Plant		
Parameters	**Values**	**Unit**
PGM Candidates	[4.5, 5, 11, 15, 20, 36, 40]	MW
Power Capacity of Shipboard Generation Plant	80	MW
Quantity Limits of the PGMs Installed for a Shipboard Power System	Min = 4, Max = 5	
Adjusting Range of the Power Factor	$pf_{lead,\max} = 0.95 \quad pf_{lag,\min} = 0.5$	

Table 6.2 The design alternative list of the shipboard power system design

Index	**Power Ratings**					**Unit**
1	5	15	20	40		MW
2	20	20	20	20		MW
3	4.5	4.5	11	20	40	MW
4	4.5	4.5	15	20	36	MW
5	5	5	15	15	40	MW
6	5	15	20	20	20	MW
7	11	11	11	11	36	MW
8	15	15	15	15	20	MW

We arbitrarily choose three mission segments to create our own mission profile, covering low speed (10 knots), medium speed (20 knots), and high speed (30 knots). The specifications of the shipboard power loads are provided in [38], as shown in Table 6.3.

At any moment, the total load connected to an independent primary distribution bus is the sum of the propulsion motor load and the lumped load allocated to that bus, as indicated in (40). The reactive power equation is only for the MVAC system. P_{load} and Q_{load} are the equivalent real and reactive power loads of the power generation plant connected to a primary distribution bus, respectively; P_{PPM} and Q_{PPM} denote the real and

Table 6.3 The load specifications of the theoretical shipboard power system

Propulsion Motor Load (MW)	**10 knots**	**15 knots**	**20 knots**	**30 knots**
	1.4	4.7	11.0	60.4

Lumped Loads (MW)	**Power Factor**			
	0.8			
	Cruise		**Battle**	
	Vital	**Non-Vital**	**Vital**	**Non-Vital**
	7.585	1.320	23.285	3.351

reactive power demands from the PPM on the bus, respectively; P_{lump} and Q_{lump} denote the real and reactive power demands from the notional ship lumped load on the bus, respectively.

$$\begin{aligned} P_{load} &= P_{PPM} + P_{lump} \\ Q_{load} &= Q_{PPM} + Q_{lump} \end{aligned} \tag{40}$$

The propulsion motor load is the largest potential power consumer in the system, varying significantly depending on the ship's speed. We always assume the use of variable speed ac drives to control propulsion motor speed, thus the power factor of this type of load can be constantly regarded as near unity (i.e., Q_{PPM} in (40) constantly equals to zero). The lumped loads, in contrast, are regarded to maintain the power factor at 0.8. The vital and non-vital lumped loads have different values for two ship operating modes, namely, the cruise mode and battle mode. In this dissertation, we employ the load profile of the cruise mode for the low and high speed, and employ that of the battle mode for the medium speed. The total vital load of the shipboard power system is defined as the sum of the propulsion power, which allows the ship to maintain the speed at 15 knots, and the

Table 6.4 The aggregate load during the given missions in our shipboard system design

	Mission 1	**Mission 2**	**Mission 3**
Aggregate Load (MW)	10.305	37.636	69.305
Power Factor	0.839	0.883	0.995

lumped vital loads. For the cases that the ship is running below 15 knots, the total vital load is defined as the sum of the current propulsion power and the lumped vital loads. The expression is shown in (41) (the reactive power equation is only for the MVAC system). P_{vload} and Q_{vload} are the equivalent real and reactive power demands, respectively, of the vital loads supplied by the shipboard generation plant. P_{vlump} and Q_{vlump} are the real and reactive power demands, respectively, of the lumped vital loads; P_{PPM} is the propulsion power required by the mission segment. The specifications of the aggregate load for each mission segment in our design problem are listed in Table 6.4.

$$\begin{aligned} P_{vload} &= \min\left\{P_{PPM}, \quad P_{PPM,15kts}\right\} + P_{vlump} \\ Q_{vload} &= Q_{vlump} \end{aligned} \tag{41}$$

Each mission segment is assumed to take one third period of the entire mission. In order to evaluate the system QOS, we assume a three year period of mission for the shipboard power system. The mission duration is chosen based on information in [44].

6.5. Quality Evaluation of Design Alternatives Based on the Economic Dispatch Problem

The parameter settings of the SOPSO are listed in Table 6.5. To demonstrate the optimization efficacy, we optimize the fuel consumption rate (measured in klbm/hr) for each mission segment via the SOPSO and make a comparison with that obtained in the worst-case scenario caused by the inappropriate choice of the CONOPS. The worst-case

Table 6.5 The parameter settings of the SOPSO

Population	50
Inertia Weight, *w*	$w_{\max} = 0.9, \quad w_{\min} = 0.4$
Mutation Rate	0.1
The NO. of Function Evaluation	50

scenario is determined by maximizing the fuel consumption rate via the SOPSO. Since the three mission segments in our design problem have an identical duration, the sum of their fuel consumption rates denotes the equivalent fuel consumption rate for the mission with one-third duration of the original mission. We can directly compare the equivalent fuel consumption rates of the design alternatives to differentiate their quality.

6.5.1. Optimization of the Economic Dispatch Problem for the MVAC ZEDS

The comparison of the design alternatives for the MVAC ZEDS is shown in Figure 6.4. The detailed numerical comparison is provided in Table A.1. The values of the CONOPS corresponding to the optimization results of the EDP are given in Table A.3.

From the figure, we can observe that an appropriate selection of the power generation plant at the earliest design stage has an impressive impact on the potential savings of fuel. When the CONOPS of every design alternative is optimized through the EDP, design alternative 1 outperforms all the others because it requires the minimum fuel to complete the given mission. In contrast, the worst design alternative—design alternative 8— has to consume 7.6% more fuel (i.e., 45.56 mega-lbms in three years) for the same mission.

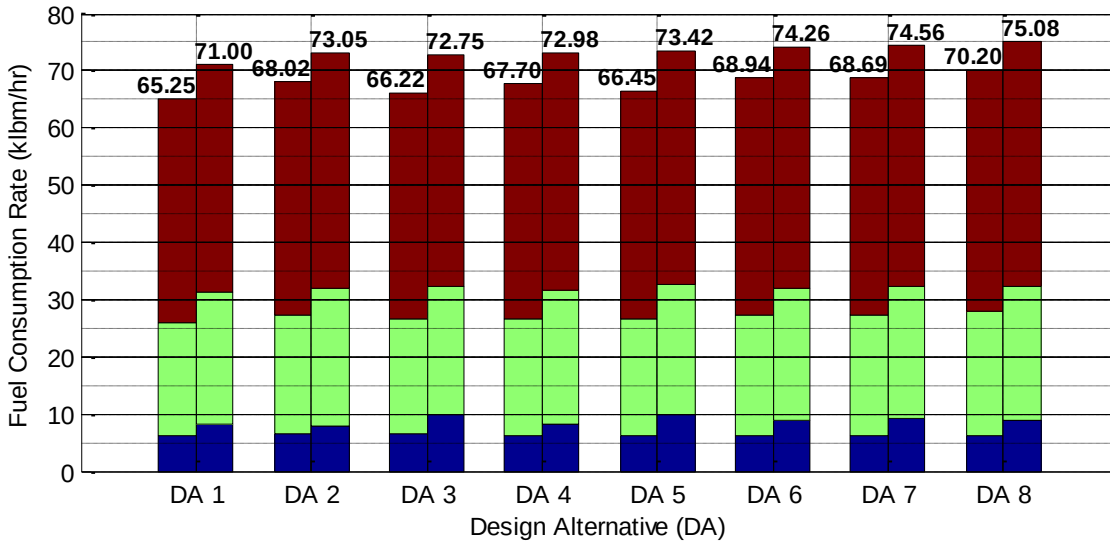

* The bar segments from bottom to top correspond to mission segment 1, 2, and 3, respectively.

Figure 6.4 The MVAC ZEDS—the fuel consumption rate minimized via the SOPSO (left) vs. the fuel consumption rate obtained in the worst-case scenario (right) of each design alternative, respectively

In addition, we can also observe that fuel consumption caused by the optimized CONOPS is far less than that in the worst-case scenario, especially for the light loading condition. In mission segment 1 when the load is under 20% of the total power capacity, optimization of the CONOPS is able to save at least 20%, up to 36.8%, of fuel for all the design alternatives. This is because optimization is always able to choose the minimum number of online PGMs to meet the power demand as well as guarantee acceptable redundancy. Besides, the operating setpoints of the online PGMs are optimally determined. In mission segment 2 when the load is about 60% of the total power capacity, the savings of fuel drop to around 10%. At the moment, the number of online PGMs determined by the optimization is quite close to the total quantity of the shipboard PGMs (in fact, design alternative 8 needs to turn on all the five generators in this case). In mission segment 3 when the load reaches near 90% of the total power capacity, the

savings of fuel due to the optimization of the CONOPS are only about 1% for all the design alternatives. This is because all the PGMs have to be turned on and everyone has to generate the power close to its rated capability, which also indicates a high efficiency. Therefore, optimal tuning of the operating setpoints does not contribute too much to the fuel savings. However, considering that a ship is mostly running in low-speed conditions (about 60% of a mission duration), sometimes in medium-speed conditions (about 30% of a mission duration), and seldom in high-speed conditions (less than 10% of a mission duration) [73], following the CONOPS optimized through the EDP can considerably reduce the fuel cost of the shipboard generation plant.

6.5.2. Optimization of the Economic Dispatch Problem for the MVDC ZEDS

For the MVDC ZEDS, the EDP for the generation plant only involves the real power dispatch and balance. The optimization results can also help us investigate the necessity of including the reactive power balance constraint in the EDP of the MVAC system. Apparently, the EDP of the MVDC system contains $1/3$ fewer setpoint variables than that of the MVAC system, reducing the simulation time by about 23%.

The optimization results of the EDP for the ac and dc system are compared in Figure 6.5. The detailed numerical comparison is provided in Table A.2.

It is noted that in our design problem, the choice of an ac or dc distribution system (or we can say "the inclusion of reactive power balance in the EDP of the MVAC ZEDS") does not affect the optimization results very much in most cases (i.e., the percent difference is around 1%). This is because the similar selection strategies for the online PGMs are employed for the two systems. Besides, the power factor values have a negligible influence to the efficiency curves of the online PGMs when the lumped load on the bus has a pretty high power factor (typically larger than 0.8) [75][76].

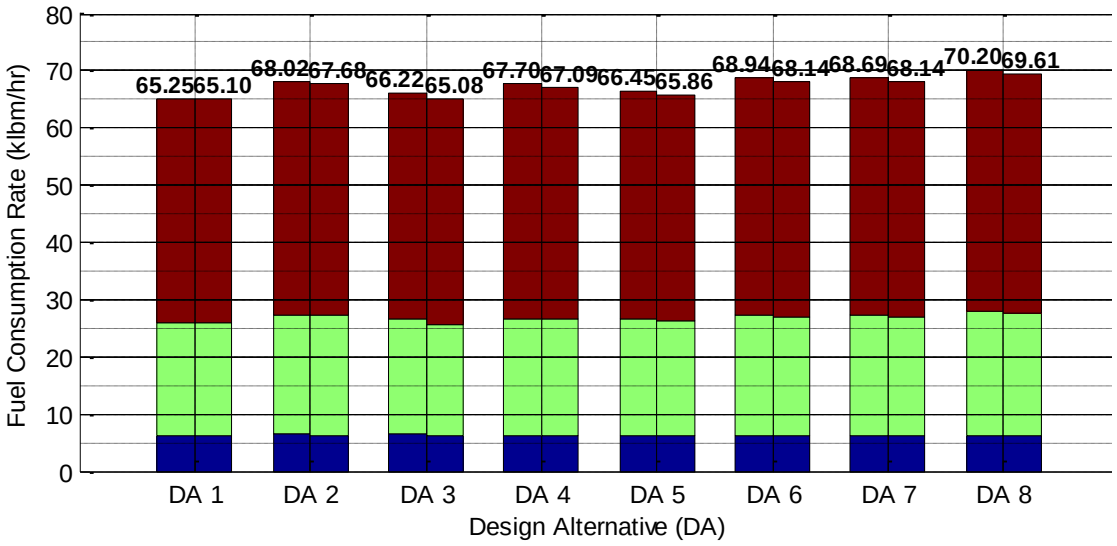

* The bar segments from bottom to top correspond to mission segment 1, 2, and 3, respectively.

Figure 6.5 Comparison of the fuel consumption rates of the design alternatives minimized via the SOPSO for the MVAC ZEDS (the bars on the left) and MVDC ZEDS (the bars on the right)

However, there is one situation that may cause big differences of the minimum fuel consumption obtained in the ac and dc systems: the optimal combination of online PGMs in the dc system only contains enough generation capacity to meet the real power demand of the load. When the reactive power generation is taken into account in the ac system, at least one more generator needs to be turned on to suffice the system, causing more fuel consumption. If the generator available to be added to the system is large, we believe the effect to the fuel consumption can hardly be negligible.

To conclude, in solving for the EDP of our design problem, the constraint of reactive power balance does not need to be taken into account for the MVAC ZEDS because the load power factor is relatively high. However, for solving the EDP of a generic micro-grid ac power system, the answer really depends on the load power demands, the load power factors, and the power ratings of the PGMs involved in the

design alternatives. If the situation that we discussed above occurs, the percent difference of the fuel consumption minimized by the EDP with and without the reactive power balance constraint can possibly turn to be very large to affect acquisition decisions.

CHAPTER 7

FORMULATION OF THE QOS OPTIMIZATION PROBLEM FOR MICRO-GRID POWER SYSTEMS

The QOS of a micro-grid power system needs to be evaluated in two aspects:

1) During normal operating scenarios without introducing any external interruption to the system, the system QOS is affected by the MTBF and MTTR values of the online PGMs because these values directly determine the frequency, duration, and magnitude of any potential power loss failure. The determinant factors of the MTBF and MTTR values of a PGM include its size, structure complexity, and operating power.
2) When some PGM failures occur, the system QOS is then reflected by the capability of the PGMs left in service to maintain the system dependability at a fairly high level, especially to mitigate the effect on the vital loads.

We have incorporated the second evaluation aspect in the EDP as the generation redundancy constraint of the PGMs in Section 6.3 because it directly affects the economic dispatch strategy as an extra condition required to meet. However, we need another independent performance metric, which is able to quantify the characteristics of the system QOS failure, to reflect the first evaluation aspect.

7.1. FORMULATION OF OBJECTIVE FUNCTION

The same categories of data defined in Section 6.1 are employed to formulate the QOS optimization problem. The objective function is the expression of the metric

relating the system QOS to the CONOPS. In this dissertation, we develop two versions of metric to evaluate different aspects of the QOS. Both of them are calculated as the reciprocal of the QOS failure metric. The first version defines the QOS failure metric in terms of failure probability of the PGMs. This metric is referred to in this dissertation as "probability-based QOS metric". In contrast, the second version defines the QOS failure metric in terms of failure magnitude and duration of the PGMs. This metric is referred to in this dissertation as "energy-based QOS metric".

The detailed formulation of these two versions of QOS metric for a mission segment is explained as follows.

7.1.1. Formulation for the Probability-Based QOS Metric

This definition evaluates how serious the power service will be affected at the moment when the online PGMs fail at certain operating setpoints. Three steps are taken to formulate the system QOS failure metric of this definition:

1) Compute the failure probability of each online GTG.
2) Multiply the failure probability of a PGM by an appropriate weight, which indicates the significance of the PGM to the system in fulfilling the mission segment (i.e., the more power a PGM generates, the more its failure affects the system power supply).
3) Add up all the weighted failure probabilities of the PGMs.

To calculate the value of the QOS metric for mission segment *k*, another weight determined by the segment duration needs to be multiplied with the derived failure metric. The longer a mission segment's duration, the more the estimated QOS for the segment should be counted in calculating the QOS for the entire mission. The mathematical expression is given in (42).

$$QOS_k = \frac{1}{f_{m,k} \cdot \sum_n \left(f_{fp,n} \cdot f_{sign,n} \right)} \tag{42}$$

where $f_{fp,n}$ denotes the failure probability of PGM n during mission segment k; $f_{sign,n}$ denotes the weight factor for the failure probability of PGM n during mission segment k; $f_{m,k}$ denotes the weight factor for the system QOS failure metric of mission segment k, equal to the fraction of time spent in mission segment k. The expressions of the three items are given in (43).

$$f_{fp,n} = \frac{T_k}{MTBF_n}, \quad f_{sign,n} = \frac{P_n}{P_k} + \frac{Q_n}{Q_k}, \quad f_{m,k} = \frac{T_k}{T} \tag{43}$$

For PGM n, $f_{fp,n}$ is defined as the ratio between T_k, which denotes the duration of mission segment k, and $MTBF_n$, which denotes its MTBF value at the operating point during mission segment k (see Secition 7.2); $f_{sign,n}$ is calculated as the sum of two ratios: one ratio denotes the PGM's contribution to the total real power demand, P_k, during mission segment k; and the other ratio denotes the PGM's contribution to the total reactive power demand, Q_k, during mission segment k.

The ultimate QOS metric for the whole mission is defined by the sum of the QOS value for each mission segment, seen in (44).

$$QOS = \sum_k QOS_k \tag{44}$$

7.1.2. Formulation for the Energy-Based QOS Metric

This definition evaluates the power plant's capability of continuously executing mission segment k when the online PGMs at certain operating setpoints encounter some operating breaks (i.e., some online generators go offline due to sudden failures or scheduled maintenances).

Each mission segment may contain several QOS failures, which can be caused by either single PGM failure or multiple simultaneous PGM failures. Each QOS failure is measured as the product of a power deficiency ΔP and its duration D, expressed as the term in the parentheses of (45). The physical meaning is that some number of the generation capacity is lost for some number of hours during a mission segment. The actual failure metric of mission segment k is defined in (45) as the sum of all the QOS failure measures during that time. The corresponding QOS metric for the mission segment is defined in (46). The ultimate QOS metric for the whole mission is the reciprocal of the aggregate QOS failures of all the mission segments, as expressed in (47)

.

$$failure_{QOS,k} = \sum \left(\Delta P_i \cdot D_i \right) \quad \left(MW \cdot h \right) \tag{45}$$

$$QOS_k = \frac{1}{failure_{QOS,k}} \quad \left(\frac{1}{MW \cdot h} \right) \tag{46}$$

$$QOS = \frac{1}{\sum_k failure_{QOS,k}} \quad \left(\frac{1}{MW \cdot h} \right) \tag{47}$$

When a QOS failure occurs at an operating setpoint but the spare offline PGMs have sufficient generation capacity to compensate the power loss, we assume that D takes a constant value equal to the time (we conservatively choose 15 minutes) for the offline PGMs to be started and synchronized to the distribution system. If all the rest of installed generation capacity is not able to meet the load demand, we consider D as the MTTR values of the broken PGMs. By this definition, the system QOS during a mission segment should be ideally infinite and should be close to zero in the worst-case scenario.

The complete procedure to calculate the system failure value for a mission segment conforms to the well-known Monte Carlo method, explained in detail as follows:

1) At each iteration step, calculate the reliability R_c (affected by the controllable factors) of each online PGM according to its operating setpoint;
2) Randomly generate a certain number of groups of reliability (affected by the uncontrollable factors) and maintainability values for each online PGM through the probability distribution models (see Section 7.2 and 7.3). The number of the groups, also known as the Monte Carlo samples, determines the accuracy level of the simulation results. The values in each group can be understood in this way: the first failure of the PGM is determined by $MTBF_1$, which corresponds to the first generated reliability $R_{uc,1}$. Following that, the time to repair the PGM is determined by $MTTR_1$, which corresponds to the first generated maintainability μ_1. The generator is restored by time ($MTBF_1$ + $MTTR_1$). The second time failure is then determined by $MTBF_2$, which corresponds to the second generated reliability $R_{uc,2}$. And the subsequent repair time is determined by $MTTR_1$, which corresponds to the second generated maintainability μ_2. The PGM is restored again by time [($MTBF_1$ + $MTTR_1$) + ($MTBF_2$ + $MTTR_2$)]. The total sum of the MTBF and MTTR values should be able to cover the duration of the mission segment T_k under investigation, as indicated in (48).

$$\sum\left(\boldsymbol{MTBF}+\boldsymbol{MTTR}\right)\geq T_k$$
$$\text{where}\quad \boldsymbol{MTBF}=\left[MTBF_1\quad\cdots\quad MTBF_i\right],\quad \boldsymbol{MTTR}=\left[MTTR_1\quad\cdots\quad MTTR_j\right] \tag{48}$$

The generation capacity of each PGM can be plotted according to its MTBF and MTTR values against time, as shown in Figure 7.1. As an example, this figure shows two maintenance breaks of PGM *n* taking place in a given mission segment. During MTBFs, the PGM is able to fully function and generate the maximum power equal to its rated value, $P_{r,n}$. During MTTRs, the PGM is under maintenance, not able to produce any power to the system.

3) Combine the reliability obtained in step 1) and 2) via (49) to calculate the instantaneous reliability for each online PGM. And then determine the actual MTBF values of the PGMs corresponding to the CONOPS.

$$R_n = R_{c,n} \cdot R_{uc,n} \tag{49}$$

It is noted that since R_c is less than one, the MTBF values obtained in step 2) will be reduced to some extent. Meanwhile, the MTTR values keep constant without being affected by the operating setpoints. Accordingly, the amount of maintenance breaks during the mission segment may increase, as shown in Figure 7.2 (one more failure as $MTTR_3$ is shown in this figure). In order to address this potential problem, at Step 2), we generate the MTBF and MTTR values to cover duration longer than a mission segment, for example, to cover twice the mission segment's duration. The corresponding stopping criterion is updated into (50).

$$\begin{aligned} &\sum\left(\boldsymbol{MTBF} + \boldsymbol{MTTR}\right) \geq 2 \cdot T_k \\ &\text{where } \boldsymbol{MTBF} = \left[MTBF_1 \quad \cdots \quad MTBF_i\right], \quad \boldsymbol{MTTR} = \left[MTTR_1 \quad \cdots \quad MTTR_j\right] \end{aligned} \tag{50}$$

4) Superpose the plots of the dynamic generation capacity of all online PGMs to produce the dynamic generation capacity of a design alternative. A QOS

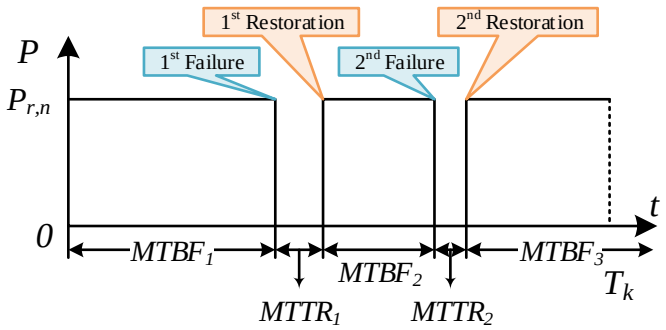

Figure 7.1 An example plot of the dynamic generation capacity of online PGM *n* based on the values of MTBFs (due to uncontrollable factors) and MTTRs

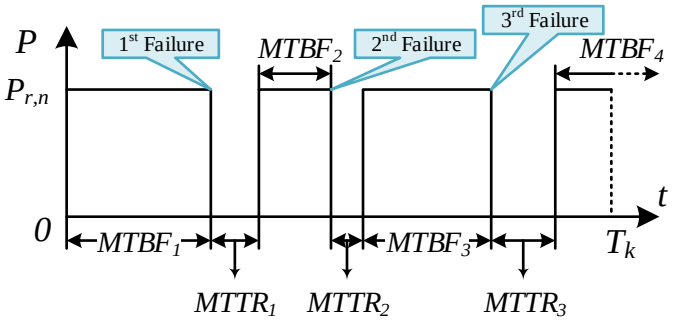

Figure 7.2 The dynamic generation capacity of PGM *n* modified by the reliability due to the controllable factors (i.e., the operating setpoints of the PGM)

failure is regarded to occur when some online PGMs fail but the rest of the functional PGMs' (including the ones staying offline) generation capacity is less than the load demand. For example, if mission segment *k* requires 40 MW for loads and if we have three PGMs, namely, 36 MW, 20 MW, and 10 MW, in service (the plots of the dynamic generation capacity are shown in Figure 7.3), the durations of the QOS failures are indicated by the bold lines. By definition, the QOS failure can be calculated in (51).

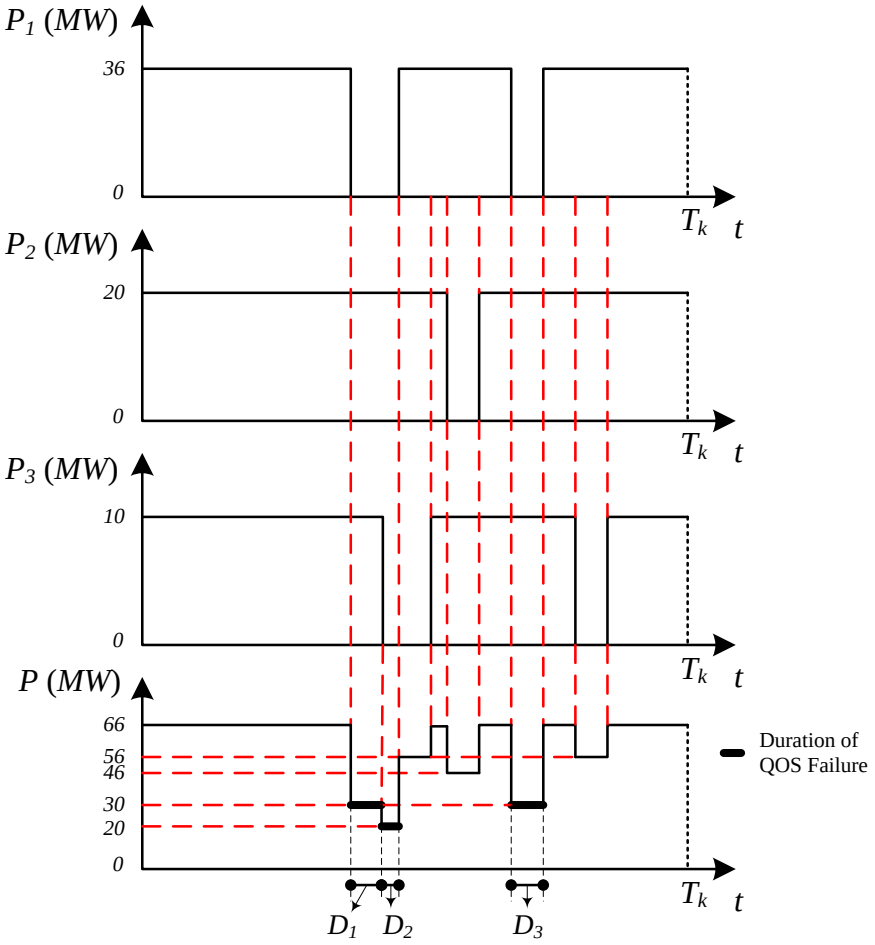

Figure 7.3 Identification of the QOS failure magnitude and duration for an example system with three online PGMs during a given mission segment

$$\begin{aligned} failure_{QOS} &= \sum_{i=1}^{3} \Delta P_i \cdot D_i \\ &= (40-30)D_1 + (40-20)D_2 + (40-30)D_3 \\ &= 10(D_1 + D_3) + 20D_2 \quad (MW \cdot h) \end{aligned} \tag{51}$$

5) Repeat step 4) for every group of data generated in step 2) based on the same R_c to calculate the corresponding value of the system QOS failure. The ultimate system QOS failure for the mission segment is determined by averaging the values of the system QOS failure obtained from all the groups.

7.2. ESTIMATION OF THE MTBF VALUES OF A PGM

The MTBF of a PGM can be directly related to the reliability of the PGM through the two-parameter cumulative distribution function for the Weibull distribution, as expressed in (52) [28]. The parameters β and η can be measured for a generic PGM model (usually provided by the manufacturers) and applied for the other models at the same power level. As long as the reliability R can be determined, the MTBF value can be obtained via (53).

$$R = 1 - e^{-\left(\frac{MTBF}{\eta}\right)^{\beta}} \tag{52}$$

$$MTBF = \eta \cdot \sqrt[\beta]{\ln\left(\frac{1}{1-R}\right)} \tag{53}$$

As we discussed in Section 3.1.3, the reliability of a PGM is simultaneously determined by the uncontrollable factors and controllable factors. In statistics, the reliability R_{uc} due to the uncontrollable factors follows the uniform distribution.

In solving for the probability-based QOS metric, we employ the Monte Carlo method to determine the average MTBF value for each PGM. Specifically, we first randomly generate a large number of R_{uc} (such as 1000 samples). For each R_{uc} the corresponding MTBF value is calculated in (53). Then we average this group of MTBF to represent the average MTBF value of each PGM. The corresponding R_{uc} can be obtained in (52).

In solving for the energy-based QOS metric, for each Monte Carlo simulation, we randomly generate the MTBF values through the uniform distribution one by one until (50) is satisfied.

The controllable factors are reflected on the reliability of a PGM through the natural exponential function introduced in [34]. Given constantly sufficient cooling capability of the power system, it is well understood that the wear-and-tear of a PGM running at a fixed frequency is directly proportional to its generated power (see Section 3.1.3). Therefore, the failure rate λ_c of a PGM can be calculated in (54) in terms of its generated real power. The corresponding reliability rate at this loading condition can be obtained from (55).

$$\lambda_c(t) = \lambda_o e^{\beta \cdot P_L(t)} \tag{54}$$

$$R_c(t) = 1 - \lambda_c(t) \tag{55}$$

The ultimate reliability of a PGM during an operation is calculated in (49). In solving for the probability-based QOS metric, R_{uc} here is the reliability corresponding to the average MTBF value; for the energy-based QOS metric, R_{uc} becomes an array data corresponding to a series of MTBF values over a mission segment.

7.3. ESTIMATION OF THE MTTR VALUES OF A PGM

For each PGM, we adopt the maintainability expression introduced in [28], as shown in (56), to relate maintainability with the MTTR. Since MTTR is only affected by uncontrollable factors, the maintainability value μ can be estimated by the uniform distribution. The MTTR value corresponding to maintainability μ is determined in (57).

$$\mu = \Phi\left(\frac{\ln MTTR - \gamma}{\sigma}\right) \tag{56}$$

$$MTTR = \exp\left[\sigma \cdot \Phi^{-1}(\mu) + \gamma\right] \tag{57}$$

where the function $\Phi(\cdot)$ is the standard normal distribution cumulative function; the function $\Phi^{-1}(\cdot)$ is the standard normal inverse distribution cumulative function.

7.4. Formulation of Optimization Constraints

The optimization constraints developed for the EDP in Section 6.3 are also applicable to the QOS optimization problem.

7.5. Quality Evaluation of Design Alternatives Based on the QOS Optimization Problem

We still employ the parameter settings of the SOPSO in Table 6.5. Instead of comparing the optimized QOS with the QOS obtained in the worst-case scenario, in this section we compare the QOS determined by maximizing the QOS via the SOPSO with the QOS obtained from minimizing the fuel consumption to investigate the performance tradeoffs.

7.5.1. Employment of the Probability-Based QOS Metric

For the MVAC ZEDS, the QOS comparison of the design alternatives is plotted in Figure 7.4. The detailed numerical comparison is provided in Table B.1. We can see that performance tradeoffs do exist between fuel consumption and the system QOS in most cases when choosing the CONOPS to execute a mission. This is because in order to minimize the fuel consumption, the number of online PGMs is generally expected to be as small as possible. However, for a high QOS, the power should be dispatched among as many online PGMs as possible, so that a single point PGM failure will not instantaneously affect the power supply that much. In very few cases, the minimum fuel consumption and the maximum QOS can be reached simultaneously, indicating the unique optimal CONOPS (e.g., design alternative 1 in mission segment 1 and 2).

The performance tradeoffs between the QOS and fuel consumption of the design alternatives are plotted in Figure 7.5. The increases of QOS and fuel consumption are

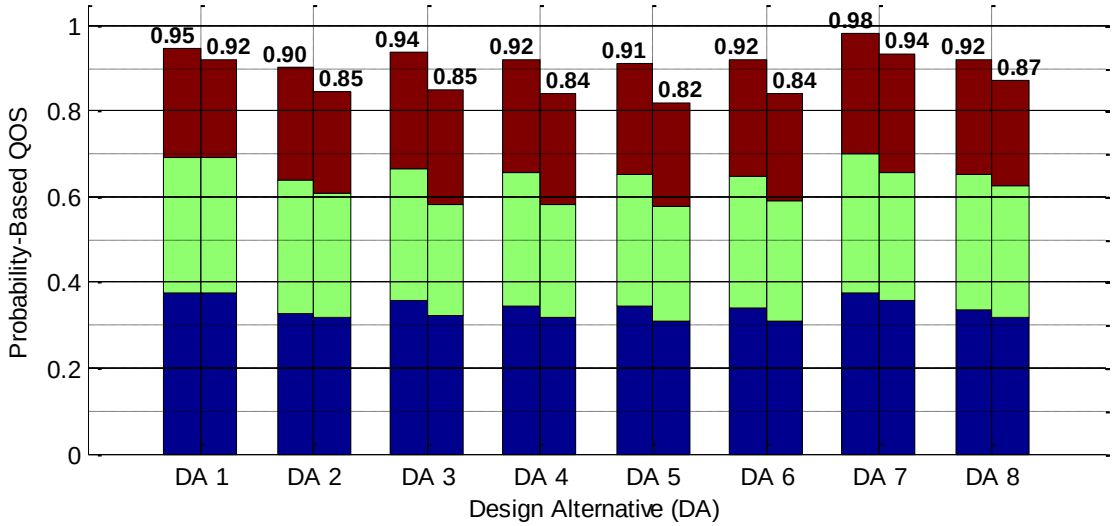

* The bar segments from bottom to top correspond to mission segment 1, 2, and 3, respectively.

Figure 7.4 The MVAC ZEDS—the QOS determined by maximizing the QOS via the SOPSO (left) vs. the QOS obtained from minimizing the fuel consumption (right) of each design alternative, respectively

measured from the values yielded by the CONOPS optimized to minimize the fuel consumption to those yielded by the CONOPS optimized to maximize the QOS. We can see that in light loading conditions, such as mission segment 1, the increase of the QOS always causes a relatively larger increase of the fuel consumption. For example, design alternative 4 requires 19% more fuel to obtain only an 8% increase in the QOS. This is because the CONOPS optimized for maximizing the QOS incorporates more online PGMs (usually the large ones) than that derived from the EDP. However, in medium and heavy loading conditions, such as mission segment 2 and 3, a slight increase of fuel consumption can yield a relatively greater improvement of the QOS. For example, design alternative 3 is able to accomplish an 18% improvement of the QOS by just consuming

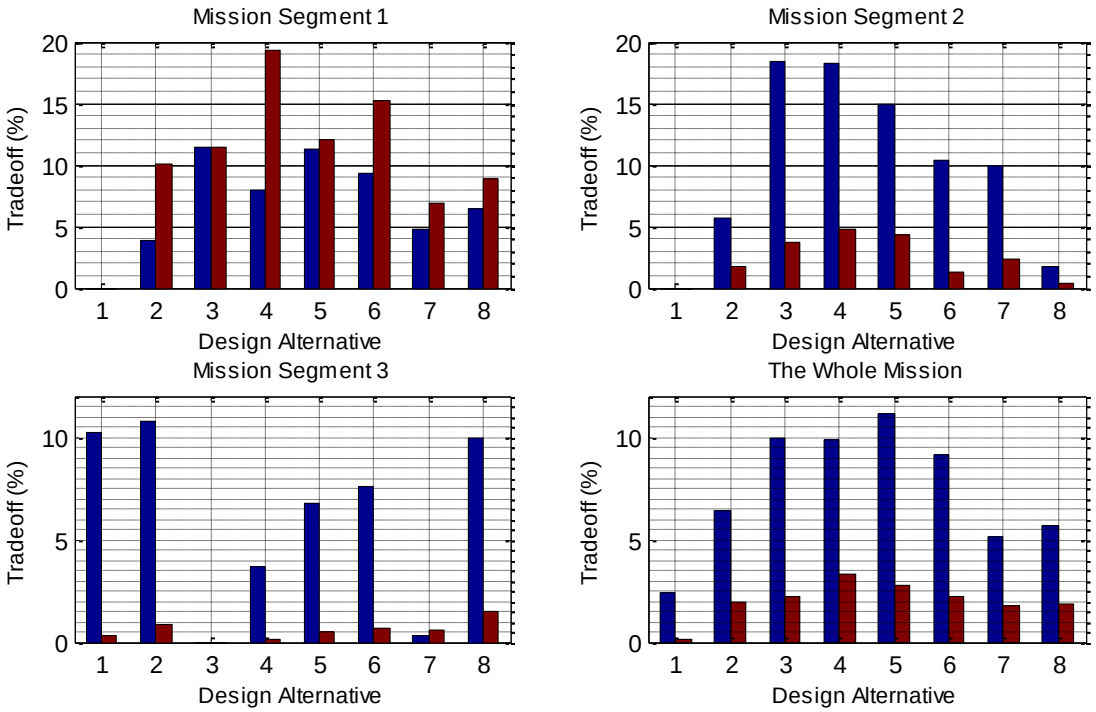

Figure 7.5 The MVAC ZEDS— the maximal percent improvement of the QOS by consuming more fuel (blue) vs. the corresponding percent increase in fuel consumption from the minimum value (red) of each design alternative, respectively

less than 4% more fuel in mission segment 2; design alternative 8 is able to obtain a 10% improvement in the QOS by consuming about 2% more fuel in mission segment 3. In these loading conditions, almost every installed PGM has to be turned on for the power supply. Therefore, the solutions to the QOS optimization problem and the EDP just indicate different operating setpoints of the PGMs, which does not involve too much variation in fuel consumption compared with the addition to the online PGMs. However, since the CONOPS optimized for maximizing the QOS dispatches the power generation more evenly, the instant effect of any PGM failure to the power supply can be mitigated.

To conclude, the usage of the probability-based QOS metric indicates a favorable tradeoff relationship between the QOS and fuel consumption in medium and heavy

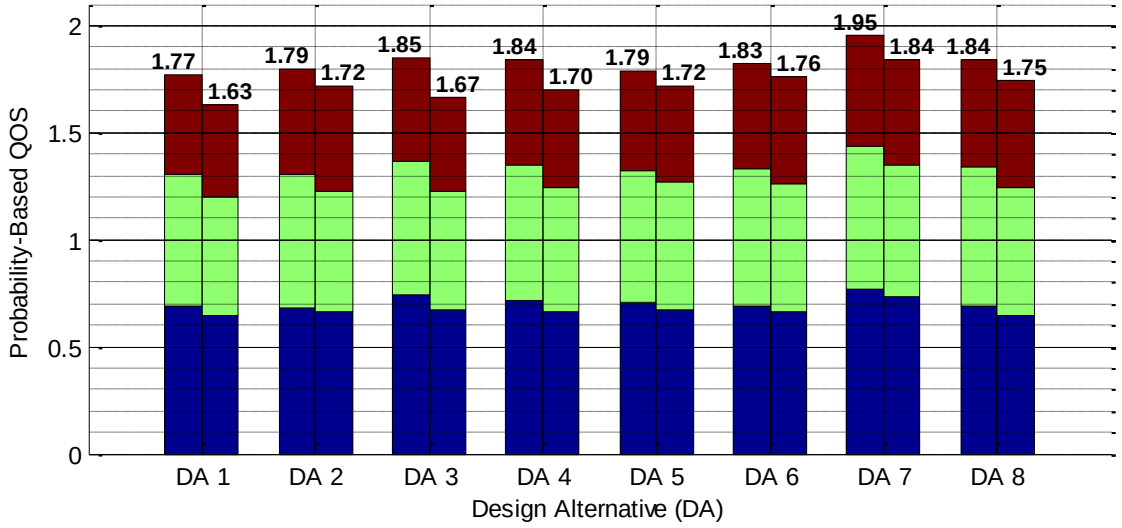

* The bar segments from bottom to top correspond to mission segment 1, 2, and 3, respectively.

Figure 7.6 The MVDC ZEDS— the QOS determined by maximizing the QOS via the SOPSO (left) vs. the QOS obtained from minimizing the fuel consumption (right) of each design alternative, respectively

loading conditions. Since our design problem defines an identical duration for the light, medium, and heavy load support, we can see from Figure 7.5 that optimization of the QOS over the whole mission can always be obtained by a smaller increase in fuel consumption. However, if a ship mission mainly contains low speed cruise, the optimization of this QOS metric may not produce desirable CONOPS.

The QOS comparison of the design alternatives for the MVDC ZEDS is shown in Figure 7.6. The corresponding performance tradeoffs are shown in Figure 7.7. Since the weight factor, $f_{sign,n}$, of the QOS failure metric defined in (43) does not contain the second term related to the reactive power generation for the MVDC system, the overall QOS of the design alternatives in the MVDC system is almost two times that in the MVAC system. However, the optimization results obtained for these two types of electrical architecture indicate the same relationship of performance tradeoffs.

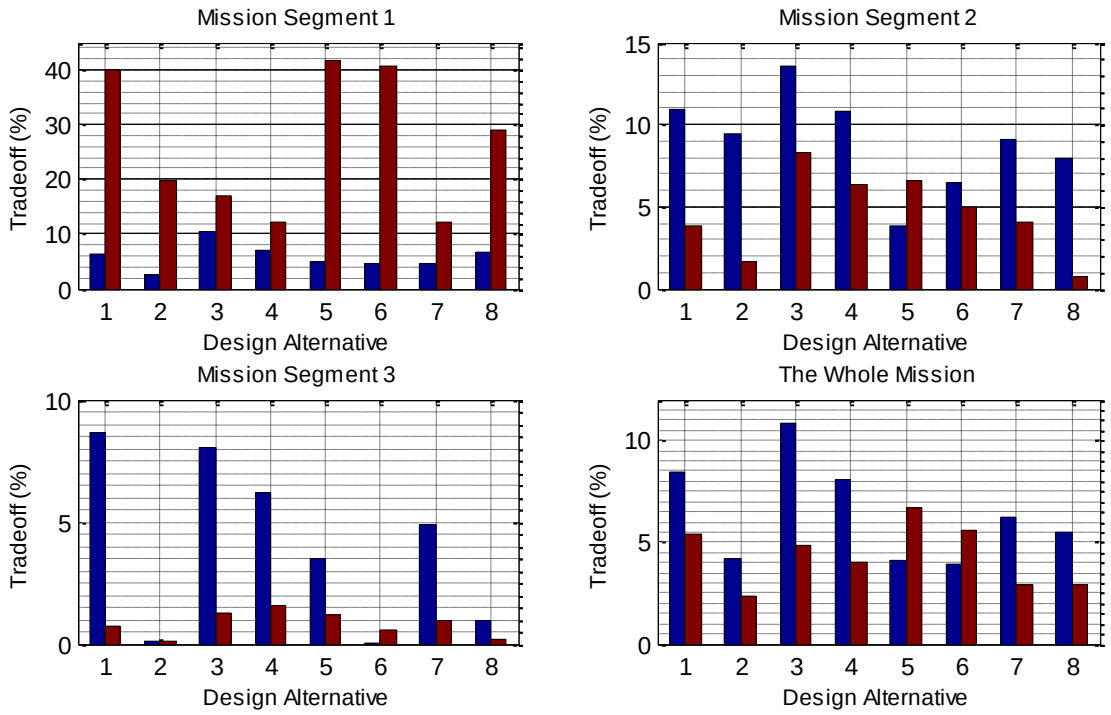

Figure 7.7 The MVDC ZEDS—the maximal percent improvement of the QOS by consuming more fuel (blue) vs. the corresponding percent increase in fuel consumption from the minimum value (red) of each design alternative, respectively

Design alternative 7 is consistently the optimal choice disregarding the electrical architecture, but the other design alternatives' ranks are changed. Therefore, we can also conclude that the inclusion of the reactive power balance constraint for the MVAC system will greatly impact acquisition decisions using the probability-based QOS metric at the earliest design stage.

7.5.2. Employment of the Energy-Based QOS Metric

Considering the compromise between the simulation speed and accuracy, we generate 100 groups (Monte Carlo simulation samples) of random MTBF (based on uncontrollable factors) and MTTR values of the online PGMs to describe the dynamic generation capacity in each mission segment. This number of groups is able to give us

95% confident that the true mean of the distribution lies within 2% of our estimate with 100 samples [80][81].

For better understanding, we use the value of the QOS failure metric instead of the QOS metric to investigate the performance tradeoffs. Specifically, we compare the energy-based QOS failure values determined by minimizing the QOS failure via the SOPSO with the QOS failure values obtained from minimizing the fuel consumption. The comparison of the design alternatives for the MVAC system is shown in Figure 7.8. The detailed numerical comparison is provided in Table B.3 for every mission segment and the whole mission. The performance tradeoffs between the energy-based QOS failure and fuel consumption of the design alternatives are shown in Figure 7.9.

We can see that in light loading conditions such as mission segment 1, the CONOPS obtained by solving the EDP for half of the design alternatives, namely, design alternative 2, 4, 5, and 6, have been able to guarantee near-flawless reliability to the system. This is because the EDP has integrated generation redundancy to prevent single-point failures of the PGMs. For the other half of the design alternatives, some multi-point failures are observed. However, the yielded power outages can be quickly recovered by turning on an offline PGM; therefore, the QOS failure does not appear to be abundant. For example, design alternative 7 represents the worst situation, but only loses about 3.75 MW·h in one year. By optimization, the CONOPS of all the design alternatives are able to completely reject any possible QOS failure. However, to this end, more PGMs are kept online, causing considerably more fuel consumption, up to 35%.

In the medium loading condition such as mission segment 2, the CONOPS determined by solving the EDP start causing serious QOS failures because the online

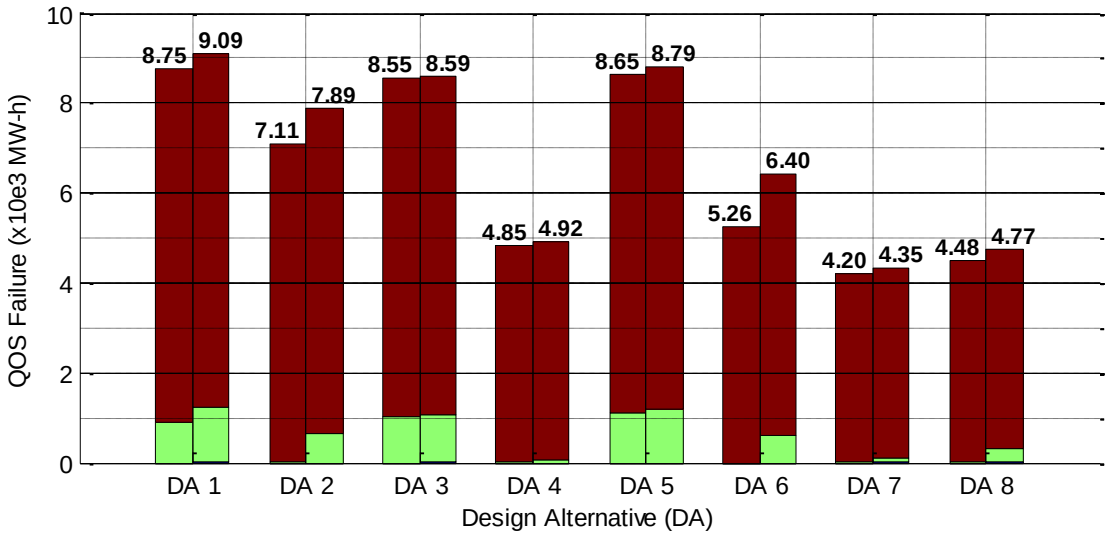

* The bar segments from bottom to top correspond to mission segment 1, 2, and 3, respectively. Since the scale of the QOS failure in mission segment 1 is far smaller than that in mission segment 2 and 3, it cannot be clearly shown in the bar chart. Detailed numerical information is available in Table B.3.

Figure 7.8 The MVAC ZEDS— the QOS failure determined by minimizing the QOS failure via the SOPSO (left) vs. the QOS failure obtained from minimizing the fuel consumption (right) of each design alternative, respectively

power generation capacity is managed to be very close to the load power; any PGM failure is likely to cause a power outage. However, by optimizing the CONOPS, the QOS failure can be significantly reduced by just increasing the fuel consumption a little bit, less than 10% for all the design alternatives. The changes of the CONOPS involve either adding one more small PGM in service all the time or dispatching the power generation in a way that every PGM works at a light loading condition (i.e., the probability of heating and bearing issues can be reduced.).

In the heavy loading condition such as mission segment 3, every design alternative encounters significant QOS failures because no backup PGMs are available at the moment. Any operating break of a PGM will result in a complete system power loss close to its power rating. In this situation, optimization of the CONOPS can barely

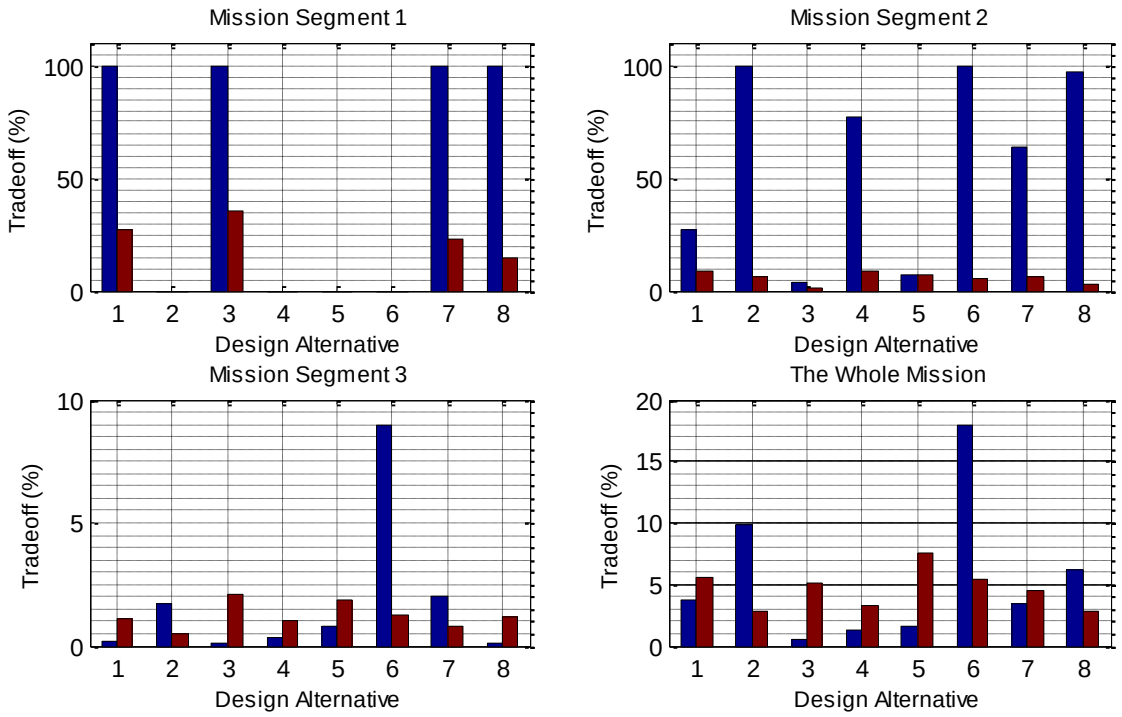

Figure 7.9 The MVAC ZEDS—the maximal percent decrease of the QOS failure by consuming more fuel (blue) vs. the corresponding percent increase in fuel consumption from the minimum value (red) of each design alternative, respectively

improve the system QOS for most of the design alternatives. The reduction of the QOS failure is just around 2%.

To conclude, the usage of the energy-based QOS metric indicates a favorable tradeoff relationship between the QOS and fuel consumption in light and medium loading conditions. The improvement of QOS is significantly noticeable because the CONOPS can be adjusted in a wide range. In heavy loading conditions, since all the PGMs run near full capacity, fine tuning of their operating setpoints does not contribute too much in terms of either fuel consumption or QOS enhancement. Considering that a typical ship mission is mostly composed of low-speed modes, we suggest employing this energy-

based QOS in evaluating the optimality of the shipboard generation plant in terms of power supply reliability.

The quality of the design alternatives in terms of the energy-based QOS for the MVDC system is compared in Figure 7.10. The performance tradeoffs between the QOS and fuel consumption are plotted in Figure 7.11. The numerical optimization results are available in Table B.4. Without considering reactive power generation, the PGMs in the dc system are operated at a lower power level, resulting in larger MTBF values and less MTTR breaks. This phenomenon is especially noticeable when the load power factor in the ac system is small. Therefore, the overall value of the QOS failure in the dc system is smaller than that in the ac system, by up to 15%. However, the conclusion about the performance tradeoffs derived from the ac system is still applicable for the dc system. In addition, in our design problem, the ac and dc systems share the same winner and loser design alternatives in terms of the energy-based QOS metric: design alternative 7 outperforms all the others, consistently suffering the least QOS failure; design alternative 1 is the worst choice for the given mission because it will most likely cause the highest value of the QOS failure. The quality of the design alternatives significantly differs: design alternative 7 is able to provide 93% better reliable service than design alternative 1.

7.6. Discussion of the Necessity to Implement Co-Optimization of the CONOPS

No matter which QOS metric is applied, we have always observed the tradeoffs of the QOS and fuel consumption when accounting for the CONOPS to evaluate the quality

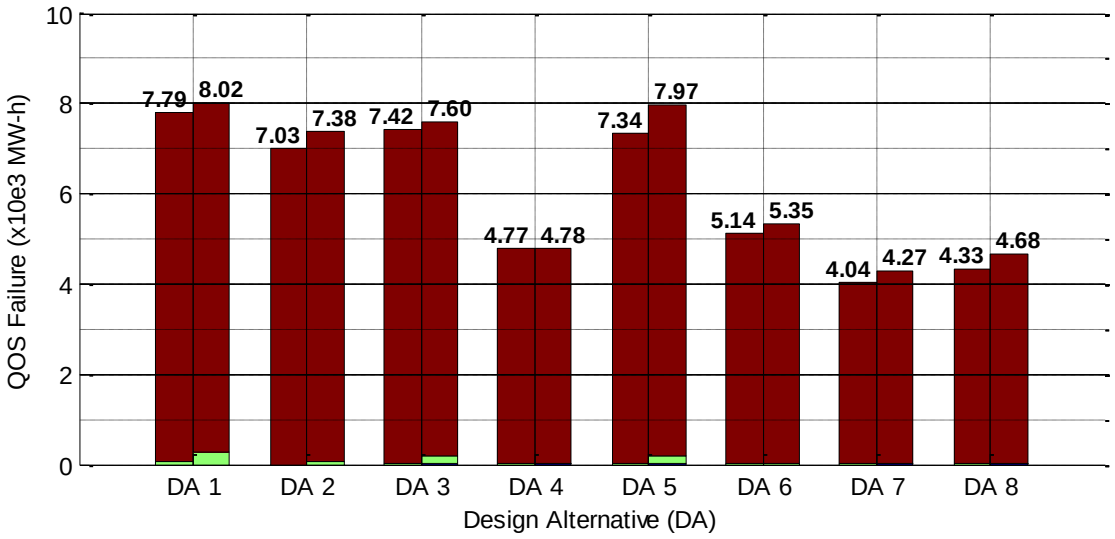

* The bar segments from bottom to top correspond to mission segment 1, 2, and 3, respectively. Since the scale of the QOS failure in mission segment 1 is far smaller than that in mission segment 2 and 3, it cannot be clearly shown in the bar chart. Detailed numerical information is available in Table B.4.

Figure 7.10 The MVDC ZEDS— the QOS failure determined by minimizing the QOS failure via the SOPSO (left) vs. the QOS failure obtained from minimizing the fuel consumption (right) of each design alternative, respectively

of a design alternative. This tradeoff is obviously large enough to affect acquisition decisions.

In Chapter 6, we identify design alternative 1 as the optimal selection of the shipboard power generation plant because compared with the others, it saves a considerable amount of fuel to complete the given mission. However, in this Chapter, we discover that design alternative 1 offers inferior QOS among all the design alternatives even with the optimal CONOPS. This decision conflict can never be discovered from either single objective optimization of the CONOPS. Instead, design alternative 2 and 7, which are regarded as mediocre choices in Chapter 6, are now identified to be the optimal solutions depending on the definition of the QOS metric.

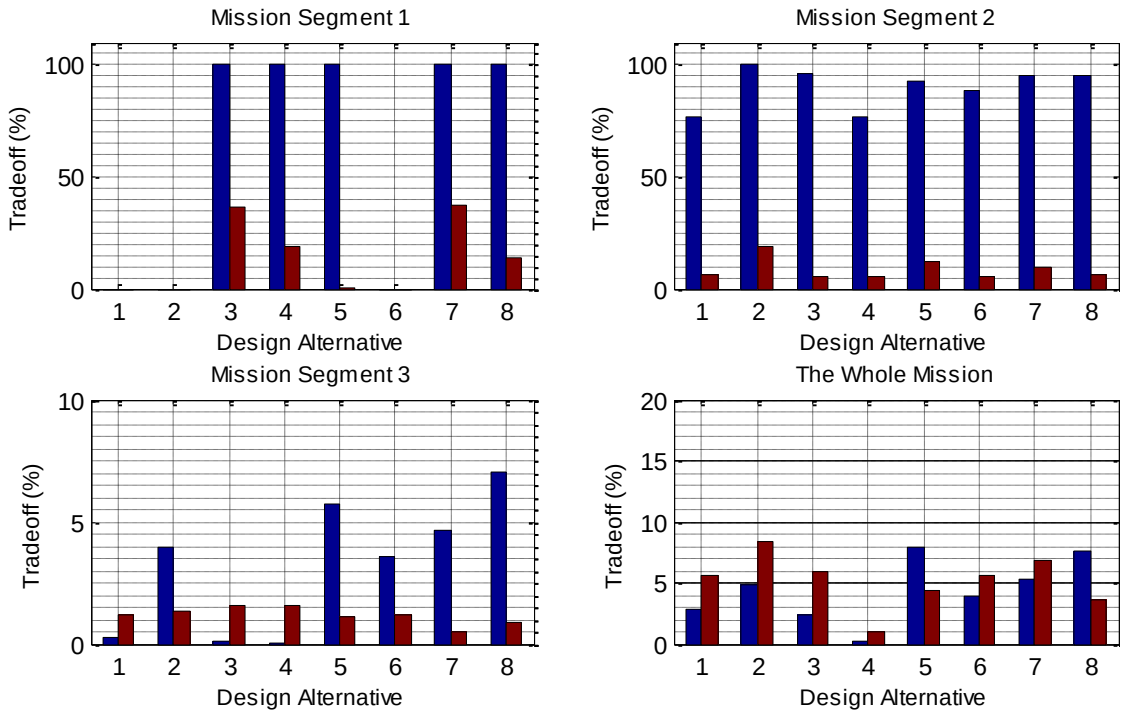

Figure 7.11 The MVDC ZEDS—the maximal percent decrease of the QOS failure by consuming more fuel (blue) vs. the corresponding percent increase in fuel consumption from the minimum value (red) of each design alternative, respectively

In fact, the quality of every design alternative in terms of one performance metric can be adjusted in a certain range depending on the choice of the CONOPS, but also constrained by the demanded value of the other performance metric. Therefore, in order to identify the real optimal CONOPS of a design alternative for a given mission, it is essential to co-optimize the QOS and fuel consumption. Further investigation will be continued in Chapter 8.

CHAPTER 8

IMPLEMENTATION OF THE CO-OPTIMIZATION APPROACH FOR THE CONCEPT EVALUATION METHOD

8.1. THEORETICAL BASIS OF OPTIMIZATION STRUCTURE

An optimization structure is developed in the form of hierarchical layers following the definition of control architecture. A hierarchical layer in the optimization structure describes the optimization method of a control function, which corresponds to a layer in the control architecture. Thus, the hierarchies in the optimization structure are also organized based on the temporal responses of control functions. Within a hierarchical layer, a certain number of optimization problem formulation structures are defined for the corresponding control function with respect to the individual performance metrics of interest. These performance metrics should be common to all the system applications at the corresponding control level. The mathematical model of an optimization problem is usually composed of an objective function subject to a set of system and component operating constraints. The objective function is formulated to calculate a specific performance metric in terms of the design variables identified in the control architecture.

The data processed in the optimization structure always conform to the five categories of data defined in Section 6.1 in spite of the specific mathematical models developed to process the data. For example, one may adopt different forms of the objective function and constraints to define the EDP for a particular micro-grid power

system application (see Section 3.1.1), but the data involved in the EDP always conform to the five categories. However, it has to be noted that, for different micro-grid system applications (e.g., ship, community power supply), the optimization structure may involve a different number of categories of data. For example, the *dynamic constraint* (i.e., generation redundancy) of the EDP can be eliminated for small scale power generation systems because they need all the installed PGMs turned on most of the time to be able to support the load. In addition, for different applications, the optimization structure may involve different performance metrics, affecting the development of the co-optimization structure. For example, the QOS optimization problem is not necessary to a system whose duration of the mission is far shorter than the MTBF values of its PGMs.

Since the determination of the CONOPS is carried out at the earliest design stage, this work has fairly low design fidelity, only considering the system steady state and neglecting any control implementation or stability issues. Therefore, we only consider one control function in the control architecture for the primary power generation and distribution level. Accordingly, we develop the optimization structure at this level with only one layer, including the formulation structure of the optimization problems with respect to fuel consumption and the QOS. Next, we will discuss the optimization problem formulation structures and identify their coupling relationship in the optimization structure for co-optimization.

8.2. Problem Formulation Structure of the Economic Dispatch Problem

The problem formulation structure of the EDP is plotted in Figure 8.1. The essential data required for the problem formulation cover all the five categories. The

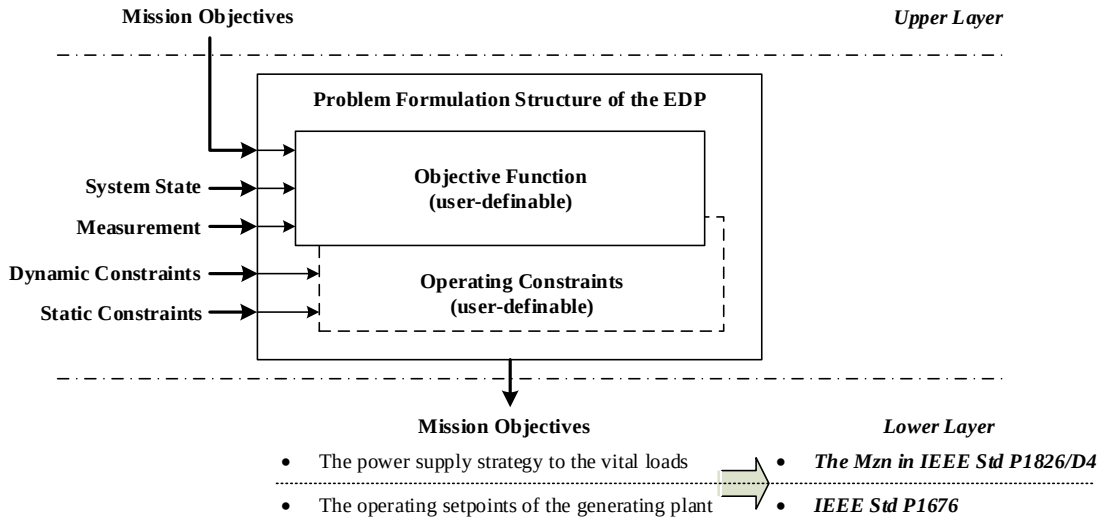

Figure 8.1 The block diagram of the problem formulation structure of the EDP

Table 8.1 Parameter list of the problem formulation structure of the EDP

Category of Data	**Required Parameter Information**	
Mission Objective	Electrical mission profile describing the power demands for each mission segment of the micro-grid power system	
System State	• Electrical architecture type (AV/DC) • The number of primary power distribution buses • The coupling location and operating status of the PDMs and PCMs • Online status of the non-vital loads for each primary distribution buses	
Static Constraint	• Power ratings of the PGMs • Operating ranges of the PGMs' power factors	
	Required Parameter Information	**Optional Parameter Information**
Measurement	• Generators' power efficiency curves • Prime Movers' thermal efficiency curves	• Start-up fuel consumption of the PGMs • Power efficiency curves of the PDMs and PCMs
Dynamic Constraint	Vital load profile	The minimum required number of online PGMs

setpoint variables are the design variables of the EDP, involved in the objective functions and operating constraints (not shown in the figure). The data of the other four categories are treated as regular parameters in the EDP. Their values are determined by the

equipment database available to the designers, the system concept under study, and the system application background, as explained in detail in Table 8.1.

The optional information of *measurement* and *dynamic constraints* is for improving the calculation accuracy. We have defined typical values of these parameters in the optimization process as follows: the efficiency of PDMs and PCMs are regarded to be constant at any operating power; the minimum required number of online PGMs is always considered to be two; the startup fuel consumption of PGMs is neglected. However, one is also free to provide user-preferred values instead, if necessary. The derived solution of the EDP prepares the *mission objectives* for the components in the ZEDS and for the power electronic devices to implement (i.e., these operations should follow the IEEE Std P1826/D4 and IEEE Std 1676).

8.3. Problem Formulation Structure of the QOS Optimization Problem

Similarly, all the five categories of data are required to construct the problem formulation structure of the QOS optimization problem, as shown in Figure 8.2. This figure also demonstrates an example that the categories of data defined with a problem formulation structure accommodate different mathematical models of the objective functions. The specific data required for evaluating a generic metric of the QOS is explained in Table 8.2. No matter which QOS metric—probability-based or energy-based—is employed, *mission objectives*, *measurements* and *static constraints* are required to generate the MTBF values of the online PGMs; *system states* and *dynamic constraints* are required to modify the equation format for specific system concepts and to generate optimization constraints. For probability-based QOS metric, *mission*

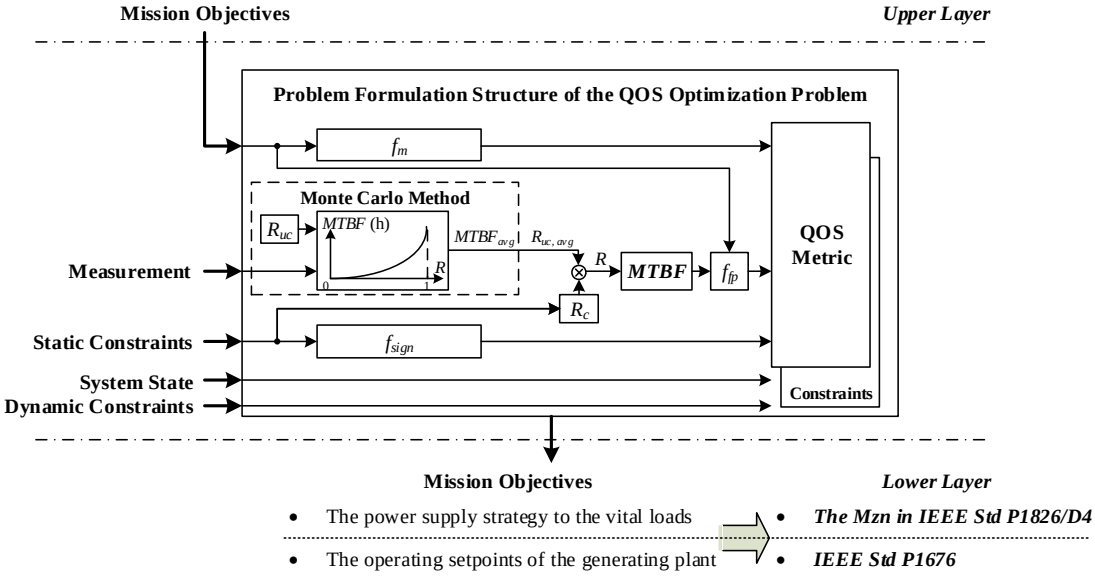

(a) Based on the probability-based QOS metric

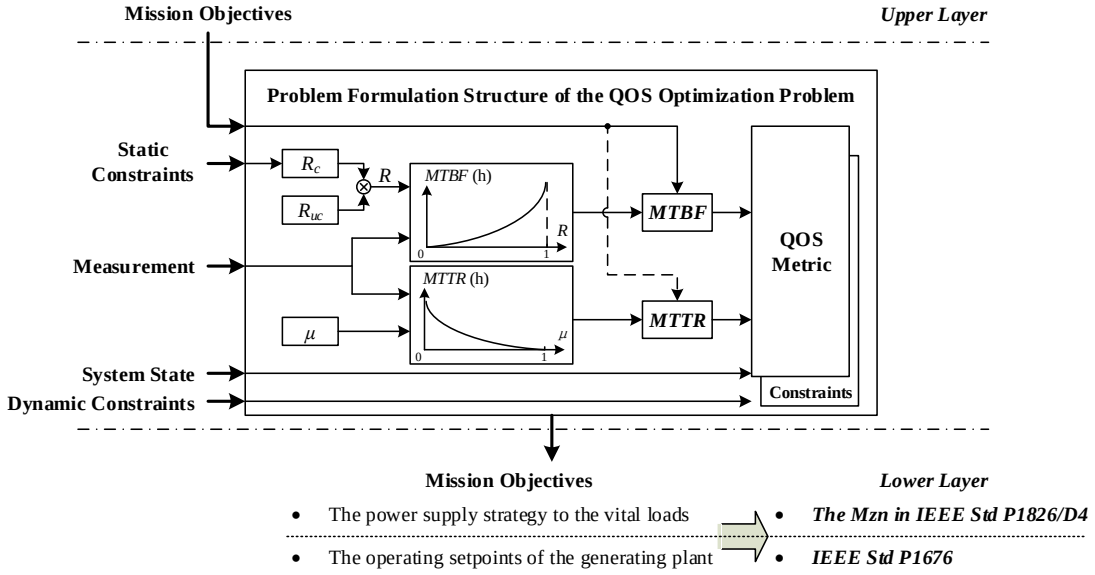

(b) Based on the energy-based QOS metric

Figure 8.2 The block diagram of the problem formulation structure of the QOS optimization problem

objectives is also used to determine a weight factor of the QOS failure metric in each mission segment. In contrast, energy-based QOS metric also uses *mission objectives* to

Table 8.2 Parameter list of the problem formulation structure of the QOS optimization problem

Category of Data	**Required Parameter Information**	
Mission Objective	Electrical mission profile describing the power demands for each mission segment of the micro-grid power system	
System State	• The number of primary power distribution buses • Online status of the non-vital loads for each primary distribution buses	
Static Constraint	• Power ratings of the PGMs • Operating ranges of the PGMs' power factors	
Measurement	Reference points of the MTBF values for fitting the distribution models	
	Required Parameter Information	**Optional Parameter Information**
Dynamic Constraint	Vital load profile	The minimum required number of online PGMs

determine the number of MTBF and MTTR breaks.

The design variables of this problem formulation structure are still the *setpoint variables*. Different from the problem formulation structure of the EDP, the output here determines the optimal CONOPS that is intended to maximize the system QOS. The output is also regarded as the *mission objectives* of the lower level components. This structure shares the same data requirements of the *static constraints* and *dynamic constraints* with that of the EDP for reflecting the system and equipment operating limits.

8.4. DEVELOPMENT OF OPTIMIZATION STRUCTURE

We develop the complete optimization structure for the primary power generation and distribution level, as shown in Figure 8.3, to identify the co-optimizing algorithm of the performance metrics.

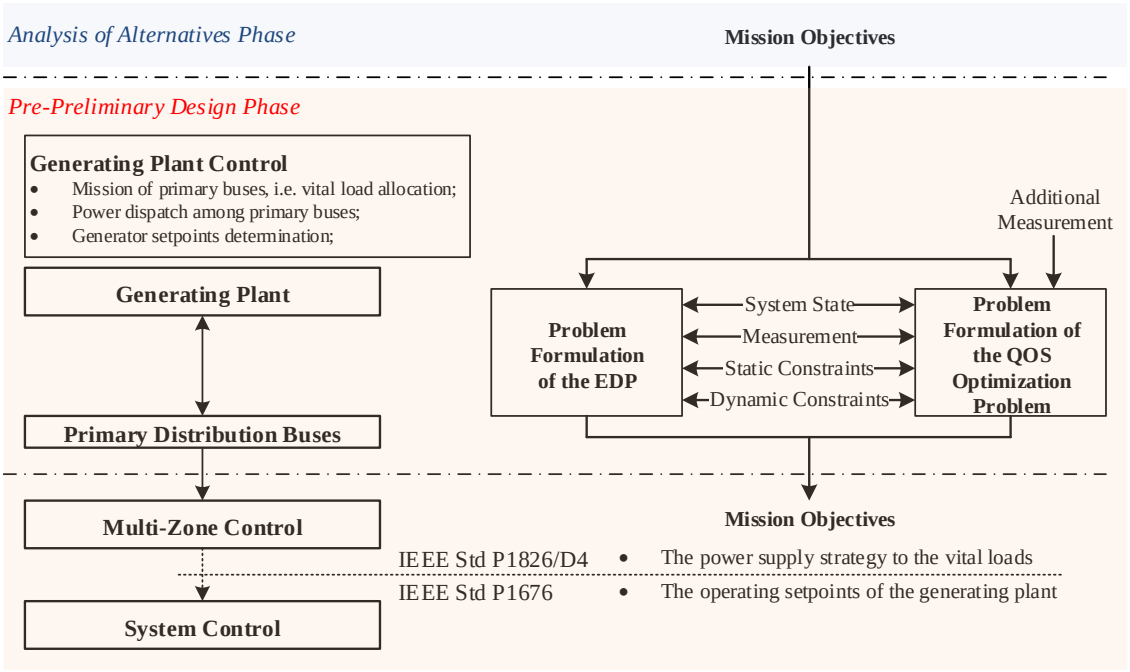

Figure 8.3 The block diagram of the optimization structure for the primary power generation and distribution level (right) corresponding to the control architecture for the same level (left)

The left block diagram is the control architecture that we develop to reflect the control function at the primary power generation and distribution level. The right block diagram is the optimization structure containing the optimization design methods for that control function. As we can see, the two optimization problems share most parameter data that are used to characterize a system concept and a design alternative, except that the QOS optimization problem needs to collect additional *measurements* for identifying reliability and maintainability distribution models of the PGMs.

8.5. Development of Data Structure for Software Implementation of the Co-Optimization Process

The optimization structure can be imposed on any regular system concept (see Section 4.1). In order to automatically implement this procedure, we suggest the software

coupling method between S3D and MATLAB as follows. The corresponding data structure is shown in Figure 8.4.

1) As the prerequisite to the design of a micro-grid power generation plant, an electrical mission profile of the power system should be determined prior to the design phase of Analysis of Alternative [5][6]. This work can be done by simulating the system dynamics in a series of scheduled operating scenarios through an appropriate engineering software tool (e.g., VTB). A mission segment defines the fraction of time or specific period of time, during which the power system is regarded to demand an approximately constant power. This power value is determined by both the electric power for carrying out the desired system dynamics and kinetics (e.g., ship speed) and the estimated power consumed by the lumped electric loads. Since the optimization problem of the CONOPS is formulated and resolved in MATLAB, the generated mission profile should be directly readable by MATLAB, or it should be read, filed, and then delivered to MATLAB with the other data as a bundle by S3D later.
2) S3D provides a collaborative simulation environment for building system concepts. For a created topology of architecture, MATLAB needs to formulate the co-optimization problem of the CONOPS for every independent primary distribution bus (PDB). To this end, the *system states* and *measurements* that characterize the PDBs should be collected and provided to MATLAB. Specifically, the *system states* should be sufficient to quantify the amount of independent PDBs; the *measurements* should be able to describe the loading

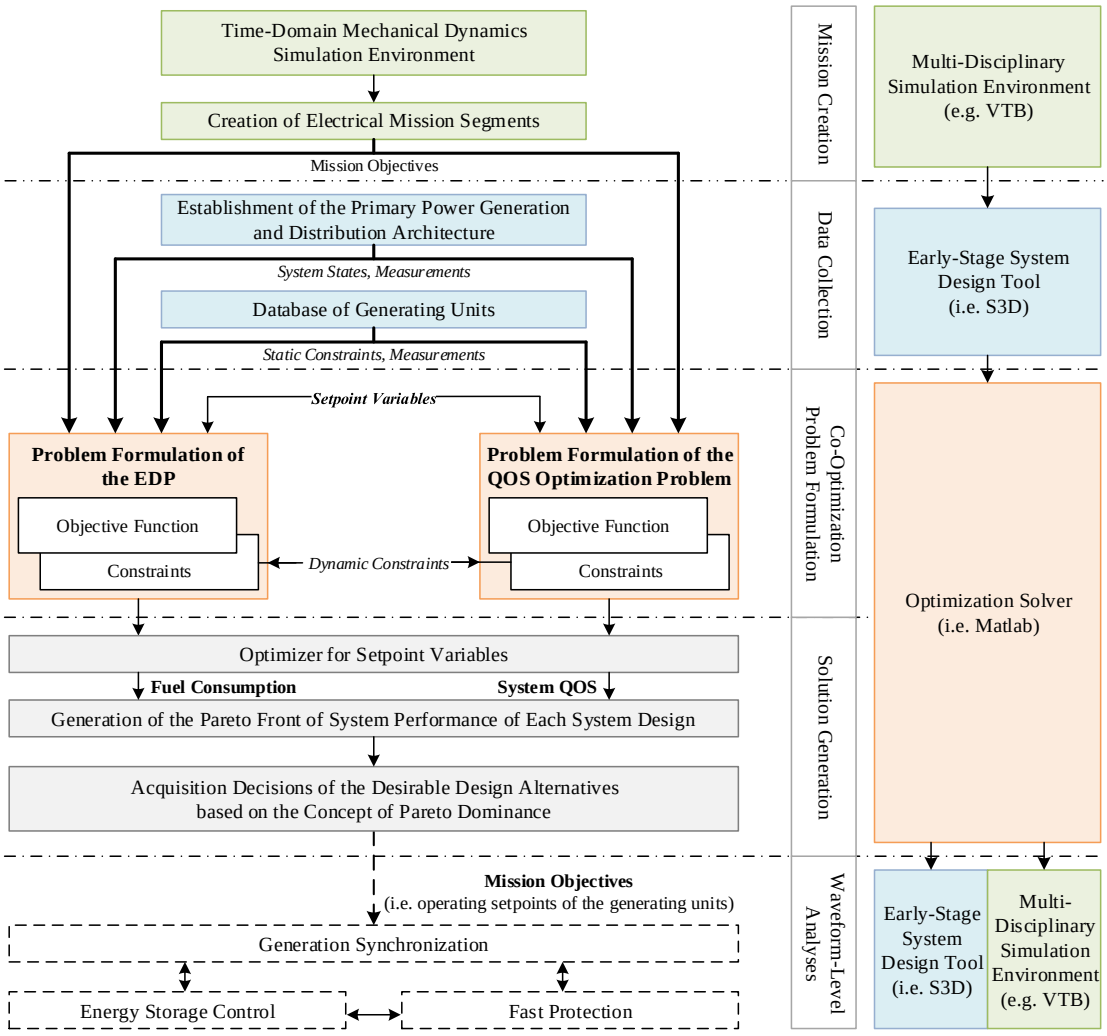

Figure 8.4 The block diagram of the data structure for software implementation of SBD accounting for the co-optimization of the CONOPS

condition of each independent PDB during a mission segment and to approximate the steady-state efficiencies of the power modules. In some cases, *measurements* should also inform MATLAB of the amount of non-vital and vital loads in service for every mission segment because their power supply strategies are treated differently in the problem formulation. A non-vital load is regarded to always receive power from one fixed PDB, while a

vital load has multiple channels to obtain power from all the buses. The data transmission from S3D to MATLAB can be realized in two different ways:

   a. S3D directly sends the *system states* and *measurements* to MATLAB for identifying the distribution architecture of a system concept;
   b. S3D first analyzes the *system states* and *measurements*, and then sends the derived conclusion (i.e., quantity of independent PDBs, loading conditions of PDBs, and online non-vital loads) to MATLAB.

3) S3D also provides MATLAB with the database of PGMs to explore the design space (i.e., produce feasible design alternatives). MATLAB should be able to know the operating characteristics (e.g., efficiency, reliability rate, maintenance rate) of the PGM candidates in order to formulate the objective functions of the optimization problems, and to know the operating limits (e.g., the nameplate ratings, valid ranges of the power factor) of the PGMs to formulate the optimization constraints. These two pieces of information also need to be delivered to MATLAB from S3D.
4) Based on the data received from S3D (and VTB), MATLAB starts formulating the co-optimization problem for each independent PDB of every design alternative. When more than one independent PDB exist, there might be several possibilities to distribute PGMs among them. We suggest two rules to address this concern:

   a. The generation capacity assigned to each PDB must be sufficient for the power demands of the loads connected to that bus during any mission segment;

Table 8.3 The concept of Pareto dominance when applying a MOPSO to the EDP and QOS optimization problem

For A design alternative of a PGM combination $P=(P_1, \cdots, P_k)$, a set of *setpoint variables* $V=[P_{gout,1},\cdots,P_{gout,k} \quad pf_1,\cdots pf_k \quad u_1,\cdots,u_k \quad v_1,\cdots,v_k]$ is said to dominate another set $V^*=[P^*_{gout,1},\cdots,P^*_{gout,k} \quad pf_1^*,\cdots pf_k^* \quad u_1^*,\cdots,u_k^* \quad v_k^*,\cdots,v_k^*]$ if and only if $f=\left[f_{EDP} \quad \frac{1}{QOS} \right]$ is partially less than $f^*=\left[f^*_{EDP} \quad \frac{1}{QOS^*} \right]$, i.e., $\left[\left(f_{EDP} \le f^*_{EDP} \right) \wedge \left(\frac{1}{QOS} \le \frac{1}{QOS^*} \right) \right] \wedge \left[\left(f_{EDP} < f^*_{EDP} \right) \vee \left(\frac{1}{QOS} < \frac{1}{QOS^*} \right) \right]$, where

$P_{gout,\,k}$ is the real power output of PGM *k*;

pf_k is the power factor of PGM *k*;

u_k is the online status (0=offline, 1=online) of PGM *k*;

v_k is the power factor status (0=lagging, 1=leading) of PGM *k*;

f_{EDP} is the fuel consumption derived from the EDP defined in (24);

QOS is the solution to the QOS metric defined in (42) or (46).

b. The generation capacity of each design alternative will be distributed among the PDBs as evenly as possible, so as to guarantee the most balanced power supply;

5) During the co-optimization of the *setpoint variables* in MATLAB, we employ the concept of Pareto Front to identify the optimal tradeoffs of the performance metrics. The Pareto front is determined by applying the concept of Pareto dominance to all feasible setpoint values that satisfy the constraints of the co-optimization problem. The setpoints, at which the performance tradeoffs are not fully dominated, are picked to construct the Pareto front, as explained in Table 8.3. By comparing the Pareto fronts of all design

alternatives, one can find the design alternatives that outperform the others and their advantageous operating areas. This step is indicated as "Solution Generation" in Figure 8.4. MATLAB generates a 2D Cartesian coordinate system to help visualize the performance dominance among individual CONOPSs of each design alternative and the performance dominance among design alternatives.

This work is of great help for software engineers to understand which data should be processed and communicated at the coupling interface between S3D and MATLAB, so that SBD accounting for the co-optimization problem of the CONOPS can be automatically implemented via software at the earliest design stage. The software demo will be developed in our future work.

8.6. CONCEPT EVALUATION VIA CO-OPTIMIZATION OF THE ECONOMIC DISPATCH PROBLEM AND QOS OPTIMIZATION PROBLEM

The objective functions and constraints of our co-optimization problem are highly nonlinear, discontinuous, and non-convex. Both equality and inequality constraints exist. Even the MOPSO improved in Section 5.3 cannot solve this type of problem. As a result, we develop a method to convert the original problem into some sub-problems only containing the real *setpoint variables*. Specifically, for each system concept, all feasible combinations of online PGMs are enumerated.

For each system concept and mission segment, all possible combinations of the online PGMs are first generated through dynamic programming. And then, each combination is evaluated against three conditions in sequence: 1) whether it contains the number of PGMs more than the minimum required value; 2) whether its generation

capacity is large enough to support the load; 3) whether its generation capacity is still large enough to support the lumped vital loads when the largest online PGM suddenly fails. Only the combinations satisfying all the conditions are regarded to be "feasible". Finally, the EDP and QOS optimization problem are only formulated for each feasible combination. The logic flow chart of this enumeration process is shown in Figure 8.5. In addition, we set all the PGMs only working with lagging power factors because we observe from the single-objective optimization that if any PGM has a leading power factor, the system performance in terms of fuel consumption will be considerably compromised. Accordingly, the EDP and QOS optimization problem no longer contain any binary variables. Then we can directly apply our developed MOPSO for solutions. The parameter settings of the MOPSO are given in Table 8.4.

8.6.1. Employment of the Probability-Based QOS Metric

All types of quasi-optimal performance tradeoffs that each design alternative is able to achieve in every mission segment are shown through Figure 8.10 to Figure 8.12 for the MVAC ZEDS and from Figure 8.13 to Figure 8.15 for the MVDC ZEDS. For a mission segment, each dot corresponds to a type of optimized CONOPS. In other words, for that mission segment, there exists no other eligible CONOPS that is able to yield both lower fuel consumption and higher QOS. We refer to the CONOPS corresponding to a dot as the "non-dominated" CONOPS, and refer to the contour formed by the dots as the "Pareto front" of system performance.

As we can see, the border values on the Pareto front of every design alternative accurately match the solutions derived through the single-objective optimization problems. The percent error is less than 2% in the worst-case scenario. The CONOPS corresponding to the border values of a Pareto front yield the two types of extreme

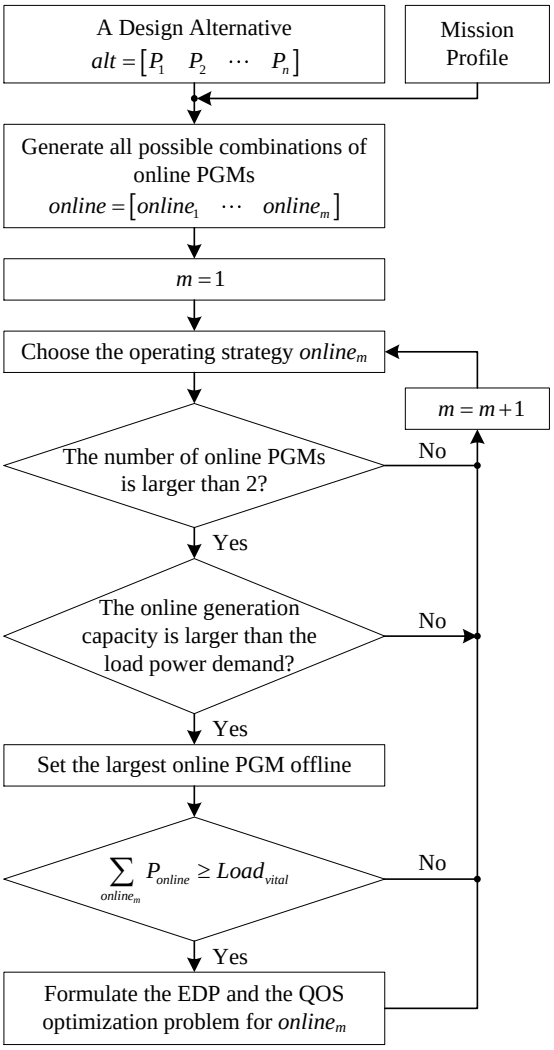

Figure 8.5 The data flow chart of converting the mixed-integer co-optimization problem into the sub-problems only containing the real variables

performance tradeoffs (i.e., the CONOPS of the leftmost border value requires the smallest fuel consumption but yields the lowest QOS, while the CONOPS of the rightmost border value demands the largest fuel consumption but yields the highest QOS). The other CONOPS on a Pareto front yield non-dominated performance tradeoffs at different degrees (i.e., a certain degree of increase in the QOS causes a certain amount of increase in fuel consumption).

Table 8.4 The parameter settings of the MOPSO

Population	150
Inertia Weight, w	$w_{\max} = 0.9, \quad w_{\min} = 0.4$
Mutation Rate	0.1
The Number of Iterations	10000

We have to follow two steps in order to integrate the Pareto fronts of the mission segments to generate the Pareto front for the whole mission:

1) Generate all possible combinations that include one dot on the Pareto front from each mission segment;
2) Apply the concept of Pareto dominance to identify the Pareto front among all the combinations.

The Pareto fronts of the design alternatives for the MVAC and MVDC ZEDS are compared in Figure 8.6 and Figure 8.7, respectively. The *x*-axis denotes the average fuel consumption rate over the whole mission. The *y*-axis denotes the aggregate value of the QOS of the mission segments. The contour of the Pareto front is a monotonically increasing curve, which can be generally divided into three segment types for identifying the optimal CONOPS of a design alternative according to the stakeholders' preference on the performance metrics:

1) When one puts more emphasis on reducing fuel consumption, he should choose the CONOPS corresponding to the dot located at leftmost end of a contour segment with a slow changing rate. Compared with the other dots on the contour segment, this dot is able to reduce a huge amount of fuel by causing just a moderate compromise of the QOS.

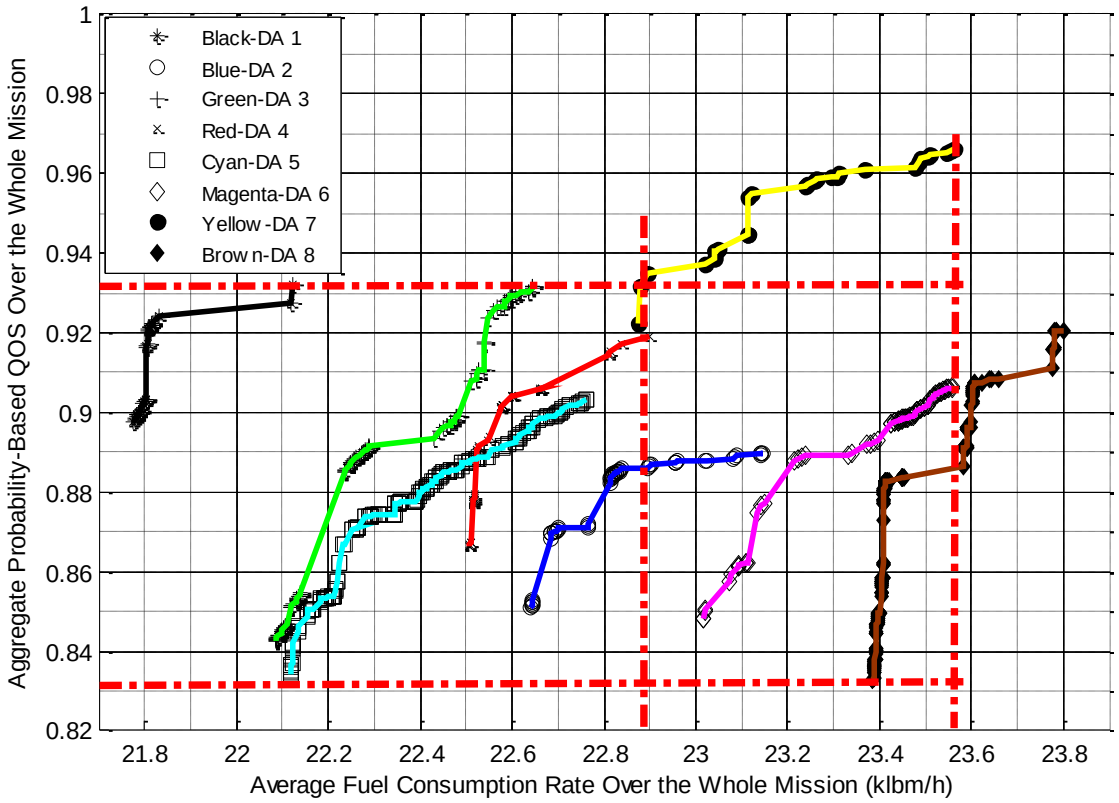

Figure 8.6 Comparison of the Pareto fronts of all the design alternatives (DAs) over the whole mission for the MVAC ZEDS, based on the probability-based QOS metric

2) When one puts more emphasis on improving the QOS, he should choose the CONOPS corresponding to the dot located at the rightmost end of a contour segment with a fast changing rate. Compared with the other dots on the contour segment, this dot is able to considerably increase the QOS by just consuming a negligible amount of more fuel.

3) If both performance metrics are weighted equally, the CONOPS corresponding to the dots located at a contour segment with a medium changing rate should be chosen. The dots on the contour segment indicate that an improvement of either performance metric will not cause a considerable compromise of the other.

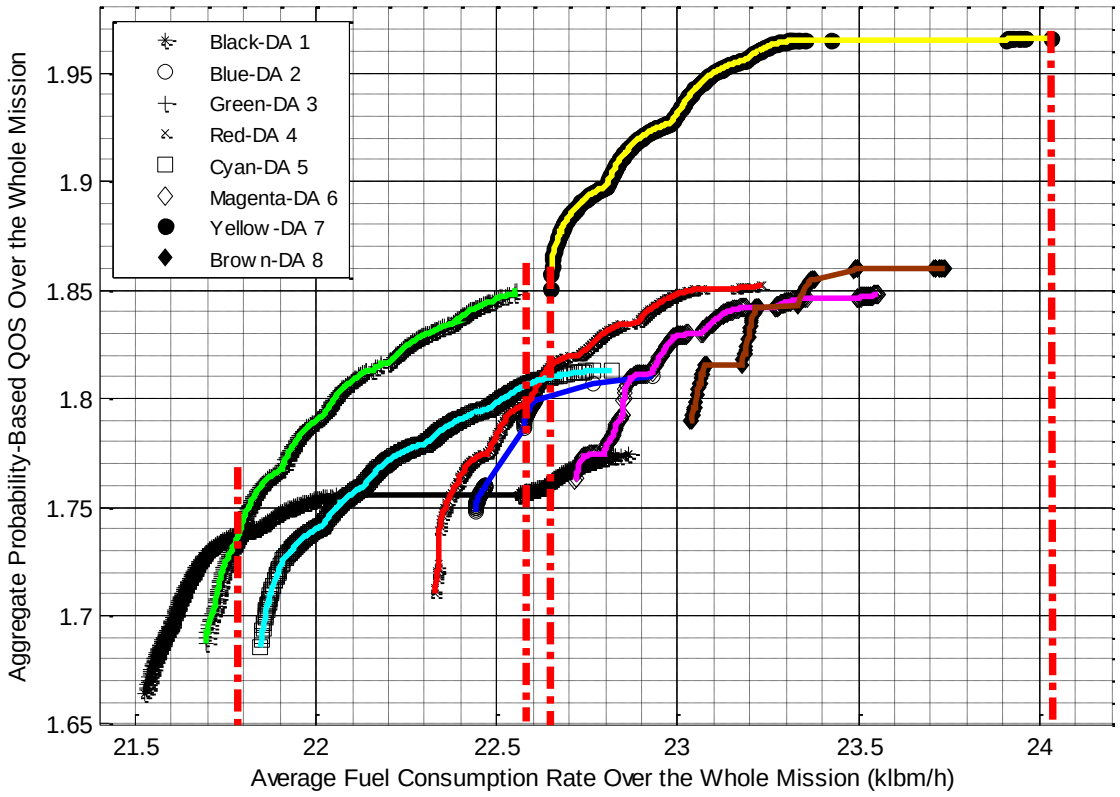

Figure 8.7 Comparison of the Pareto fronts of all the design alternatives (DAs) over the whole mission for the MVDC ZEDS, based on the probability-based QOS metric

From Figure 8.6 we can see that based on the choice of the CONOPS, every design alternative is able to complete the mission with low fuel consumption, or high QOS, or somewhere in between. However, design alternative 1 outperforms the others when the QOS is below 0.932 because it always consumes the lowest fuel with the appropriate CONOPS. When the system QOS is required to reach above 0.932, design alternative 7 stands out because all the other design alternatives cannot yield that high QOS no matter how much fuel is consumed. Apparently, design alternative 1 and 7 always dominate the other design alternatives at certain points but neither completely dominates the other. Therefore, we can conclude that for our defined mission, when the probability-based QOS and fuel consumption are evaluated, design alternative 1 and 7 are

the quasi-optimal choices for the shipboard generation plant, yielding non-comparable performances.

For the MVDC ZEDS, besides design alternative 1 and 7, design alternative 3 is also one quasi-optimal choice for certain performance requirements. When the average fuel consumption rate is limited between 21.78 klbm/h and 22.59 klbm/h, design alternative 3 generates the highest QOS compared to the others, as shown in Figure 8.7. Apparently, for a given mission and system concept, the quality of a design alternative is also affected by the electric architecture. This effect can be directly investigated at the earliest design stage by applying our concept evaluation method.

8.6.2. Employment of the Energy-Based QOS Metric

When the energy-based QOS metric is used, the Pareto fronts of the design alternatives for the mission segments are shown through Figure 8.16 to Figure 8.19 for the MVAC ZEDS and through Figure 8.20 to Figure 8.23 for the MVDC ZEDS. The *x*-axis still denotes the average fuel consumption rate over the whole mission, but the *y*-axis denotes the aggregate value of the QOS failure of the mission segments. The percent errors of the border values compared to the results obtained through the single-objective optimization problems are always limited within 3%. One is still able to use the decision philosophy introduced in Section 8.6.1 to pick the optimal CONOPS for each design alternative.

For the MVAC ZEDS, the Pareto fronts of the design alternatives for the whole mission are compared in Figure 8.8. There are four non-dominated design alternatives representing distinct types of performance tradeoffs at different degrees. Design alternative 1 has an overwhelming advantage in saving fuel but offers horrible QOS. When the average fuel consumption rate is allowed to be slightly increased up to

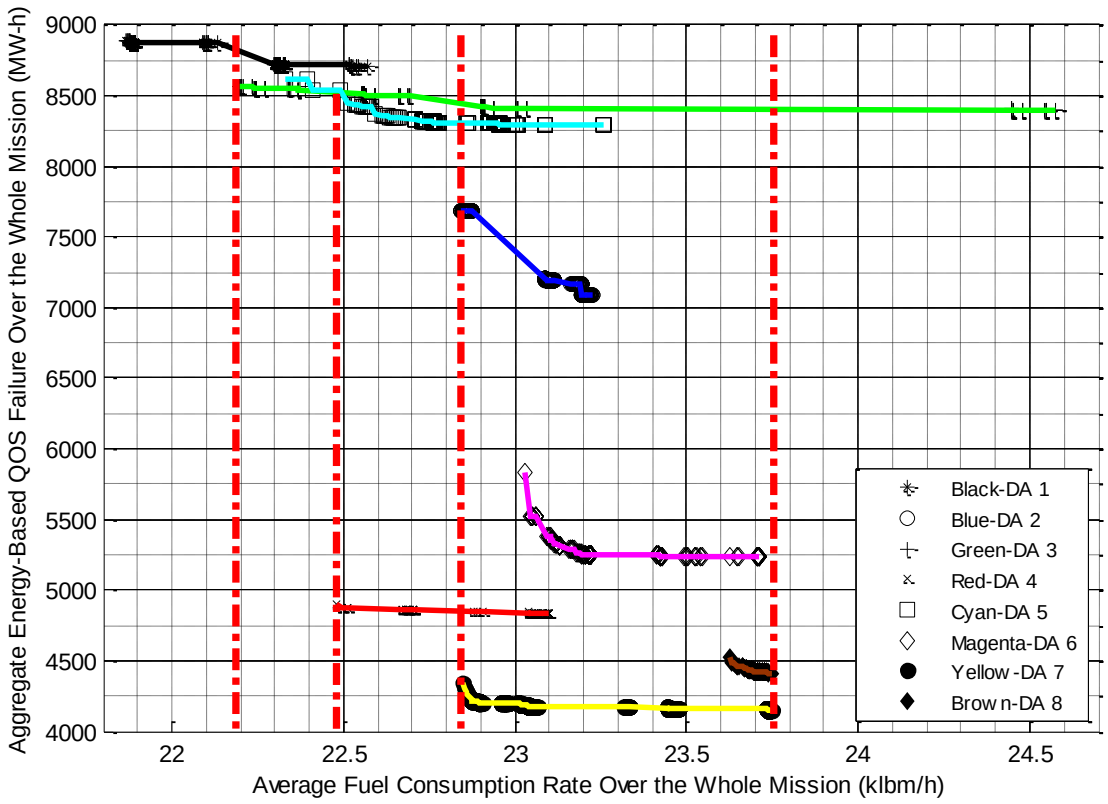

Figure 8.8 Comparison of the Pareto fronts of all the design alternatives (DAs) over the whole mission for the MVAC ZEDS, based on the energy-based QOS metric

22.19 klbm/h, design alternative 3 starts dominating all the others because it is able to limit the QOS failure to the relatively minimum level. When the average fuel consumption rate reaches 22.49 klbm/h, design alternative 4 becomes the optimal choice of the power generation plant. It can reduce the QOS failure value caused by the other design alternatives by at least 40%. When the fuel consumption rate of the ship is allowed to go higher than 22.84 klbm/h, design alternative 7 turns out to be the absolute optimal choice, which is able to further reduce the QOS failure.

As compared to the MVAC ZEDS, the MVDC ZEDS substitutes design alternative 5 for design alternative 3 as one of the quasi-optimal choices, as shown in

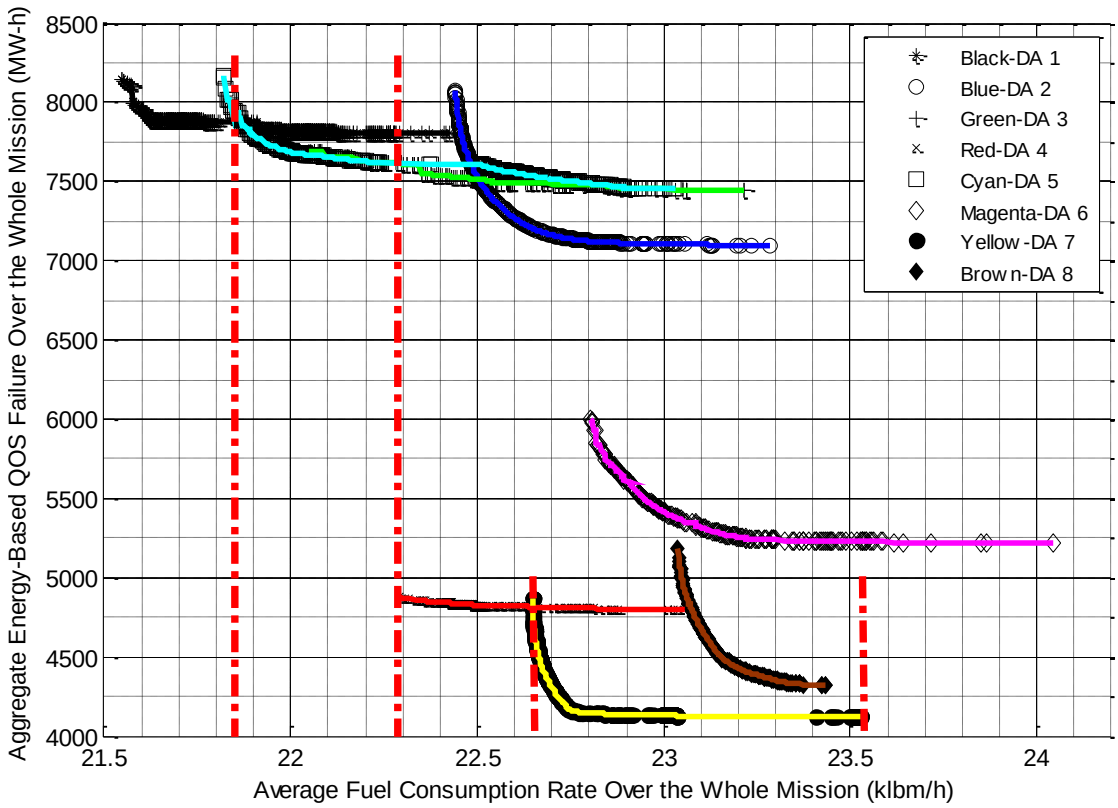

Figure 8.9 Comparison of the Pareto fronts of all the design alternatives (DAs) over the whole mission for the MVDC ZEDS, based on the energy-based QOS metric

Figure 8.9. In addition, we also observe the different performance tradeoffs yielded by the same quasi-optimal design alternatives, namely, design alternative 1, 4, and 7, in the ac and dc system. For example, design alternative 1 is only regarded as being optimal for the dc system when the average fuel consumption rate is less than 21.86 klbm/h (other than 22.19 klbm/h in the ac system).

To sum up, the selection of a design alternative at the earliest stage has predetermined the performance a system design can best achieve in the final product and also commits the costs to obtain the performance. It is very important to inform stakeholders with this information as early as possible, so that they do not waste large

investments on developing the detailed power electronic applications. Our concept evaluation method considering the optimization of the CONOPS has been successfully demonstrated to assist stakeholders' with acquisition decisions at the earliest design stage by visualizing the quality comparison.

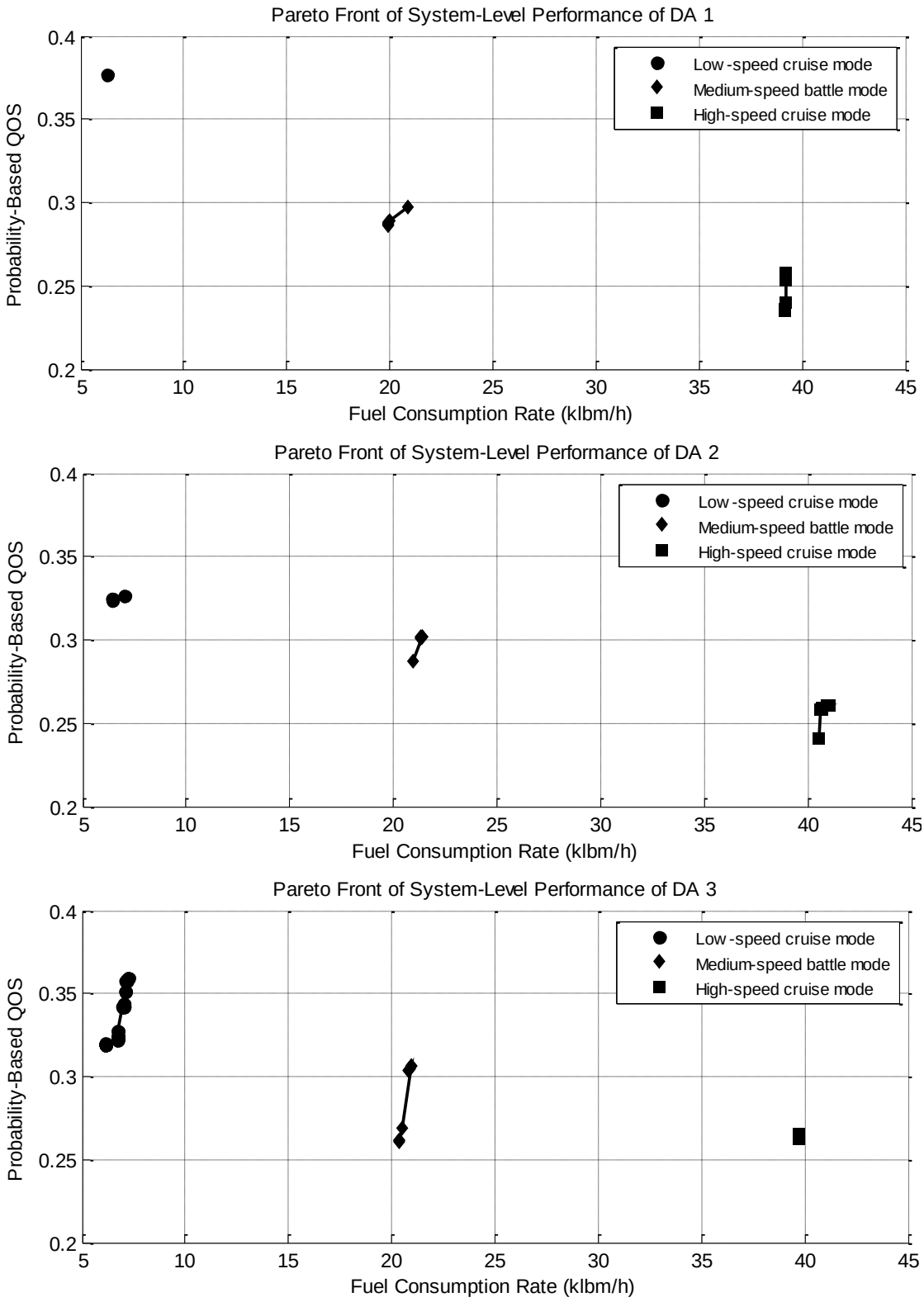

Figure 8.10 The MVAC ZEDS—the Pareto fronts for the mission segments of design alternative 1, 2, and 3, based on the probability-based QOS metric

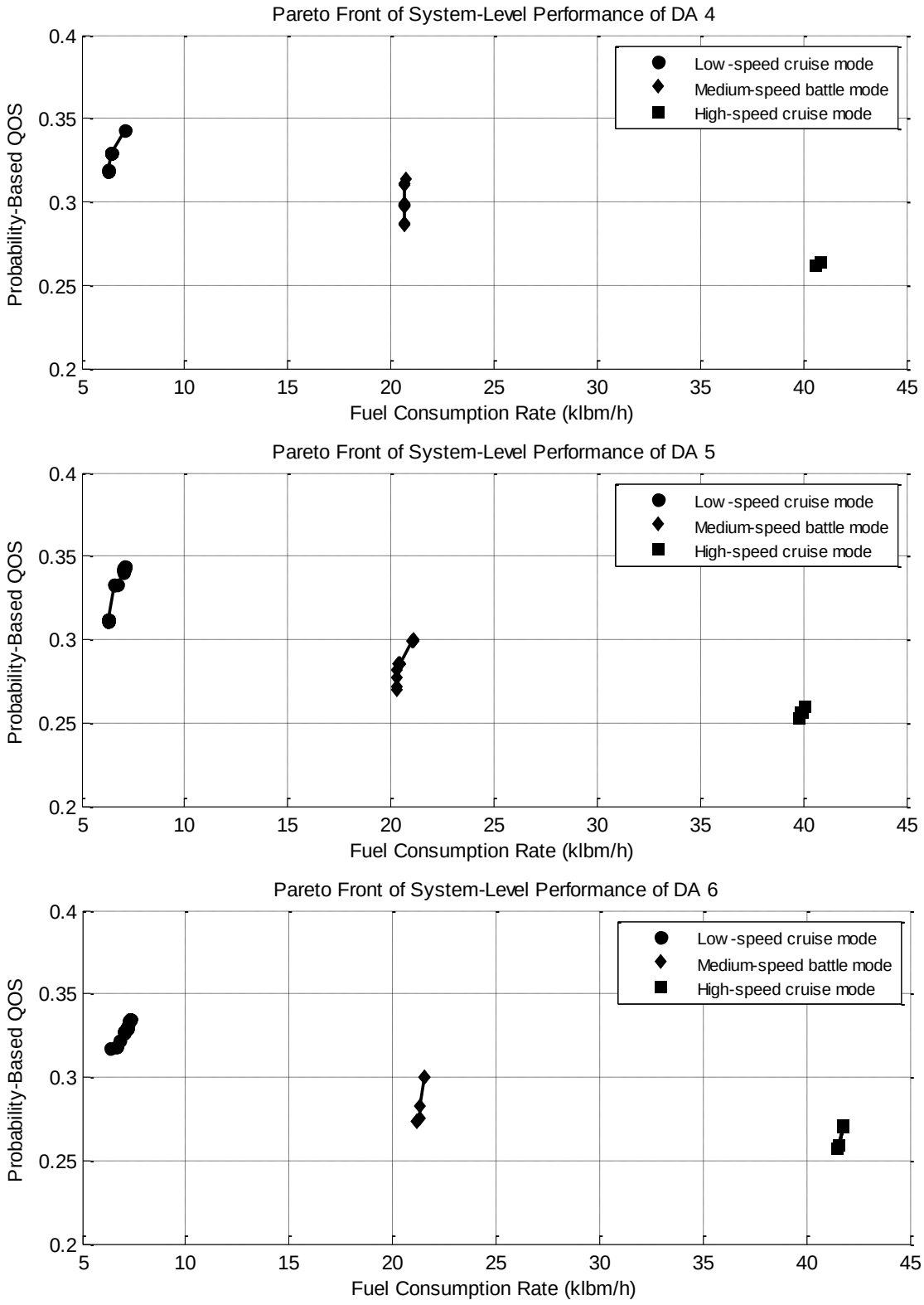

Figure 8.11 The MVAC ZEDS—the Pareto fronts for the mission segments of design alternative 4, 5, and 6, based on the probability-based QOS metric

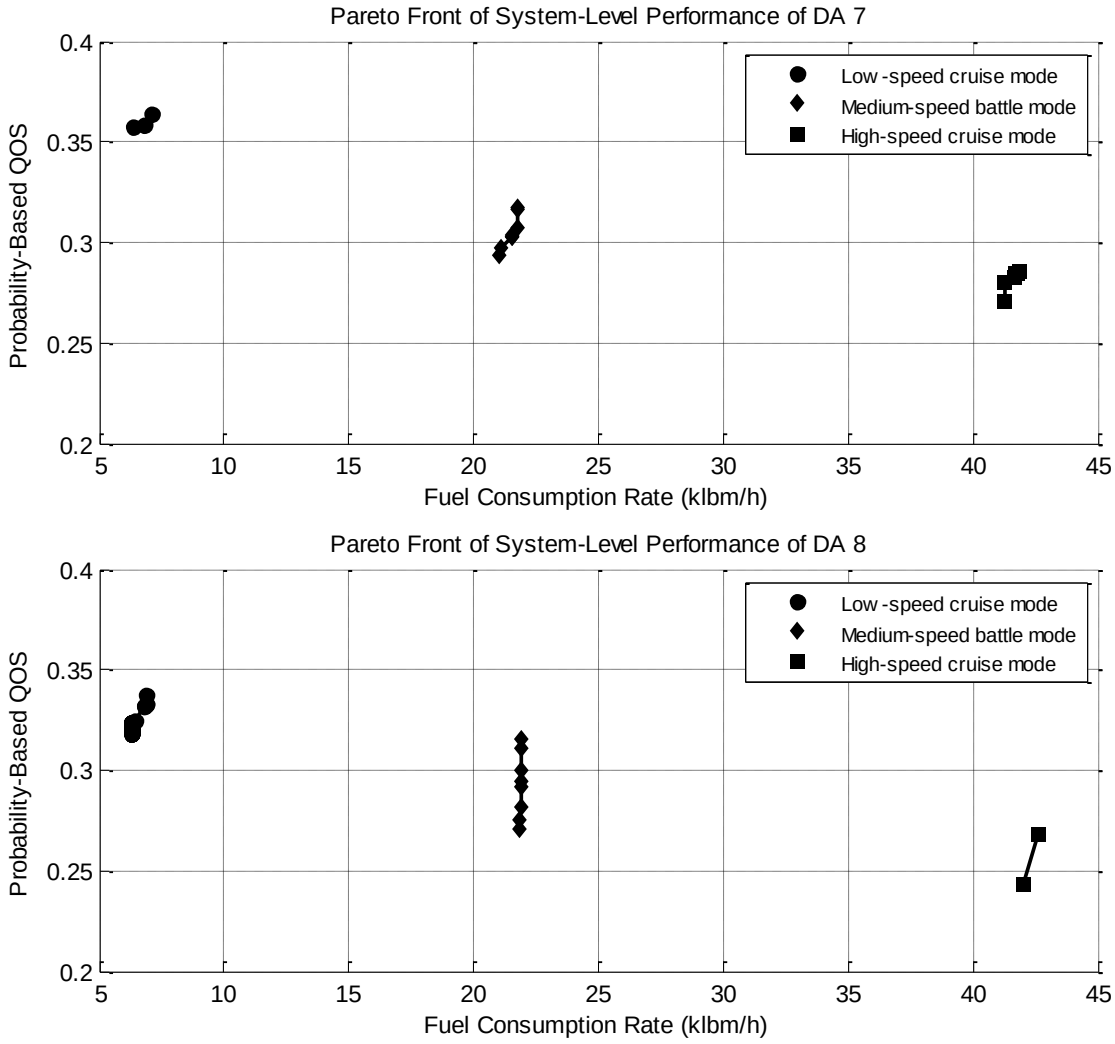

Figure 8.12 The MVAC ZEDS—the Pareto fronts for the mission segments of design alternative 7 and 8, based on the probability-based QOS metric

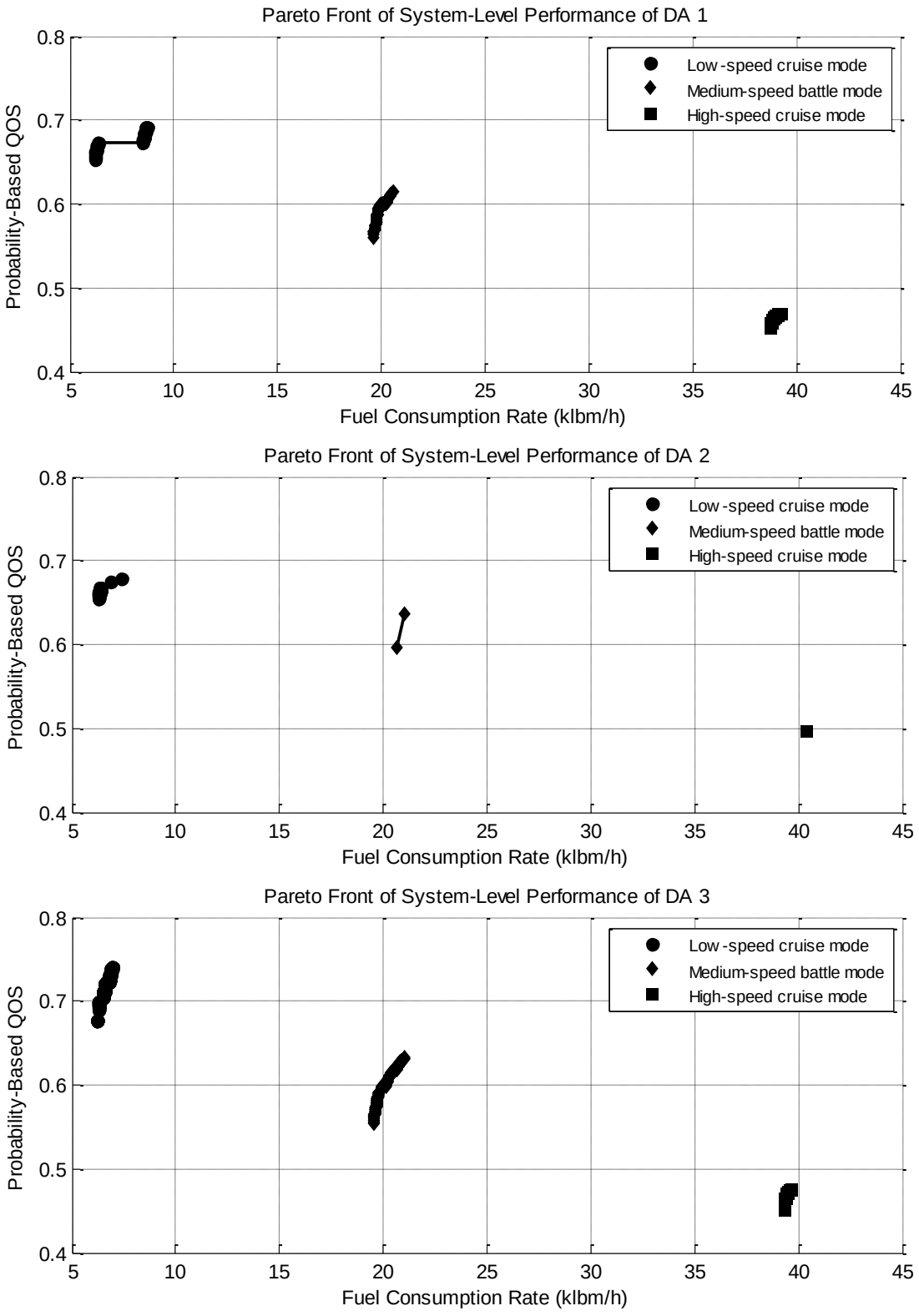

Figure 8.13 The MVDC ZEDS—the Pareto fronts for the mission segments of design alternative 1, 2, and 3, based on the probability-based QOS metric

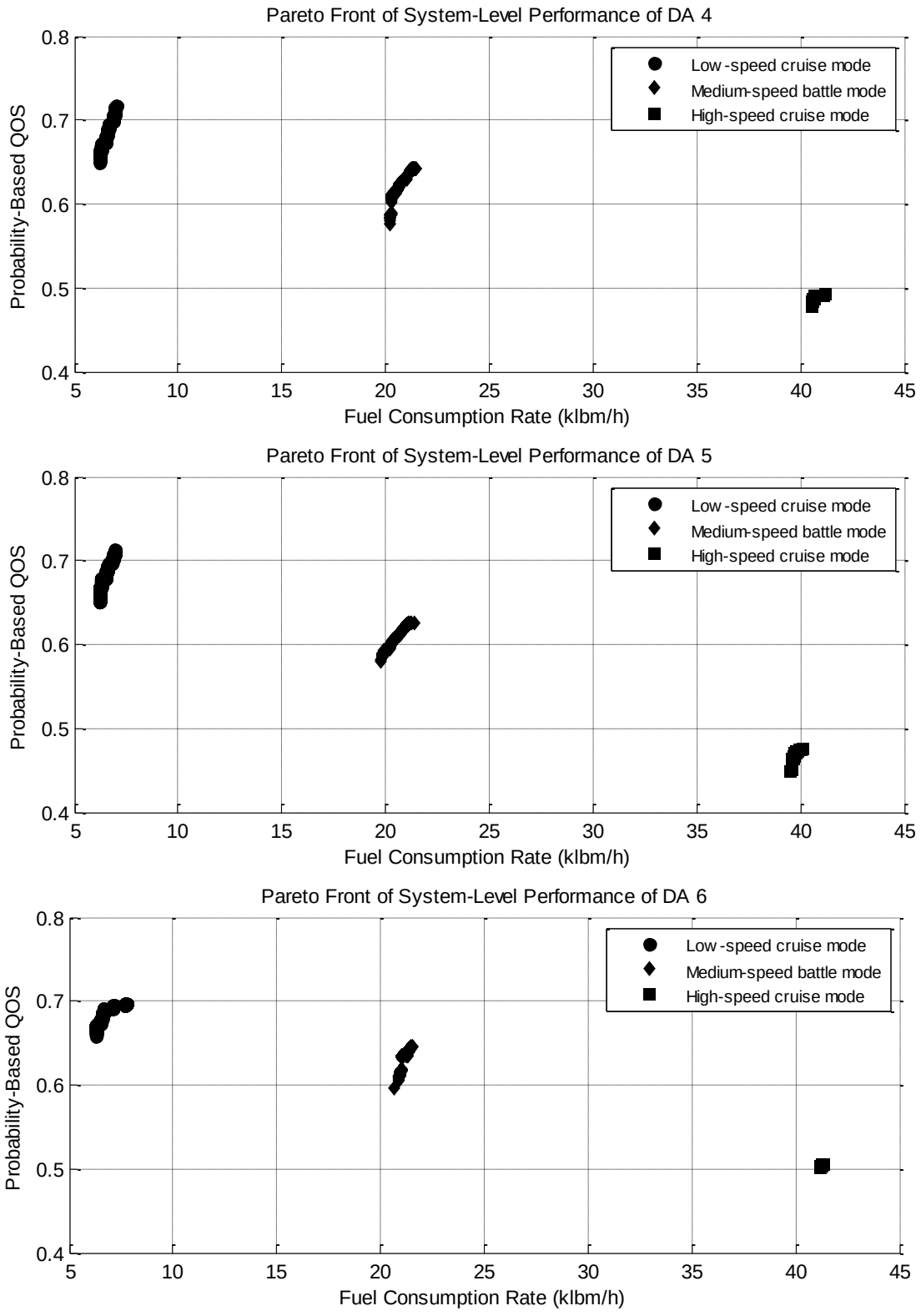

Figure 8.14 The MVDC ZEDS—the Pareto fronts for the mission segments of design alternative 4, 5, and 6, based on the probability-based QOS metric

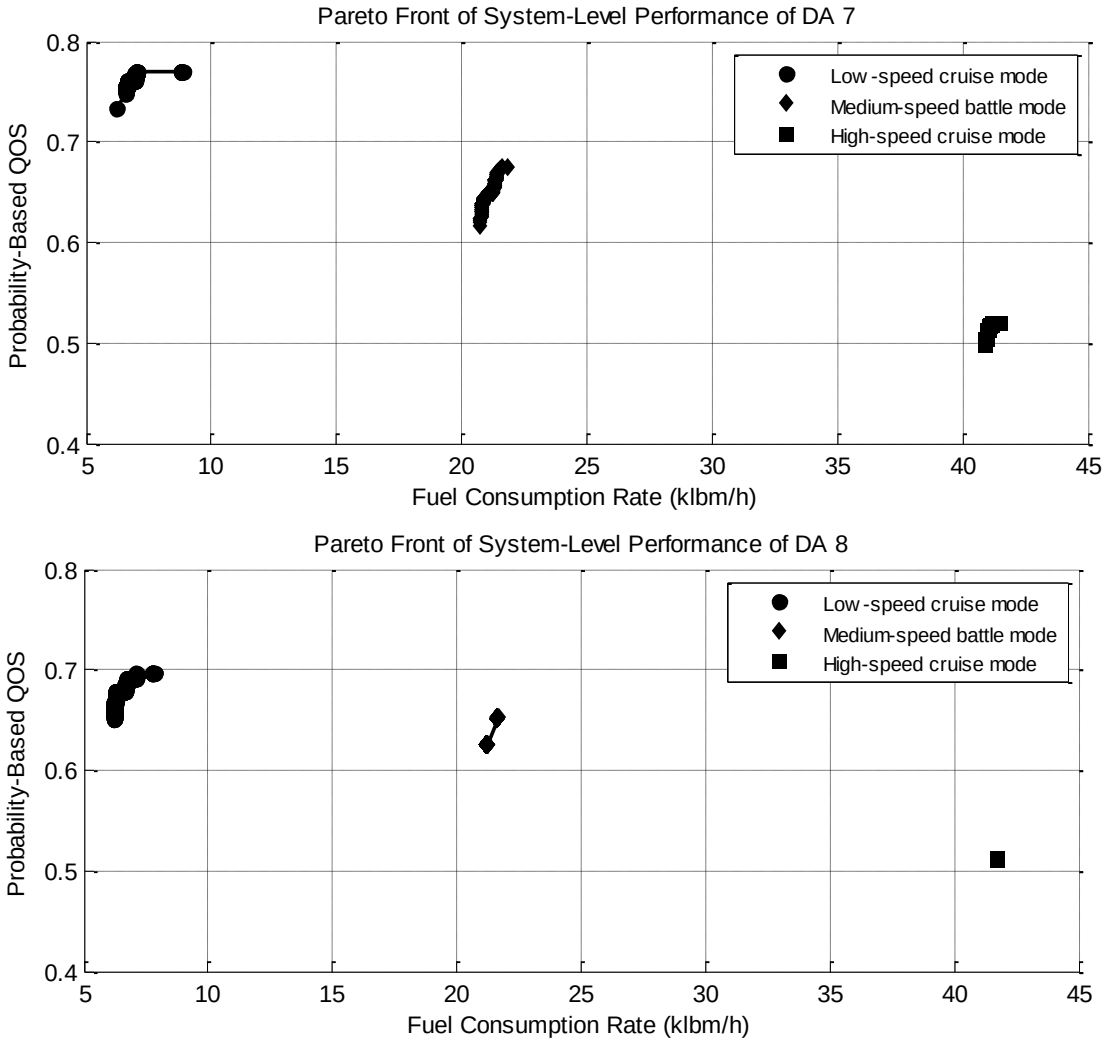

Figure 8.15 The MVDC ZEDS—the Pareto fronts for the mission segments of design alternative 7 and 8, based on the probability-based QOS metric

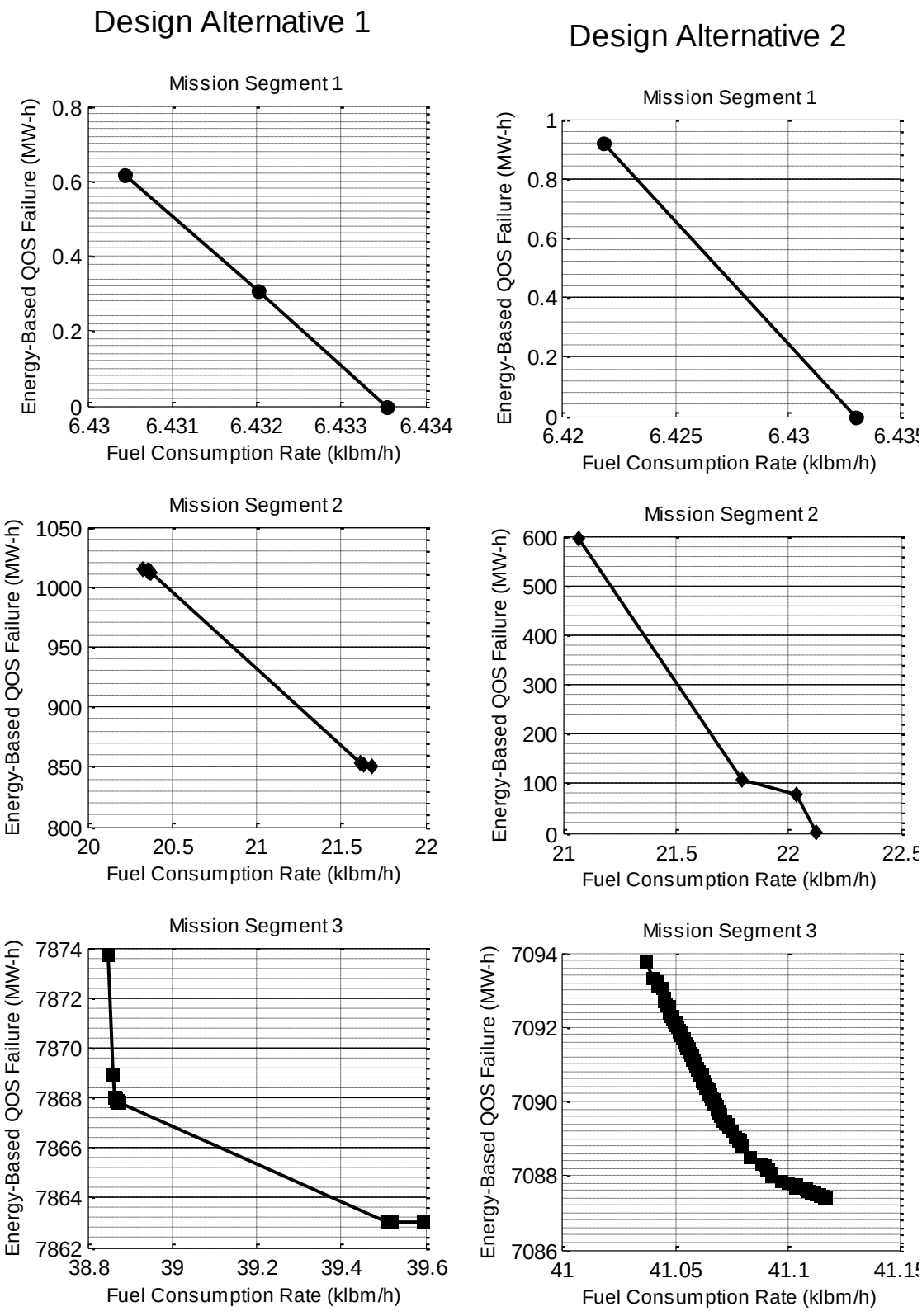

Figure 8.16 The MVAC ZEDS—the Pareto fronts for the mission segments of design alternative 1 and 2, based on the energy-based QOS metric

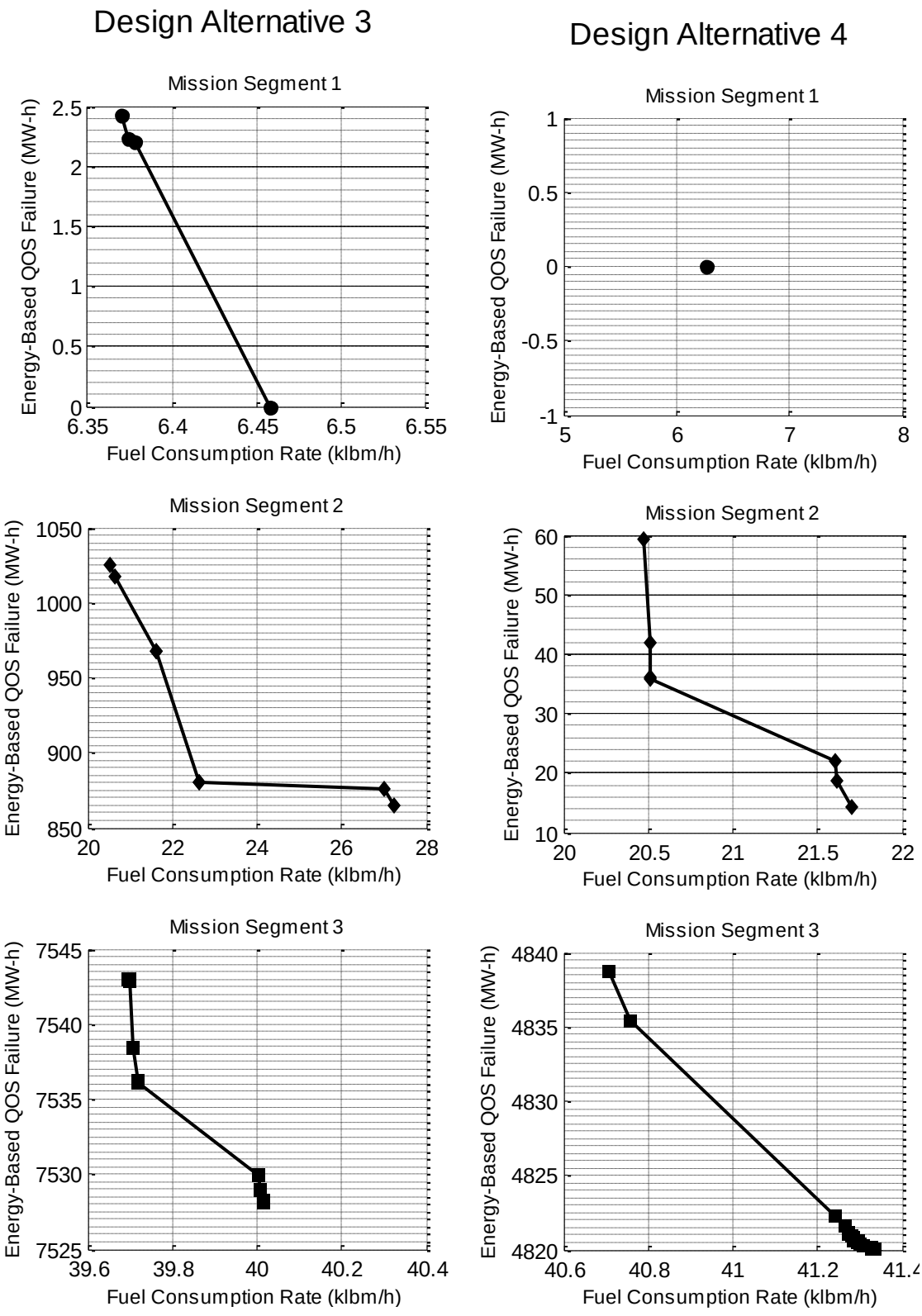

Figure 8.17 The MVAC ZEDS—the Pareto fronts for the mission segments of design alternative 3 and 4, based on the energy-based QOS metric

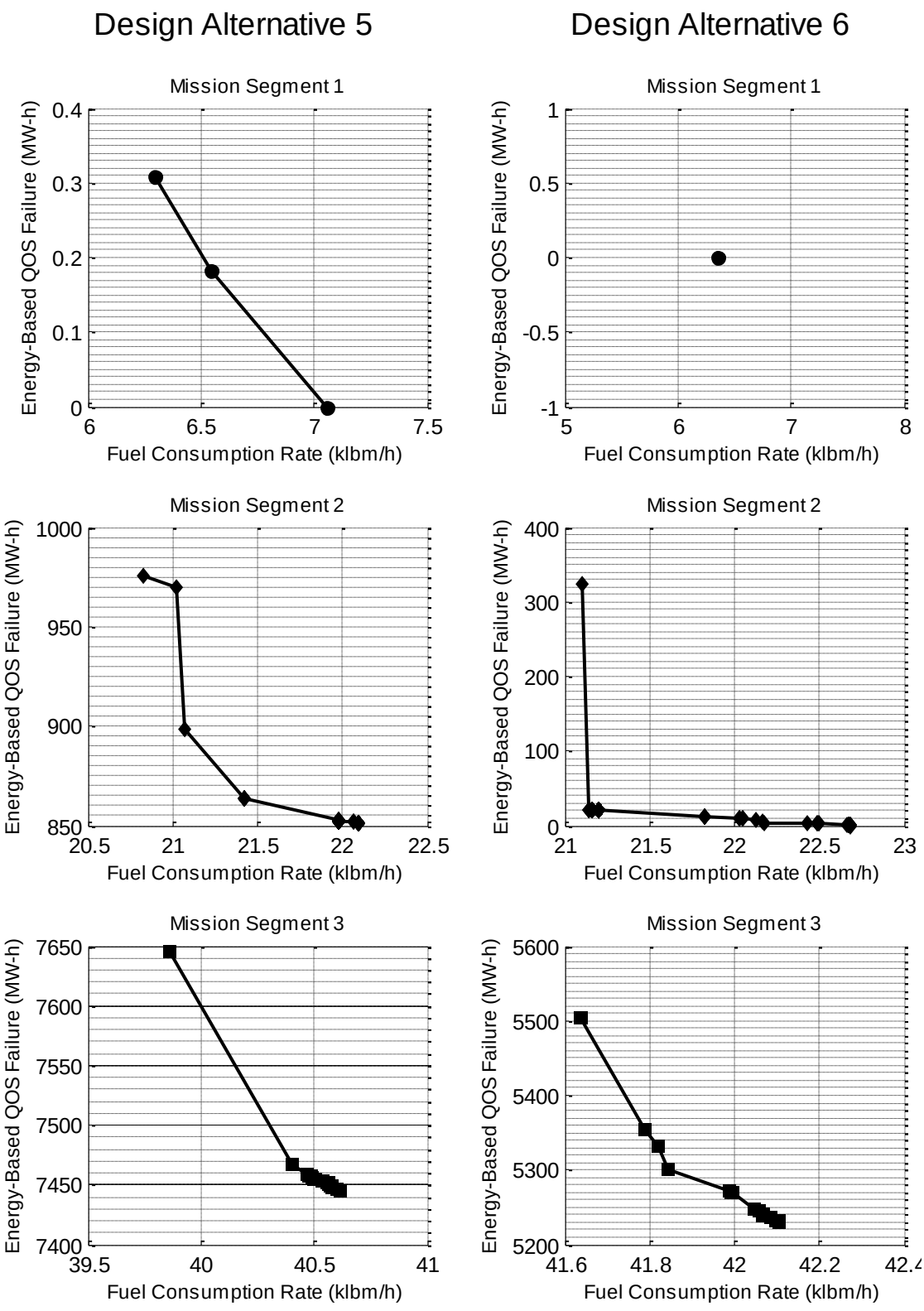

Figure 8.18 The MVAC ZEDS—the Pareto fronts for the mission segments of design alternative 5 and 6, based on the energy-based QOS metric

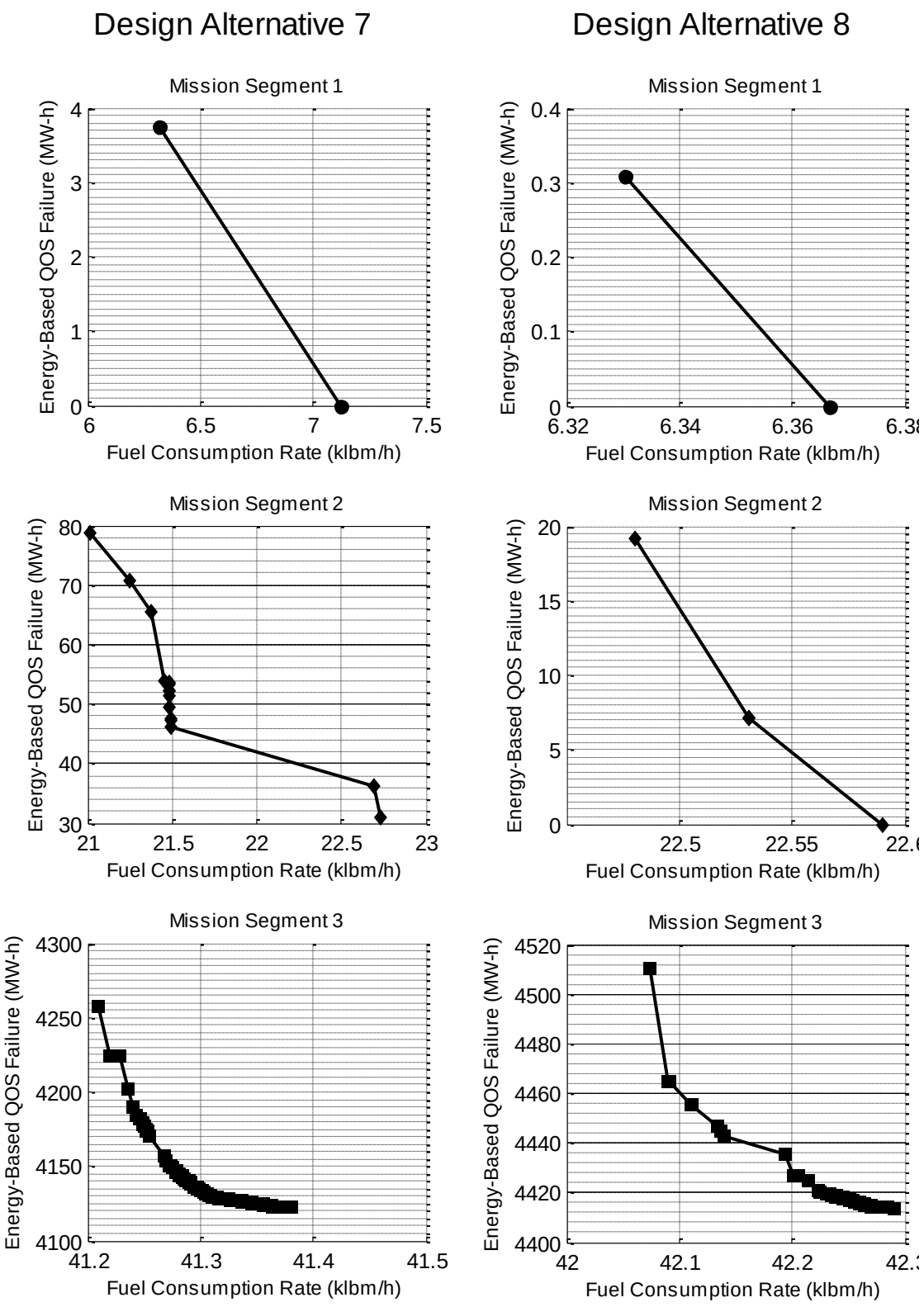

Figure 8.19 The MVAC ZEDS—the Pareto fronts for the mission segments of design alternative 7 and 8, based on the energy-based QOS metric

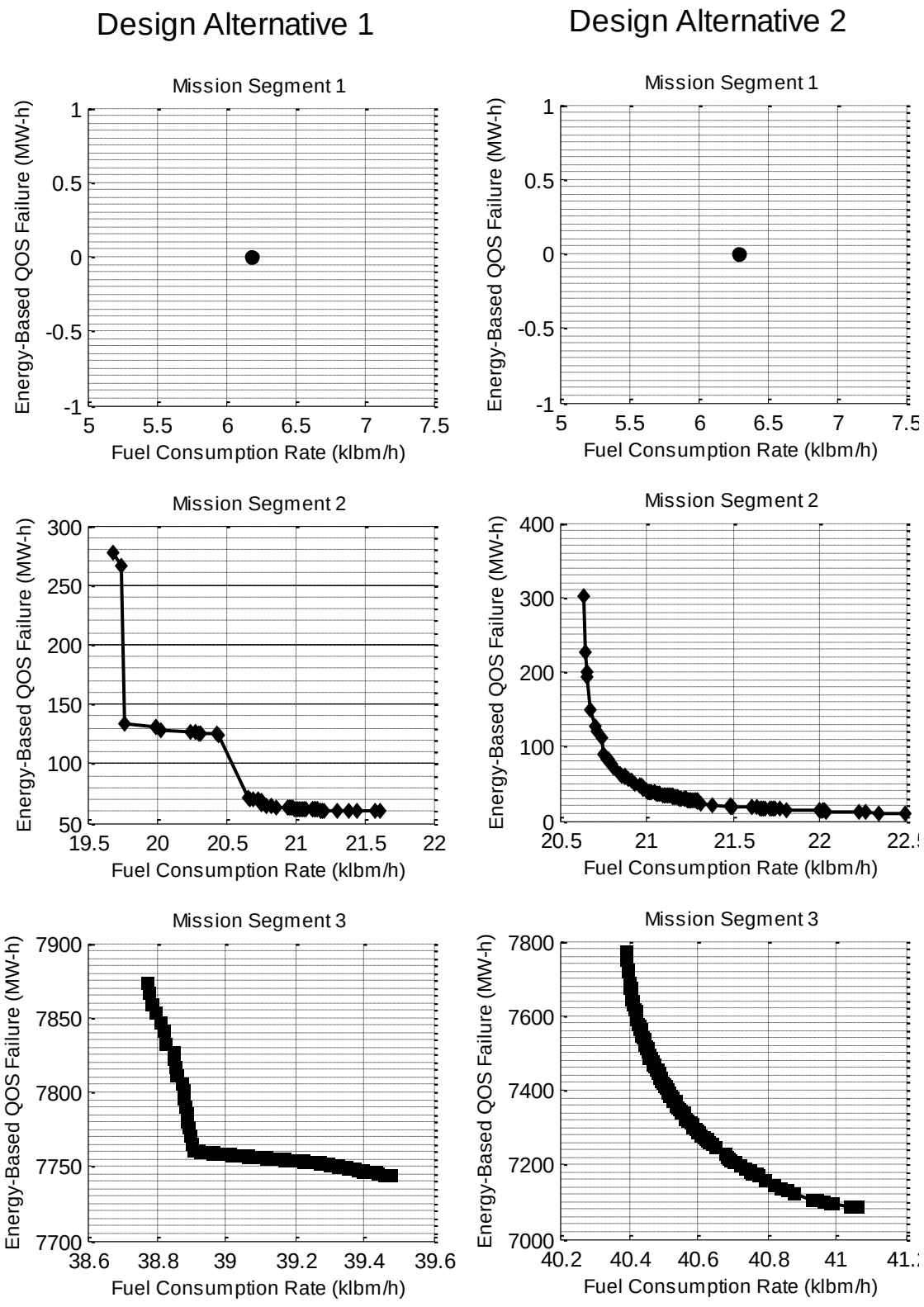

Figure 8.20 The MVDC ZEDS—the Pareto fronts for the mission segments of design alternative 1 and 2, based on the energy-based QOS metric

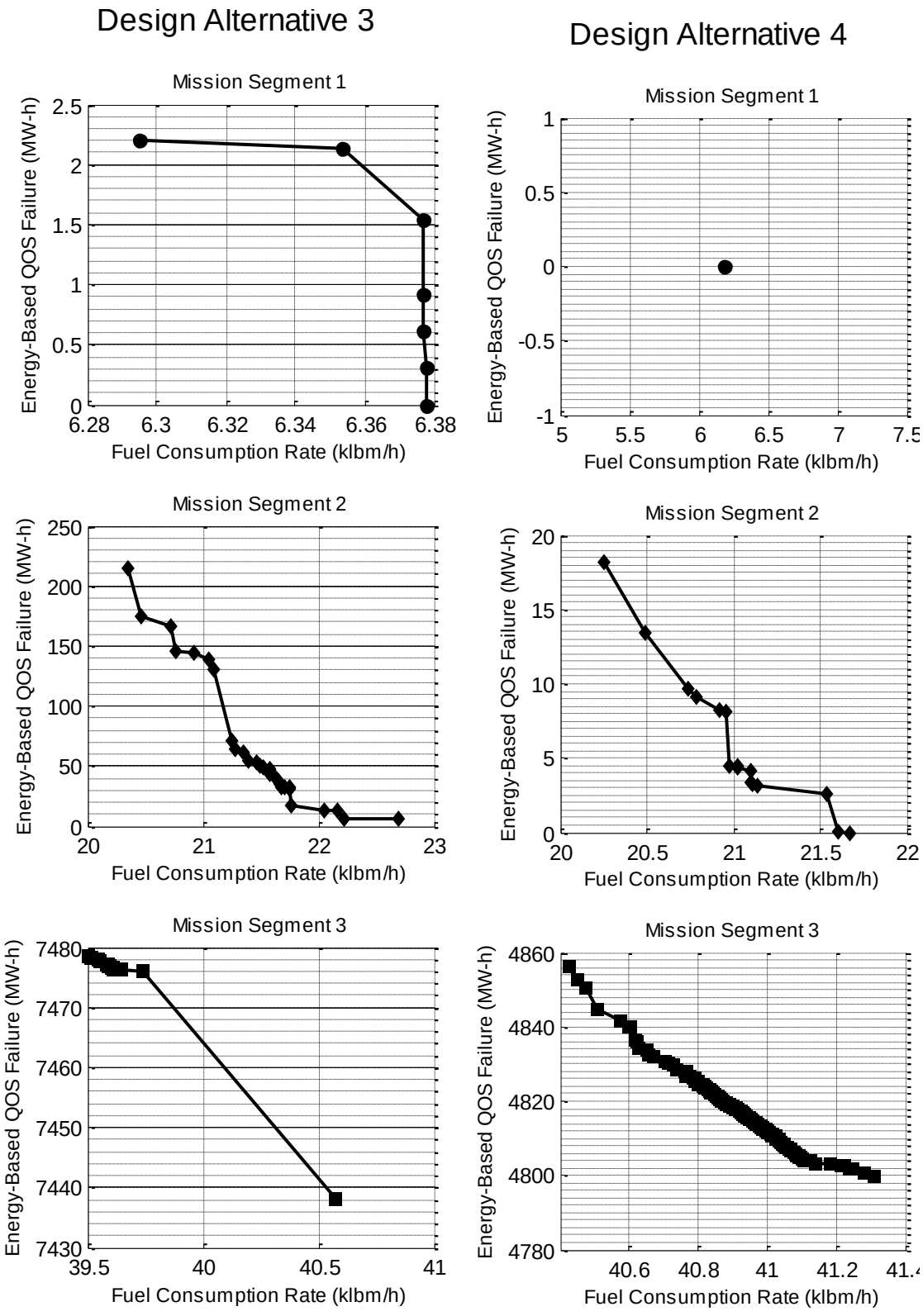

Figure 8.21 The MVDC ZEDS—the Pareto fronts for the mission segments of design alternative 3 and 4, based on the energy-based QOS metric

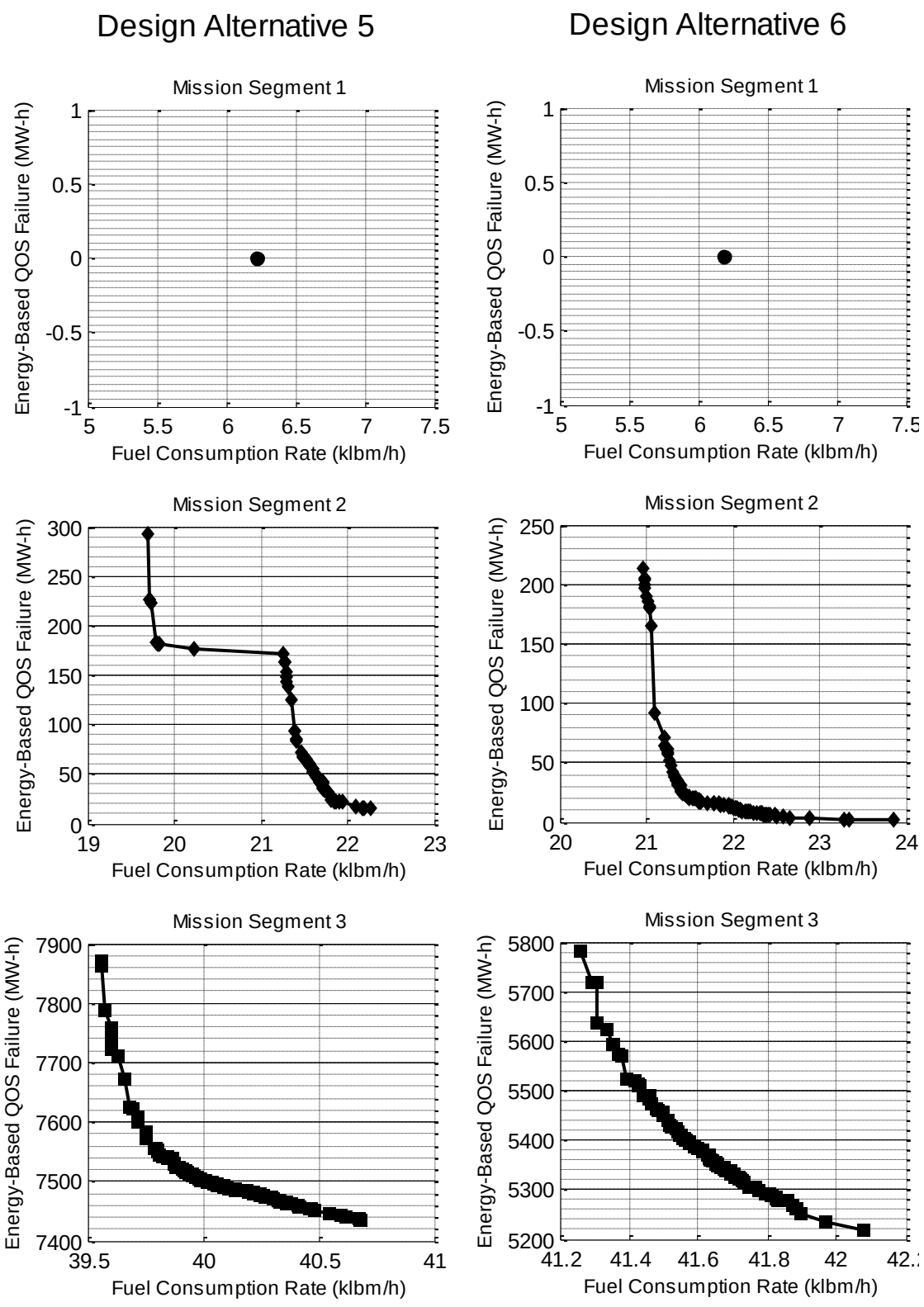

Figure 8.22 The MVDC ZEDS—the Pareto fronts for the mission segments of design alternative 5 and 6, based on the energy-based QOS metric

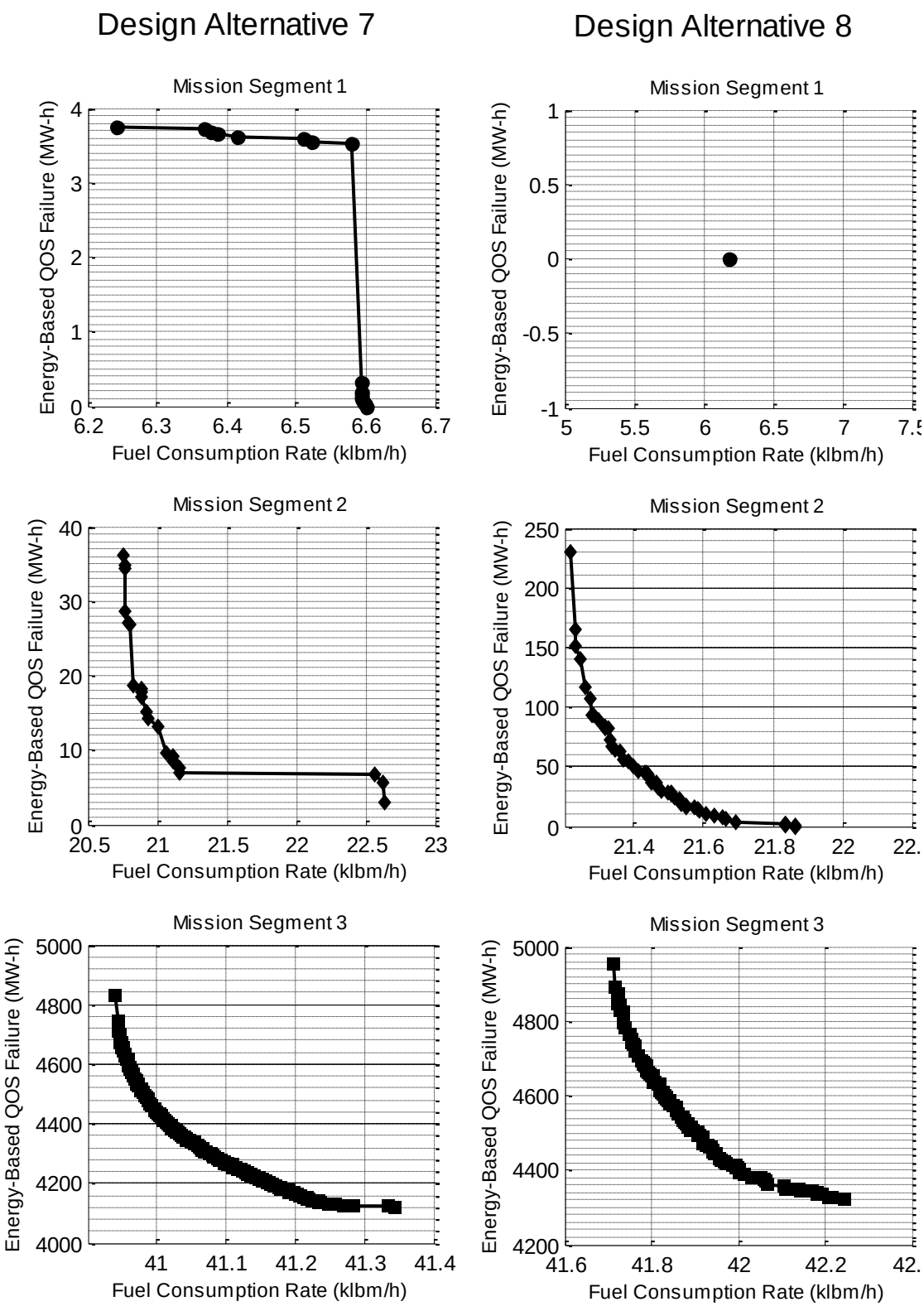

Figure 8.23 The MVDC ZEDS—the Pareto fronts for the mission segments of design alternative 7 and 8, based on the energy-based QOS metric

CHAPTER 9

CONCLUSIONS AND FUTURE WORK

9.1. CONCLUSIONS

This dissertation is motivated by the decision conflicts when selecting or designing the power generation plant for a micro-grid power system at the earliest design stage. For a given mission, the fuel consumption and system QOS have been the emphasized performance metrics for evaluating the quality of a design alternative. Apparently, this concept evaluation work requires incorporating the appropriate design of CONOPS. However, much literature has not developed the appropriate optimization problems of the CONOPS with respect to these two performance metrics. Recent advancement in the state of the art has been reviewed in Chapter 3 and some major drawbacks as listed below.

1) The EDPs are developed mainly for the installed terrestrial power generation plant instead of helping designers choose the optimal power generation plant. Due to the characteristics of terrestrial power systems, the EDPs neglect the study on the optimal control of reactive power balance and fail to address the generation redundancy.
2) The QOS optimization problem has never been appropriately formulated. Much recent literature mainly stays on the qualitative analyses or requires detailed time-domain studies, which are not available for the early design stages.

3) The performance tradeoffs of design alternatives have never been investigated by any optimization algorithm in a quantitative analysis, not to mention the development of the simulation environment for automatically doing this job during the SBD process.
4) Due to the complicated mathematical expression of the EDP and logics in calculating the QOS, the existing optimization algorithms are not effective enough to resolve these problems.

To address these drawbacks, this dissertation redevelops the EDP and QOS optimization problem particularly for the earliest stage design of micro-grid power system. We adopt both ac and dc shipboard NGIPS ZEDS for study. Then we apply our developed optimization algorithms to address the single-objective and multi-objective optimization of these problems. Finally we discuss the significance of this research.

Noticing the complexity of the mixed-integer optimization problems of the CONOPS and the weakness of the current optimization algorithms, in Chapter 5, we develop a SOPSO and MOPSO with the performance improvements. For the SOPSO, we add a dynamic mutation operator and an archive operator to improve the PSO's capability of avoiding premature convergence. In addition, we incorporate the multi-stage penalty function to enhance the PSO's searching capability for more accurately locating the global optimum. The simulation results indicate that our SOPSO is able to consistently find the results closer to the global optimum with 32% smaller standard deviation than the current PSOs based on the same number of simulation trials. For the MOPSO, we introduce the same dynamic mutation operator and multi-stage penalty function to handle the constraints. Our simulation results indicate that our MOPSO is able to solve the

complicated constrained problems that cannot be solved by the current MOPSOs at all in a reasonable time.

In Chapter 6, we develop the new EDP for micro-grid power systems. Referring to the development of control architecture, we first define the standard categories of data for the power level analysis, so as to generalize the formulation of the optimization problems of the CONOPS for a generic system concept. This EDP considers both real and reactive power balance (for ac systems only) of a generation power plant, as well as the requirement of generation redundancy. The simulation results obtained via the SOPSO successfully demonstrate the efficacy of this EDP in reflecting the quality of the design alternatives in saving fuel. In addition, we discover that the inclusion of reactive power balance constraint for ac systems does not affect the calculation of fuel consumption in the most cases, however, when the load power demand is close to the generation capacity of the online PGMs (determined by real power balance), the inclusion may change the results large enough to affect acquisition decisions.

In Chapter 7, we define two versions of QOS metric to evaluate different aspects of the power supply reliability of a micro-grid power system. The optimization problem of the CONOPS with respect to each metric is developed individually. The probability-based QOS metric evaluates how serious the system service will be affected at the moment when the online PGMs fail all of a sudden at certain operating setpoints. The energy-based QOS metric evaluates the power plant's capability of continuously executing a mission segment when the online PGMs at a certain operating setpoint encounter some operating breaks. In optimizing these two metrics, the methods for estimating the condition-based MTBF and MTTR of a PGM are taken into account. The

simulation results obtained via the SOPSO indicate that the probability-based QOS metric reflects a favorable tradeoff relationship between the QOS value and fuel consumption in heavy loading conditions, while the energy-based QOS metric does in light and medium loading conditions.

In Chapter 8, we develop the optimization architecture to generalize the co-optimization problem formulation of the CONOPS. Based on this, we implement the co-optimization of the EDP and the QOS optimization problem for our design problem. The concept of Pareto optimality is used to generate and visualize the optimal performance tradeoffs of individual design alternatives and the comparison of the design alternatives. Thus we are able to identify the favorable choices of CONOPS for each design alternative and identify the quasi-optimal design alternatives with a high level of confidence at the earliest design stage. In addition, the software coupling method is also suggested in this chapter for software engineers to automatically realize this concept evaluation process.

9.2. FUTURE WORK

The potential research directions based on this dissertation are suggested as follows:

1) Further improve the MOPSO to directly handle constrained mixed-integer co-optimization problems. In this dissertation, we have just improved the searching capability of the MOPSO in solving for constrained real-variable-based problems. Therefore, in Chapter 8, we have to capitalize on appropriate enumeration techniques to convert the original mixed-integer problem, which consequently adds much intensive computation to the optimization solver and

significantly increases the simulation time. The success of this work can significantly accelerate the concept evaluation process.

2) Develop a modeling method to reduce the complexity degree of the EDP. Currently, the EDP involves many non-linear equations (e.g., the power and thermal efficiency curves of the PGMs, the calculation of the condition-based MTBF values) that need to be dealt with at each iteration step. Our test results show that only linearizing the curve-fitting equation of the PGM power efficiency can lead to about 64% faster simulation speed. Therefore, we believe that an effective simplification of these equations without hurting the computation accuracy can significantly reduce the time investment on the concept evaluation process.
3) Incorporate the vital load allocation strategy into the formulation of the optimization problems of the CONOPS. The power generation and distribution architecture of a micro-grid power system is usually reconfigurable depending on the operations of circuit breakers. For reliability purposes, the vital loads usually have multiple channels to receive power supply, different from the single-channel-based regular non-vital loads. Based on our primary research, the configuration of system architecture is expected to largely affect the quality estimation of the design alternatives.
4) Develop the software coupling between S3D and MATLAB to implement real automatic concept evaluation process. We have defined the coupling method in Chapter 8; however, the detailed difficulties are required to be further investigated. The ultimate goal is to let designers create the system concept in

S3D and invoke MATLAB as the optimization solver through a window interface in S3D to visualize the optimality comparison of the design alternatives.

REFERENCES

[1] N. Doerry, "Designing Electrical Power Systems for Survivability and Quality of Service," Naval Engineers Journal, vol. 119, Issue 2, pp. 25-34, Oct. 2007.

[2] D.J. Singer, N. Doerry, and M.E. Buckley, "What is Set-Based Design?" Naval Engineering Journal, Vol. 121, No. 4, pp. 31-43, 2009.

[3] W.L. Mebane, C.M. Carlson, C. Dowd, D.J. Singer, and M.E. Buckley, "Set-Based Design and the Ship to Shore Connector," Naval Engineers Journal, Vol. 123, Issue 3, pp. 79-92, Sep. 2011.

[4] T.A. McKenney, L.F. Kemink, and D.J. Singer, "Adapting to Changes in Design Requirements Using Set-Based Design," Naval Engineers Journal, Vol. 123, Issue 3, pp. 66-77, Sep. 2011.

[5] Secretary of the Navy (SECNAV 2008a), "Department of the Navy (DON) Requirements and Acquisition Process Improvement," SECNAVNOTE 5000 of February 26, 2008.

[6] Secretary of the Navy (SECNAV 2008b), "Implementation and Operation of the Defense Acquisition System and the Joint Capabilities Integration and Development System," SECNAVINST 5000.2D of October 16,, 2008.

[7] N. Doerry, "Next generation integrated power systems for the future fleet," Presentation given at IEEE Electric Ships Technology Symposium, Baltimore, MD, April 21, 2009.

[8] N. Doerry, "Institutionalizing the Electric Warship," Naval Engineers Journal, Vol. 118, Issue 4, pp. 57-64, Oct. 2006.

[9] Doerry, N., and Fireman, H., "Designing All Electric Ships," Presented at International Marine Design Conference, Ann Arbor, MI, May 16-19, 2006.

[10] M.R. AlRashidi, M.E. El-Hawary, "A Survey of Particle Swarm Optimization Applications in Electric Power Systems," IEEE Transactions on Evolutionary Computation, Vol. 13, No. 4, 2009.

[11] M.A. Abido, “Multiobjective particle swarm optimization for environmental/economic dispatch problem,” Electric Power Systems Research, Vol. 79, Issue 7, pp. 1105-1113, Jul. 2009.

[12] K.Y. Lee and J.B. Park, “Application of particle swarm optimization to economic dispatch: advantages and disadvantages,” IEEE Trans. Power Syst., pp. 188-192, 2006.

[13] D.N. Jeyakumar, T. Jayabarathi, and T. Raghunathan, “Particle swarm optimization for various types of economic dispatch problems,” International Journal of Electrical Power & Energy Systems, Vol. 28, Issue 1, pp. 36-42, Jan. 2006.

[14] Zwe-Lee Gaing, “Particle swarm optimization to solving the economic dispatch considering the generator constraints,” IEEE Trans. Power System, vol.18, pp. 1187-1195, Mar. 2003.

[15] S.O. Orero and M.R. Irving, “Economic dispatch of generators with prohibited operating zones: a genetic algorithm approach,” IEE Proc. Gener. Transm. Distrib., Vol. 143, No. 6, Nov. 1996.

[16] H.T. Yang, P.C. Yang, and C.L. Huang, “Evolutionary programming based economic dispatch for units with nonsmooth incremental fuel cost functions,” IEEE Transcations on Power System, Vol. 11, Issue 1, pp. 112-118, Feb. 1996.

[17] K.P. Wong and Y.W. Wong, “Genetic and genetic/simulated-annealing approaches to economic dispatch,” IEE Proceedings of Generation, Transmission and Distribution, Vol. 141, Issue 5, pp. 507-513, Sep. 1994.

[18] S. Affijulla and S. Chauhan, “A New Intelligence Solution for Power System Economic Load Dispatch,” Environment and Electrical Engineering (EEEIC), 2011 10th International Conference on, pp. 1-5, May 2011.

[19] W. Sugsakarn, P. Damrongkulkamjorn, “Economic dispatch with nonsmooth cost function using hybrid method,” Electrical Engineering/Electronics, Computer, Telecommunications and Information Technology, 2008. ECTI-CON 2008. 5th International Conference on, pp. 889-892, May 2008.

[20] T.A.A. Victoire and A.E. Jeyakumar, “Hybrid PSO-SQP for economic dispatch with valve-point effect,” Electric Power Systems Research, Vol. 71, pp. 51-59, 2004.

[21] P. Attaviriyanupap, H. Kita, E. Tanaka, and J. Hasegawa, “A hybrid EP and SQP for dynamic economic dispatch with nonsmooth fuel cost function,” IEEE Transactions on Power Systems, Vol. 17, Issue 2, pp. 411-416, May 2002.

[22] W.M. Lin, F.S. Cheng, and M.T. Tsay, “Nonconvex Economic Dispatch by Integerated Artificial Intelligence,” IEEE Transactions on Power Systems, Vol. 16, No. 2, pp. 307-311, May 2001.

[23] W. Wu, D. Wang, A. Arapostathis, and K. Davey, “Optimal Power Generation Scheduling of a Shipboard Power System,” IEEE Electric Ship Technologies Symposium, Arlington, VA, pp. 519-522, May 2007.

[24] S. Vijlee, A. Ouroua, L. Domaschk, and J. Beno, “Directly-coupled gas turbine permanent magnet generator sets for prime power generation on board electric ships,” 2007 Electric Ship Technologies Symposium, pp.340-347, May 2007.

[25] N. Doerry, “Designing Electrical Power Systems for Survivability and Quality of Service,” Naval Engineers Journal, vol. 119, Issue 2, pp. 25-34, Oct. 2007.

[26] J. Chalfant, B. Langland, S. Abdelwahed, C. Chryssosotomidis, R. Dougal, A. Dubey, T.E. Mezyani, J. Herbst, T. Kiehne, J. Ordonez, S. Pish, S. Srivastava, and Ed Zivi, “A Collaborative Early-Stage Ship Design Environment,” ESRDC Technical reports, 2012.

[27] C.J. Zapata, A. Alzate, and M.A. Rios, “Reliability Assessment of Substations using Stochastic Point Processes and Monte Carlo Simulation,” IEEE Power and Energy Society General Meeting, Minneapolis, MN, July 2010.

[28] F.J.G. Carazas and G.F.M. de Souza, “Availability Analysis of Gas Turbines Used in Power Plants,” International Journal of Thermodynamics, Vol. 12, No. 1, pp. 23-37, March 2009.

[29] L. Wang and C. Singh, “Artificial Immune System Based Reliability Appraisal Methodology of Power Generation Systems with Wind Power Penetration,” IEEE Systems and Information Engineering Design Symposium, Charlottesville, VA, Apr. 2007.

[30] A. Ehsani, M. Fotuhi, A. Abbaspour, and A.M. Ranjbar, “An Analytical Method for the Reliability Evaluation of Wind Energy System,” 2005 IEEE TENCON Region 10, Nov. 2005.

[31] "Performance of Generating Plant: New Realities, New Needs," A report of the World Energy Council, Section 1, pp. 15-17, Aug. 2004.

[32] Y. Wu and W. Chang, "A Study on Optimal Reliability Indices in an Electrical Distribution System," Proceedings of International Conference on Power System Technology 2000, Vol. 2, pp. 727-732, Perth, WA, 2002.

[33] "Handbook of Reliability Prediction Procedures for Mechanical Equipment," Logistics Technology Support, CARDEROCKDIV, NSWC-10, Chapter 14, Jan. 2010.

[34] G. Velotto, "Optimal Dispatching of Generators with Load Dependent Failure Rates," RT&A #02 (21), Vol. 2, June 2011.

[35] A.M. Cramer, S.D. Sudhoff, and E.L. Zivi, "Metric Optimization-Based Design of Systems Subject to Hostile Disruptions," IEEE Transactions on Systems, Man and Cybernetics-Part A: Systems and Humans, Vol. 41, No. 5, pp. 989-1000, Sep. 2011.

[36] A.M. Cramer, S.D. Sudhoff, and E.L. Zivi, "Performance Metrics for Electric Warship Integrated Engineering Plant Battle Damage Response," IEEE Transactions on Aerospace and Electronic Systems, Vol. 47, No. 1, pp. 634-645, Jan. 2011.

[37] R.R. Chan, S.D. Sudhoff, Y. Lee, and E.L. Zivi, "A Linear Programming Approach to Shipboard Electrical System Modeling," 2009 IEEE Electric Ship Technologies Symposium, pp. 261-269, Apr. 2009.

[38] J. Chalfant, D. Hanthorn, and C. Chryssostomidis, "Development of a Vulnerability Metric for Electric-Drive Ship Simulations," 2012 International Simulation Multi-Conference, Genoa, Italy, July 8-11, 2012.

[39] N. Kumar, A. Srivastava, and N. N. Schulz, "Shipboard Power System Restoration Using Binary Particle Swarm Optimization," 39th North American Power Symposium, Las Cruces, pp. 164-169, Sep. – Oct. 2007.

[40] T. Amba, K. Burler-Purry, and M. Falahi, "Genetic Algorithm Based Damage Control for Shipboard Power Systems," IEEE Electric Ship Technologies Symposium, pp. 242-252, Apr. 2009.

[41] S. Bose, S. Pal, C. Scoglio, B. Natarajan, S. Das and N. Schulz, "Analysis of optimized reconfiguration of power system for electric ships," North American Power Symposium, Arlington, TX, pp. 1-7, Sep. 2010.

[42] W. Xue and Y. Fu, "A two-step method for reconfiguration of shipboard power system," 2011 IEEE Electric Ship Technologies Symposium, Alexandria, VA, pp. 167-172, Apr. 2011.

[43] P. Mitra and G. K. Venayagamoorthy, "Implementation of an Intelligent Reconfiguration Algorithm for an Electric Ship's Power System," IEEE Transactions on Industry Applications, Vol. 47, No. 5, pp. 2292-2300, Sep./Oct. 2011.

[44] N. Doerry, "Shipboard Electrical Power Quality of Service," IEEE Electric Ship Technologies Symposium, Washington, DC, pp. 274-279, July 2005.

[45] S. Lahiri, K. Miu, H. Kwatny, G. Bajpai, A. Beytin, and J. Patel, "Fuel Optimization under Quality of Service Constraints for Shipboard Hybrid Electric Drive," 2011 4th International Symposium on Resilient Control Systems, pp. 137-141, Aug. 2011.

[46] IEEE Std 1676-2010, "IEEE Guide For Control Architecture for High Power Electronics (1MW and Greater) Used in Electric Power Transmission and Distribution Systems."

[47] IEEE P1826/D4, Draft Standard for Power Electronics Open System Interfaces in Zonal Electrical Distribution Systems Rated Above 100 kW."

[48] J. Chalfant, B. Langland, S. Abdelwahed, C. Chryssosotomidis, R. Dougal, A. Dubey, T.E. Mezyani, J. Herbst, T. Kiehne, J. Ordonez, S. Pish, S. Srivastava, and Ed Zivi, "A Collaborative Early-Stage Ship Design Environment," ESRDC Technical reports, 2012.

[49] http://www.mathworks.com/products/matlab/

[50] S. Lahiri, K. Miu, H. Kwatny, G. Bajpai, A. Beytin, and J. Patel, "Fuel Optimization under Quality of Service Constraints for Shipboard Hybrid Electric Drive," 2011 4th International Symposium on Resilient Control Systems, pp. 137-141, Aug. 2011.

[51] M. AlRashidi, M. El-Hawary, "Hybrid Particle Swarm Optimization approach for solving the discrete OPF problem considering the valve loading effects," IEEE Trans. on Power Systems, vol. 22, no. 4, pp. 2030-2038, Nov. 2007.

[52] P. Venkatesh, R. Gnanadass and N. Padhy, "Comparison and application of evolutionary programming techniques to combined economic emission dispatch with

line flow constraints," IEEE Trans. on Power Systems, vol. 18, no. 2, pp. 688-697, May 2003.

[53] K. Wong and Y. Wong, "Genetic and genetic/simulated-annealing approaches to economic dispatch," IEEE Proc. Gener. Trans. Distrib., vol. 141, issue 5, pp. 507-513, Sep. 1994.

[54] S. Affijulla and S. Chauhan, "A new intelligence solution for power system economic load dispatch," 10th International Conference on Environment and Electrical Engineering, pp. 1-5, May 2011.

[55] K.Y. Lee, A.S. Yome and J.H. Park, "Adaptive Hopfield Neural Networks for Economic Load Dispatch," IEEE Transactions on Power Systems, Vol. 13, No. 2, pp. 519-526, May 1998.

[56] J. Kennedy and R. Eberhart, "Particle swarm optimization," IEEE Proc. the International Conference on Neural Networks, Perth, Australia, pp. 1942-1948, 1995.

[57] C.S. Pedamallu and L. Ozdamar, "Investigating a hybrid simulated annealing and local search algorithm for constrained optimization," European Journal of Operational Research 185, pp. 1230-1245, 2008.

[58] W. Sugsakarn, P. Damrongkulkamjorn, "Economic dispatch with nonsmooth cost function using hybrid method," Electrical Engineering/Electronics, Computer, Telecommunications and Information Technology, 2008. ECTI-CON 2008. 5th International Conference on, pp. 889-892, May 2008.

[59] R.R. Tan, "Hybrid evolutionary computation for the development of pollution prevention and control strategies," Journal of Cleaner Production 15, pp. 902-906, 2007.

[60] M. Abido, "Optimal design of power-system stabilizers using Particle Swarm Optimization," IEEE Trans. on Energy Conversion, vol. 17, no. 3, pp.406-413, Sep. 2002.

[61] J.G. Ciezki and R.W. Ashton, "A Technology Overview for a Proposed Navy Surface Combatant DC Zonal Electric Distribution System," Naval Engineers Journal, Vol. 111, Issue 3, pp.59-69, May 1999.

[62] N. Doerry, "Zonal Ship Design," Naval Engineers Journal, Vol. 118, Issue 1, pp. 39-53, Jan 2006.

[63] C. Holsonback, T. Webb, T. Kiehne and C.C. Seepersad, "System-Level Modeling and Optimal Design of an All-Electric Ship Energy Storage Module," Electric Machines Technology Symposium, Philadelphia, PA. May 2006.

[64] T. Zhang, Y. Zhang, and R.A. Dougal, "Accounting for System-Level Controls During Early-System Design," Proceedings of 2013 IEEE Electric Ship Technologies Symposium, pp. 326-332, Arlington, VA, April 2013.

[65] T. Zhang, J.J. Shepherd, J. Tang, and R.A. Dougal, "The Simulation Tool for Mission-Optimized System Design," Grand Challenges in Modeling & Simulation 2011, the Hague, Netherlands, June 2011.

[66] B. Chadha, J. Wedgwood, and J. Welsh, "Next-Generation Architecture to Support Simulation-Based Acquisition," Naval Engineers Journal, Vol. 112, Issue 4, pp. 347-354, July 2000.

[67] J. Kennedy and R. Eberhart, "Particle swarm optimization," IEEE Proc. the International Conference on Neural Networks, Perth, Australia, pp. 1942-1948, 1995.

[68] L. Wang and C. Singh, "Unit commitment considering generator outages through a mixed-integer particle swarm optimization algorithm," Applied Soft Computing, vol. 9, pp.947-953, 2009.

[69] M. AlRashidi, M. El-Hawary, "Hybrid Particle Swarm Optimization approach for solving the discrete OPF problem considering the valve loading effects," IEEE Trans. on Power Systems, vol. 22, no. 4, pp. 2030-2038, Nov. 2007.

[70] J. Joines, C. Houck, "On the use of non-stationary penalty functions to solve nonlinear constrained optimization problems with GA's," IEEE Int. Conf. Evol. Comp, pp.579-585, Jun. 1994.

[71] K. Parsopoulos, M. Vrahatis, "Particle Swarm Optimization method for constrained optimization problems," Intelligent Technologies - Theory and Applications: New Trends in Intelligent Technologies, pp. 214–220. IOS Press, 2002.

[72] C.A. Coello Coello, G.T. Pulido, and M.S. Lechuga, "Handling Multiple Objective with Particle Swarm Optimization," IEEE Transactions on Evolutionary Computation, Vol. 8, No. 3, June 2004.

[73] J.S. Chalfant and C. Chryssostomidis, “Toward the Development of an Integrated Electric Ship Evaluation Tool,” Proc. Grand Challenges in Modeling and Simulation (GCMS09), Istanbul, Turkey. July 13-16, 2009.

[74] http://www.geaviation.com/engines/marine/

[75] Black Hills Corporation – Cheyenne Generating Station, Submittal of Greenhouse Gas PSD Construction Air Permit Application Revision 1 – Sept. 2011.

[76] Data sheet of BDAX 7-193ER, GE NUovo Pignone Internal DT-‘N’.

[77] F. Haglind and B. Elmegaard, “Methodologies for predicting the part-load performance of aero-derivative gas turbines,” 11th Conference on Process Integration, Modelling and Optimisation for Energy Saving and Pollution Reduction, Vol. 34, Issue 10, pp. 1484-1492, Oct 2009.

[78] M.R. Patel, “Shipboard Electrical Power System,” published by CRC Press, Dec 15, 2011.

[79] W.L. Gray, “DC to DC power conversion module for the all-electric ship”, M.S. Thesis, Massachusetts Institute of Technology, 2011.

[80] M.R. Driels and Y.S. Shin, “Determining the Number of Iterations for Monte Carlo Simulations of Weapon Effectiveness,” NAVAL POSTGRADUATE SCHOOL Monterey, California 93943-5000.

[81] C.P. Robert and G. Casella, “Monte Carlo Statistical Methods," Springer, ISBN 0-387-21239-6, 2nd ed., 2004.

APPENDIX A – NUMERICAL SOLUTION TO THE ECONOMIC DISPATCH PROBLEM

Table A.1 The MVAC ZEDS—the fuel consumption rate minimized via the SOPSO vs. the fuel consumption rate obtained in the worst-case scenario (W) of each design alternative, respectively

Index		**1**	**2**	**3**	**4**	**5**	**6**	**7**	**8**
Mission Segment1*	**SOPSO**	6.267	6.369	6.452	6.261	6.318	6.338	6.322	6.267
	W	8.332	7.899	9.853	8.241	10.006	8.963	9.294	8.706
Fuel Saving (%)		24.78	19.36	34.52	24.03	36.82	29.29	31.98	28.02
Mission Segment 2	**SOPSO**	19.825	20.911	20.302	20.503	20.257	21.071	21.107	21.838
	W	23.002	23.944	22.554	23.37	22.799	22.985	23.028	23.561
Fuel Saving (%)		13.81	12.67	9.99	12.27	11.15	8.33	8.34	7.31
Mission Segment 3	**SOPSO**	39.158	40.742	39.463	40.940	39.874	41.530	41.266	42.092
	W	39.662	41.210	40.345	41.367	40.624	42.307	42.239	42.816
Fuel Saving (%)		1.27	1.13	2.19	1.03	1.85	1.84	2.30	1.69
Total Fuel Consumption ($\times 10^3$ klbm)	**SOPSO**	**571.59**	595.86	580.06	593.09	582.09	603.90	601.77	**614.93**
	W	621.92	639.94	637.31	639.29	643.19	650.47	653.15	657.72
Fuel Saving (%)		8.09	6.87	8.98	7.23	**9.50**	7.16	7.87	6.58

* Fuel consumption rate in each mission segment is measured in klbm/hr;

Table A.2 The minimized fuel consumption rate for the MVAC ZEDS (AC) vs. the minimized fuel consumption rate for the MVDC ZEDS (DC) of each design alternative, respectively

Index		**1**	**2**	**3**	**4**	**5**	**6**	**7**	**8**
Mission Segment 1*	**AC**	6.267	6.369	6.452	6.261	6.318	6.338	6.322	6.267
	DC	6.187	6.307	6.158	6.246	6.286	6.285	6.250	6.188
Percent Difference %		1.29	0.98	4.67	0.25	0.52	0.84	1.15	1.25
Mission Segment 2	**AC**	19.825	20.911	20.302	20.503	20.257	21.071	21.107	21.838
	DC	19.775	20.832	19.527	20.224	20.026	20.634	20.760	21.550
Percent Difference %		0.25	0.38	3.89	1.37	1.15	2.10	1.66	1.33
Mission Segment 3	**AC**	39.158	40.742	39.463	40.940	39.874	41.530	41.266	42.092
	DC	39.140	40.544	39.394	40.615	39.549	41.221	41.134	41.875
Percent Difference %		0.04	0.49	0.18	0.80	0.82	0.75	0.32	0.52
Total Fuel Consumption ($\times 10^6$ lbm)	**AC**	**571.59**	595.86	580.06	593.09	582.09	603.90	601.77	**614.92**
	DC	**570.30**	592.90	570.09	587.67	576.93	596.90	596.94	**609.81**
Percent Difference %		0.23	0.50	1.73	0.92	0.89	1.17	0.81	0.83

* The fuel consumption rate in each mission segment is measured in klbm/hr.

Table A.3 The CONOPS of each design alternative corresponding to the fuel consumption values minimized in Table A.2

Index			Mission Segment 1					Mission Segment 2					Mission Segment 3				
1	PGM (MW)		**5**	**15**	**20**	**40**		**5**	**15**	**20**	**40**		**5**	**15**	**20**	**40**	
	AC	Pg (MW)		1.39	9.70				1.66	12.39	26.24		3.94	14.77	15.56	39.42	
		PF*		0.73	0.85				0.97	0.92	0.86		0.51	1.00	1.00	1.00	
	DC	Pg (MW)		1.60	9.37				6.70	4.61	28.68		2.54	11.12	20	40	
2	PGM (MW)		**20**	**20**	**20**	**20**		**20**	**20**	**20**	**20**		**20**	**20**	**20**	**20**	
	AC	Pg (MW)	8.75	2.34					14.36	14.14	11.80		19.96	17.82	15.90	20.00	
		PF	0.79	0.96					0.89	0.96	0.75		1.00	1.00	1.00	0.95	
	DC	Pg (MW)	8.44	2.53					13.18	15.92	10.89		16.53	18.60	18.83	19.72	
3	PGM (MW)		**4.5**	**4.5**	**11**	**20**	**40**	**4.5**	**4.5**	**11**	**20**	**40**	**4.5**	**4.5**	**11**	**20**	**40**
	AC	Pg (MW)		0.80	0.64	9.65			1.20	3.99	3.90	31.20	3.65	2.84	8.43	18.78	40.00
		PF		0.54	0.71	0.86			0.93	0.51	1.00	0.89	0.90	0.84	0.92	1.00	1.00
	DC	Pg (MW)			2.10	8.86				1.21	11.45	27.34	2.93	2.87	9.42	18.45	40.00
4	PGM (MW)		**4.5**	**4.5**	**15**	**20**	**36**	**4.5**	**4.5**	**15**	**20**	**36**	**4.5**	**4.5**	**15**	**20**	**36**
	AC	Pg (MW)			1.56	9.53				2.11	1.13	26.88	4.41	2.55	10.73	20.00	36.00
		PF			0.86	0.83				0.94	1.00	0.78	1.00	1.00	0.82	1.00	1.00
	DC	Pg (MW)	1.16	0.72		9.09				2.53	12.04	25.43	3.62	2.69	11.51	19.84	36.00
5	PGM (MW)		**5**	**5**	**15**	**15**	**40**	**5**	**5**	**15**	**15**	**40**	**5**	**5**	**15**	**15**	**40**
	AC	Pg (MW)			1.68	9.40			1.87	1.98	6.33	30.11	2.98	3.93	11.78	15.00	40.00
		PF			0.98	0.80			0.98	0.55	0.64	0.93	1.00	0.74	1.00	0.97	1.00
	DC	Pg (MW)			4.43	6.54				10.10	8.30	21.60	3.87	3.79	12.98	13.10	39.93

To be continued on the next page

* PF stands for power factor.

* The grey color of a block denotes the offline status of the corresponding generating unit.

Index			Mission Segment 1					Mission Segment 2					Mission Segment 3				
6	PGM (MW)		**5**	**15**	**20**	**20**	**20**	**5**	**15**	**20**	**20**	**20**	**5**	**15**	**20**	**20**	**20**
	AC	Pg (MW)		3.00	8.09					12.11	16.08	12.10	2.46	13.56	18.51	20.00	19.16
		PF		1.00	0.72					0.64	1.00	0.80	0.51	1.00	1.00	1.00	0.98
	DC	Pg (MW)		7.77	3.20					13.33	13.33	13.33	4.02	13.45	18.89	18.64	18.70
7	PGM (MW)		**11**	**11**	**11**	**11**	**36**	**11**	**11**	**11**	**11**	**36**	**11**	**11**	**11**	**11**	**36**
	AC	Pg (MW)	5.47	5.62					3.75	6.86	6.19	23.49	8.19	8.46	10.04	11.00	36.00
		PF	0.76	0.90					0.82	0.55	0.52	0.99	0.97	0.87	1.00	1.00	1.00
	DC	Pg (MW)	6.06	4.91					5.06	5.32	5.13	24.49	8.49	11.00	8.99	9.24	35.94
8	PGM (MW)		**15**	**15**	**15**	**15**	**20**	**15**	**15**	**15**	**15**	**20**	**15**	**15**	**15**	**15**	**20**
	AC	Pg (MW)				1.43	9.66	9.31	7.49	2.52	7.91	13.06	14.06	13.49	11.14	15.00	20.00
		PF				0.71	0.85	0.95	0.92	1.00	0.75	0.83	1.00	1.00	1.00	0.91	1.00
	DC	Pg (MW)				1.50	9.47		8.86	7.75	6.69	16.70	12.43	15.00	13.00	13.24	20.00

APPENDIX B – NUMERICAL SOLUTION TO THE QOS OPTIMIZATION PROBLEM

Table B.1 The MVAC ZEDS—the probability-based QOS determined by maximizing the QOS via the SOPSO vs. the probability-based QOS obtained from minimizing the fuel consumption (MF) of each design alternative, respectively

Index		**1**	**2**	**3**	**4**	**5**	**6**	**7**	**8**
Mission Segment 1	**SOPSO**	0.377	0.329	0.359	0.343	0.344	0.339	0.374	0.337
	MF	0.377	0.317	0.322	0.318	0.309	0.310	0.357	0.317
QOS Improvement %		0.00	3.79	11.40	7.99	11.29	9.35	4.82	6.40
Fuel Increase %		0.00	10.05	11.37	19.29	12.11	15.22	6.84	8.90
Mission Segment 2	**SOPSO**	0.313	0.309	0.308	0.314	0.308	0.310	0.328	0.315
	MF	0.313	0.292	0.260	0.266	0.268	0.281	0.298	0.310
QOS Improvement %		0.00	5.75	18.42	18.20	14.96	10.36	9.93	1.68
Fuel Increase %		0.00	1.73	3.66	4.71	4.21	1.27	2.41	0.36
Mission Segment 3	**SOPSO**	0.256	0.263	0.270	0.265	0.259	0.271	0.281	0.268
	MF	0.232	0.237	0.270	0.256	0.243	0.252	0.280	0.244
QOS Improvement %		10.26	10.80	0.00	3.67	6.75	7.62	0.32	9.96
Fuel Increase %		0.30	0.86	0.00	0.17	0.49	0.72	0.59	1.52
QOS Overall the Whole Mission	**SOPSO**	0.945	**0.900**	0.937	0.923	0.911	0.920	**0.983**	0.921
	MF	0.923	0.846	0.852	0.840	0.820	0.843	0.935	0.870
QOS Improvement %		2.38	6.43	9.98	9.90	11.15	9.17	5.10	5.72
Fuel Increase %		0.18	1.99	2.23	3.31	2.73	2.22	1.73	1.82

Table B.2 The MVDC ZEDS—the probability-based QOS determined by maximizing the QOS via the SOPSO vs. the probability-based QOS obtained from minimizing the fuel consumption (MF) of each design alternative, respectively

Index		**1**	**2**	**3**	**4**	**5**	**6**	**7**	**8**
Mission Segment 1	**SOPSO**	0.691	0.677	0.739	0.713	0.709	0.691	0.767	0.692
	MF	0.650	0.659	0.668	0.667	0.676	0.661	0.732	0.649
QOS Improvement %		6.34	2.73	10.55	6.94	4.88	4.57	4.77	6.59
Fuel Increase %		40.15	19.76	17.11	12.23	41.69	40.54	12.16	28.89
Mission Segment 2	**SOPSO**	0.610	0.625	0.630	0.639	0.615	0.636	0.673	0.646
	MF	0.550	0.571	0.555	0.576	0.592	0.597	0.617	0.598
QOS Improvement %		10.91	9.44	13.53	10.87	3.80	6.45	9.11	7.94
Fuel Increase %		3.82	1.71	8.32	6.41	6.53	4.96	4.05	0.75
Mission Segment 3	**SOPSO**	0.467	0.491	0.481	0.489	0.465	0.500	0.513	0.506
	MF	0.430	0.490	0.445	0.460	0.449	0.500	0.489	0.501
QOS Improvement %		8.63	0.10	8.04	6.22	3.52	0.06	4.87	1.00
Fuel Increase %		0.76	0.09	1.26	1.54	1.20	0.57	0.93	0.16
QOS Overall the Whole Mission	**SOPSO**	**1.768**	1.792	1.849	1.841	1.788	1.827	**1.953**	1.843
	MF	1.630	1.720	1.668	1.703	1.717	1.758	1.838	1.748
QOS Improvement %		8.48	4.21	10.88	8.07	4.15	3.92	6.25	5.45
Fuel Increase %		5.43	2.31	4.88	4.00	6.69	5.59	2.91	2.90

Table B.3 The MVAC ZEDS—the energy-based QOS failure determined by minimizing the QOS failure via the SOPSO vs. the energy-based QOS failure obtained from minimizing the fuel consumption (MF) of each design alternative, respectively

Index		**1**	**2**	**3**	**4**	**5**	**6**	**7**	**8**
Mission Segment 1*	**SOPSO**	0	0	0	0	0	0	0	0
	MF	0.307	0	0.032	0	0	0	3.749	0.307
Failure Improvement %		100.00	0	100.00	0	0	0	100.00	100.00
Fuel Increase %		26.75	0	35.67	0	0	0	22.95	14.91
Mission Segment 2	**SOPSO**	0.901×10^3	0.090	1.013×10^3	14.236	1.102×10^3	0	33.618	7.814
	MF	1.230×10^3	0.659×10^3	1.052×10^3	0.063×10^3	1.183×10^3	0.627×10^3	0.092×10^3	0.293×10^3
Failure Improvement %		26.76	99.98	3.68	77.40	6.80	100.00	63.46	97.33
Fuel Increase %		8.40	6.03	1.29	8.45	7.40	5.30	6.03	2.63
Mission Segment 3	**SOPSO**	7.845×10^3	7.109×10^3	7.533×10^3	4.835×10^3	7.544×10^3	5.258×10^3	4.168×10^3	4.470×10^3
	MF	7.859×10^3	7.232×10^3	7.541×10^3	4.852×10^3	7.607×10^3	5.776×10^3	4.254×10^3	4.476×10^3
Failure Improvement %		0.18	1.70	0.10	0.34	0.83	8.98	2.01	0.13
Fuel Increase %		1.13	0.52	2.09	1.03	1.87	1.29	0.77	1.22
Total QOS Failure (MW·h)	**SOPSO**	$\mathbf{8.746\times10^3}$	7.109×10^3	8.546×10^3	4.850×10^3	8.647×10^3	5.258×10^3	$\mathbf{4.202\times10^3}$	4.478×10^3
	MF	9.089×10^3	7.892×10^3	8.593×10^3	4.915×10^3	8.789×10^3	6.402×10^3	4.350×10^3	4.769×10^3
Failure Improvement %		3.78	9.91	0.54	1.33	1.63	17.89	3.40	6.11
Fuel Increase %		5.62	2.86	5.12	3.21	7.52	5.35	4.43	2.88

* The energy-based QOS failure in each mission segment is measured in MW·h.

Table B.4 The MVDC ZEDS—the energy-based QOS failure determined by minimizing the QOS failure via the SOPSO vs. the energy-based QOS failure obtained from minimizing the fuel consumption (MF) of each design alternative, respectively

Index		**1**	**2**	**3**	**4**	**5**	**6**	**7**	**8**
Mission Segment 1*	**SOPSO**	0	0	0	0	0	0	0	0
	MF	0	0	0.258	2.456	0.516	0	0.774	0.258
Failure Improvement %		0	0	100.00	100.00	100.00	0	100.00	100.00
Fuel Increase %		0	0	36.89	19.13	0.37	0	37.61	14.11
Mission Segment 2	**SOPSO**	61.00	0	6.392	2.415	15.465	2.526	1.416	1.217
	MF	0.265×10^3	62.064	0.185×10^3	10.382	0.204×10^3	22.311	29.777	25.647
Failure Improvement %		76.98	100.00	96.54	76.74	92.42	88.68	95.24	95.25
Fuel Increase %		6.54	19.15	5.10	5.37	12.23	5.79	10.01	6.04
Mission Segment 3	**SOPSO**	7.732×10^3	7.029×10^3	7.410×10^3	4.768×10^3	7.324×10^3	5.138×10^3	4.043×10^3	4.329×10^3
	MF	7.753×10^3	7.319×10^3	7.416×10^3	4.770×10^3	7.767×10^3	5.328×10^3	4.241×10^3	4.658×10^3
Failure Improvement %		0.28	3.97	0.08	0.03	5.71	3.56	4.68	7.06
Fuel Increase %		1.20	1.33	1.60	1.58	1.11	1.23	0.49	0.86
Total QOS Failure (MW·h)	**SOPSO**	$\mathbf{7.791\times10^3}$	7.029×10^3	7.416×10^3	4.771×10^3	7.339×10^3	5.141×10^3	$\mathbf{4.044\times10^3}$	4.331×10^3
	MF	8.018×10^3	7.381×10^3	7.601×10^3	4.783×10^3	7.972×10^3	5.350×10^3	4.271×10^3	4.684×10^3
Failure Reduction %		2.81	4.77	2.43	0.24	7.94	3.92	5.32	7.54
Fuel Increase %		5.67	8.39	5.98	0.98	4.39	5.55	6.83	3.64

* The energy-based QOS failure in each mission segment is measured in MW·h.